THE UNIVERSITY THOUGHT

PUBLICATION IN NATURAL SCIENCES

Vol. 10, Nº 1, 2020.

ISSN 1450-7226 (Print), ISSN 2560-3094 (Online)

THE UNIVERSITY THOUGHT - PUBLICATION IN NATURAL SCIENCES

Published by
University in Priština - Kosovska Mitrovica
Faculty of Sciences - Republic of Serbia

Focus and Scope

The University Thought - Publication in Natural Sciences is an international, peer-reviewed, open access journal, published semiannually, both online and in print, by the University of Priština, Kosovska Mitrovica, Republic of Serbia. The Journal publishes articles on all aspects of research in biology, chemistry, geography, geoscience, astronomy, mathematics, computer science, mechanics and physics.

Editorial Office

Ive Lola Ribara 29; 38220, Kosovska Mitrovica, Serbia, e-mail: editor.utnsjournal@pr.ac.rs, office.utnsjournal@pr.ac.rs, office.utnsjournal@gmail.com; fax: +381 28 425 397

Available Online

This journal is available online. Please visit http://www.utnsjournal.pr.ac.rs or http://www.utnsjournal.com to search and download published articles.

THE UNIVERSITY THOUGHT - PUBLICATION IN NATURAL SCIENCES

Vol. 10, N^{o} 1, 2020.

CONTENTS

BIOLOGY

CHEMISTRY

GEOGRAPHY, GEOSCIENCE AND ASTRONOMY

MATHEMATICS, COMPUTER SCIENCE AND MECHANICS

PHYSICS

UNIVERSITY THOUGHT
Publication in Natural Sciences, Vol. 10, No. 1, 2020, pp. 1-5.
DOI: https://doi.org/10.5937/univtho10-24743
Original Scientific Paper

HIGHLY PATTERNED PRIMARY SUCCESSION AFTER FLUVIAL DEPOSITION OF MINING WASTE

NINA NIKOLIĆ[*1]

[1]Institute for Multidisciplinary Research, University of Belgrade, Belgrade, Serbia

ABSTRACT

This study examined early stages (3-5 years) of spontaneous primary vegetation succession on a model locality drastically altered by long term fluvial deposition of copper tailings in Eastern Serbia. In a large-scale survey, 115 samples of herbaceous vegetation (with a total of 75 species) were harvested from standardized 1m x 1m quadrates, and concomitant soil samples collected and their relevant physicochemical properties analysed. Primary succession depended on the establishment of five pioneer species (*Rumex acetosella*, *Agrostis capillaris*, *Calamagrostis epigeios*, *Persicaria lapathifolia* and *Chenopodium botrys*). Unconstrained ordination showed very clear vegetation gradients, significantly correlated with the key soil constraints (from Cu excess to low pH and nutrient deficiency), while the distribution of the five edificatory pioneers showed high degree of dependence on the micro-level habitat conditions. This work demonstrates that in such a complex setup with severe abiotic filtering, sufficient sampling effort can reveal strong patterns in a process commonly considered very stochastic.

Keywords: Copper, Gradient analysis, Habitat Modeling, Primary Vegetation Succession.

INTRODUCTION

Even after a century of research, primary succession (especially in its early stages) is in general still considered an inherently stochastic process with extremely low predictability (Buma et al., 2019). Thorough understanding of vegetation succession (a species change over time in the broadest sense) is however a key issue for sustainable restoration and management, particularly on fragile post-mining land (Prach & Walker, 2011). Mining of metals has so far irreversibly destroyed about 1% of the global terrestrial area (Walker, 1999). Mining of sulphidic copper (Cu) deposits creates more waste than mining of any other metal; this waste (tailings slurry) has an extremely high potential for oxidative weathering, soil acidification and metal mobilization. In fact, low pH and high concentrations of plant available metals can become an insurmountable obstacle for *de novo* establishment of vegetation (via primary succession) on such land (Bradshaw, 1997). An immanently irregular spatial distribution of soil constraints on post-mining areas (over distances shorter than 10 m, e.g. Néel et al., 2003) further makes a gradient analysis very difficult. Notwithstanding the notion that barren post-mining landscapes provide a unique and exciting opportunity to study primary succession, (e.g. Wiegleb & Felinks, 2001; Felinks & Wiegand, 2008), such investigations are still worldwide very scarce.

This study examines early stages (3-5 years) of primary succession spontaneously initiated upon mine closure on a model locality in Eastern Serbia, created by long-term fluvial deposition of sulphidic Cu tailings over arable land. The objective is to check whether extensive sampling of soil and vegetation can discern any patterns which elucidate the distribution of major early plant assemblages over the very heterogeneous and drastically altered land.

MATERIALS AND METHODS

Research locality

The exclusive model locality of this study (Fig. 1) has been created during about 70 years of fluvial deposition of sulphidic Cu tailings waste from the Bor Copper Mine complex in Eastern Serbia. In brief, the toxic slurry from the tailing ponds was being released directly into the local river system, carried to the Timok river and deposited (via lateral accretion during regular floods) in the Timok floodplain, over the former arable land. The depth of the deposited sediments ranges from tens of cm to over a meter. Due to highly dynamic flooding regime, a complex mosaic of soil constraints ranging from extreme Cu toxicity to severe nutrient deficiency and low pH was created. About 80 km of waterways was affected and more than 10,000 ha of alluvial land is still without vegetation. For details see Nikolic et al. (2018).

Vegetation sampling

The major sampling sites were located along about 30 km of the Timok flow (Fig. 1), where the river slowly meanders and creates a braided pattern of smaller lateral channels. The sampling design comprised firstly stratification according to the dominant pioneer species followed by flexible systematic sampling according to the visual appearance of the vegetation (Smartt, 1978). Aboveground biomass was harvested from standardized 1 m x 1 m quadrates, separated by species, air dried and used for further analyses. All the samples were less than 300 m away from the riverbed or seasonally dry lateral channel; our

* Corresponding author: nina@imsi.bg.ac.rs

larger monitoring study guaranteed that the relevées were of the age of 3 to 5 years.

Figure 1. Study area. Red line denotes the Timok watershed, black cross marks the ore flotation facilities and the leaking tailing ponds. Polluted waterways are emphasized in dark blue, while purple triangles mark the major research sites.

Soil sampling and analyses

In each vegetation sample (quadrate) a composite soil sample (consisting of 3 subsamples) was taken at the rooting depth (0-20 cm), and analysed for 21 chemical and physical parameters (for details see Nikolic & Nikolic, 2012). Plant available concentrations of mineral elements were determined by different extractions: DTPA for metals, ammonium acetate-ammonium lactate (AL) for P and K, and KCl for Al.

Statistical analyses

Prior to ordination, biomass data were log-transformed by using the generalized log transform formula [b = log(x+xmin) - log(xmin)] to deal with zeroes. Biomass is a more precise measure than other common abundance indices. The unconstrained ordination (ordering of sampling units on the basis of vegetation data according to the covariation and association among the species) was done by Nonmetric Multidimensional Scaling (NMS), a robust non-parametric method based on rank distances. Soil data were passively projected (overlaid) on the ordination scores to produce joint plot. NMS was done using the PC-ORD 6.22 software (MjM Software Design, Gleneden Beach, USA). Variation in performances of the five edificatory pioneer species was related to the measured soil parameters using habitat models. Multiplicative habitat modeling was done by Non-Parametric Multiplicative Regression (NPMR) with the HyperNiche 2.3 software (MjM Software Design, Gleneden Beach, USA). NPMR was performed using Local Mean with a Gaussian weighting function; species response matrix contained biomass data relativized by total plot DW. Conservative overfitting control, better suited for the clumped data, was applied. Best soil predictors were selected for the highest tolerance and cross-validated pseudo-R^2.

RESULTS AND DISCUSSION

The natural revegetation process on this locality depends on the arrival and establishment of the five keystone pioneers (Fig. 2). These species are: perennial rhizomatous grasses *Agrostis capillaris* L. and *Calamagrostis epigeios* (L.) Roth, a perennial forb with strong vegetative propagation *Rumex acetosella* L. (Polygonaceae), and two therophytes (annuals), *Persicaria lapathifolia* (L.) Gray (Polygonaceae) and *Chenopodium botrys* L. (Chenopodiaceae). Of these five, only *P. lapathifolia* occurs but never dominates in the referent, pre-pollution natural vegetation of the study area (alluvial poplar forests of the Populion albae Br.-Bl. 1931 alliance), and only *C. epigeios* occassionaly occurs in a matrix of xerothermic calcicole vegetation surrounding the affected floodplain (to a distance of at least 5 km). Our other long-time monitoring shows that if any of the keystone pioneers (except *Calamagrostis*) would not get established, certain (well defined) patches would remain barren and the succession arrested (Nikolic, 2014)

Over the initial period (3-5 years) the keystone pioneers act as facilitators of the primary succession, allowing the gradual immigration of the accompanying 70 species, increase in biomass production and in biodiversity (Table 1). These are mostly pseudometallophytes (many are ruderals), about 27% of which are shared among the five assemblages. High and fluctuating number of species, and unusual and unstable species compositions ("Frankenstein" assemblages) like those encountered here, are typical for very early stages of primary succession, in particular on man-made habitats (e.g. Tischew & Kirmer, 2007).

Unconstrained ordination (Fig. 3.) shows three strong gradients which capture 83% of variation in these early vegetation stands. The gradients in species composition of the early vegetation are significantly correlated with the measured soil parameters. The strongest separation of the early vegetation samples (stands dominated by *R. acetosella*, *A. capillaris* and *P. lapathifolia*, against the stands of *Ch. botrys* and *C. epigeios*) occurs along the first two ordination axes, which are correlated with the two main soil gradients: increasing soil pH, phosphorus (P), Cu vs increasing aluminum (Al) and iron (Fe) concentrations along the Axis 2; and increasing potassium (K), total nitrogen (N_{tot}) and organic carbon (C_{org}) along the Axis 1 (Fig. 3). On the other hand, NMS Axis 3 captures significant variation in

vegetation data, but is only weakly (Pearson's correlation coefficient of only 0.12) correlated with the single soil parameter, total sulphur (S_{tot}) concentration in soils. This parameter (which, per se, has no direct effect on plant growth) was previously shown to be a good indicator of the amount of pollution deposited in the research area, and to be highly correlated with the development of later successional forest vegetation (Nikolic et al., 2016, 2018), and even with the weed vegetation in partially polluted but still cropped fields at the outer edge areas of the polluted alluvium (Nikolic et al., 2014). This indicates that micro-scale patterning (sometimes over the distances of only a few meters) of soil constraints is decisive for the very early primary succession, but that a more "coarser scaled" behavior could be expected along the spatial pollution gradients in the lather stages. It is commonly not feasible to include such tiny variations into the sampling design (Néel et al., 2003), what contributes to the increased "randomness" of this early process.

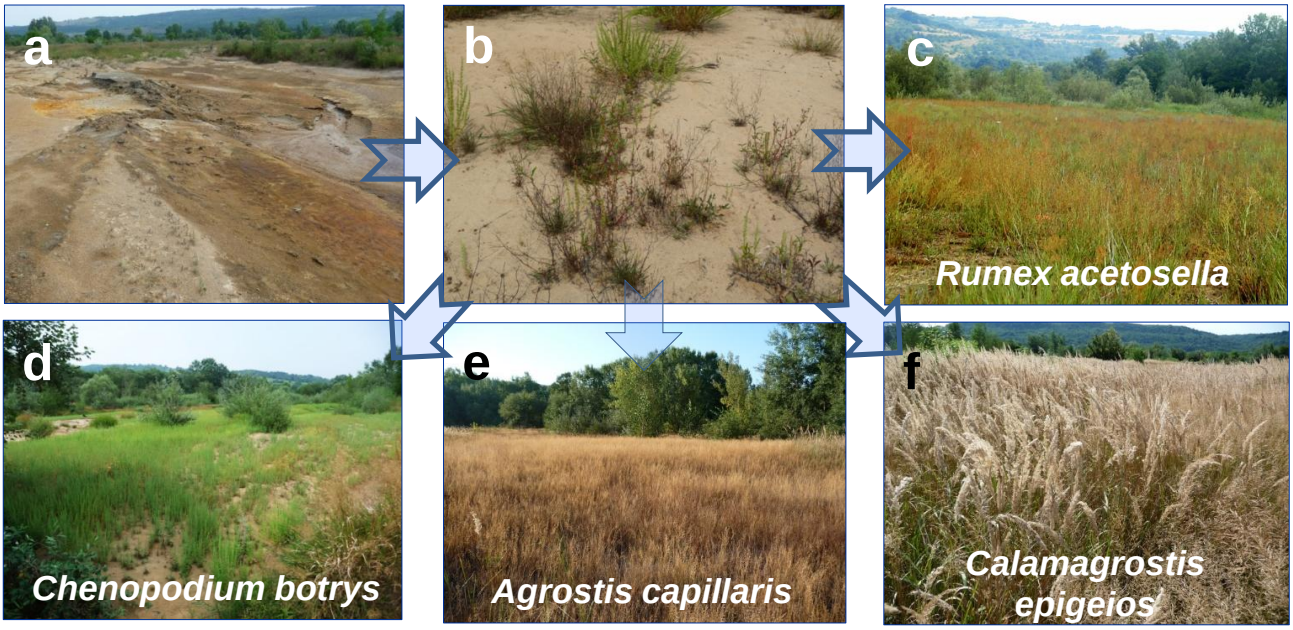

Figure 2: Primary succession on the barren land polluted by mining effluents in the Timok floodplain (a) does not start without five keystone pioneer species: *Rumex acetosella*, *Agrostis capillaris*, *Persicaria lapathifolia* and *Chenopodium botrys* (b). Their niches broadly overlap, but each achieves dominance (c-f) at distinct sections of the soil gradient. "Dominance" refers to about 50% of the biomass per m^2.

Table 1: Overview of the major 5 types of pioneer vegetation on the barren land polluted by the fluvially deposited Cu tailings. Edificatory species: A - *Rumex acetosella*; B - *Agrostis capillaris*; C - *Persicaria lapathifolia*; D - *Chenopodium botrys*; E- *Calamagrostis epigeios*.

Parameters	Pioneer vegetation dominated by:				
	A	B	C	D	E
No. of samples	27	31	17	20	20
Total species no.	64	62	38	40	65
Average species no. per m^2	9.4	8.0	7.8	6.7	14.0
Average aboveground biomass (g DW m^{-2})	184	199	173	83	547
Average within-group distance (Sørensen)[a]	0.53	0.46	0.47	0.50	0.37

[a] group is defined by the dominant pioneer specie

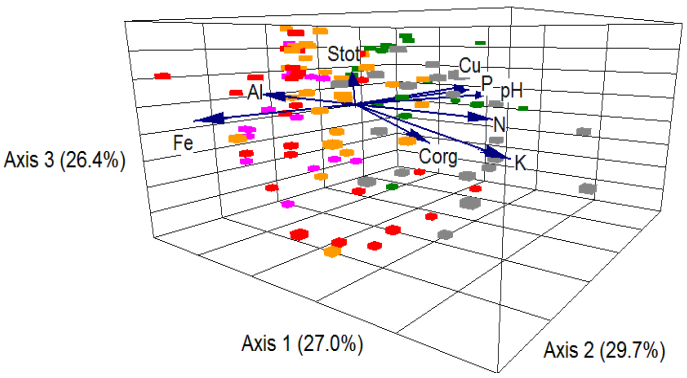

Figure 3: Unconstrained ordination (Nonmetric Multi-dimensional Scaling, NMS) of early vegetation relevées dominated by one of the five pioneer species occurring on the polluted floodplain. Selected soil parameters (plant available fractions of P and metals, and total concentrations of N and Corg), correlated with the ordination scores by > 10%, are overlaid. The values in parenthesis denote the proportion of variance represented by each axis. The angles and lengths of the radiating lines indicate the direction and strength of relationships of the soil variables with the ordination scores. Data matrix: 75 species, 115 stands, log-transformed biomass data, Sørensen distance, varimax rotation; final stress for 3-d solution 14.52. Assemblages dominated by each key pioneer are colour coded: red – *R. acetosella*; orange - *A. capillaris*; purple – *P. lapathifolia*; grey – *C. epigeios*; green – *Ch. botrys*.

Though the ordination of early vegetation shows very strong gradients, the Pearson's correlation coefficient of ordination with the measured soil parameters ranges from 0.12 to about 0.4. This might not be sufficient to clearly predict the occurrence of certain assemblages, but it is more of correlation than so far reported (e.g. Wiegleb & Felinks, 2001). On the other hand, the separation of preferred habitats of the keystone pioneers (modeled distribution along the gradient of soil constraints) is much clearer (Fig. 4). Putting together the data of this study, certain trends can be discerned:

1. *P. lapathifolia* and *Ch. botrys*-dominated patches occupy the smallest area and have the lowest biomass production; the former prefers microsites with stagnating water (low sand content), while the latter is a weak competitor which avoids acidic sites and thrives on Cu rich outcrops where other species are excluded by extreme Cu availability (median about 300 mg kg^{-1} of DTPA-extractable Cu).
2. *Calamagrostis*-dominated stands produce most biomass, and facilitate the establishment of the highest number of immigrating species. *Calamagrostis* avoids wet habitats (with higher availability of Fe), occurs with the increased incidence of uncontrolled burning (from the neighbouring crop fields – indicated by high K availability in soils), and generally prefers nutrient richer soils.
3. *R. acetosella* and *A. capillaris* dominate the landscape. They establish on nutrient poor, acidic and moist microsites, and are competitively excluded from more fertile sites.

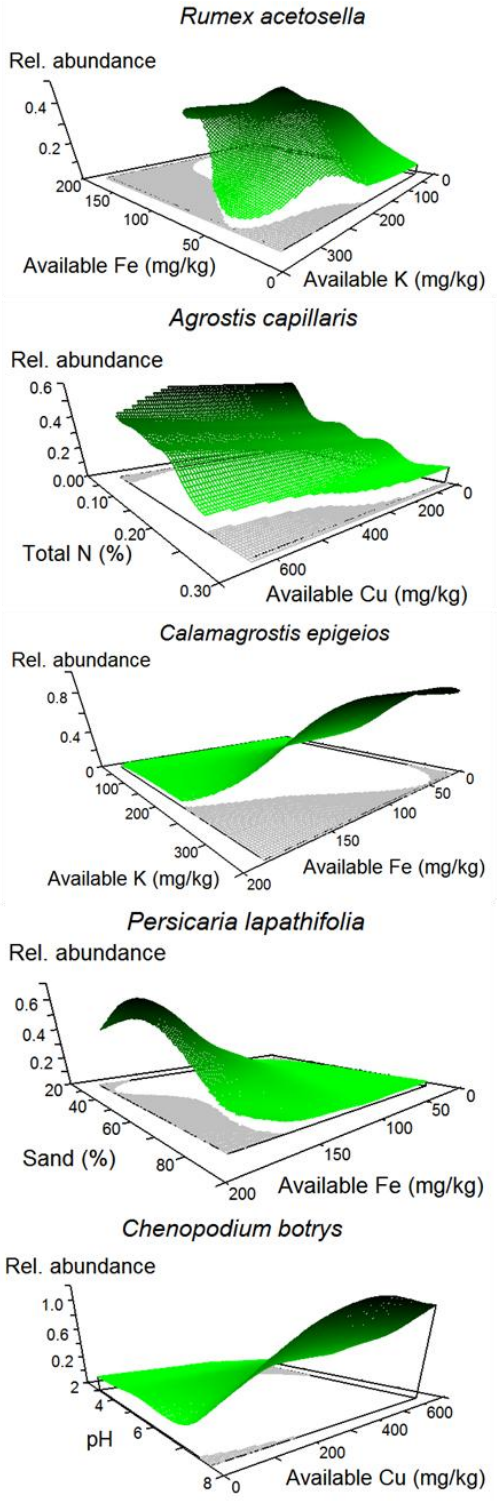

Figure 4: Habitat modeling (responses of the pioneers to the key soil parameters) by Non-Parametric Multiplicative Regression (NPMR). Relative abundance – share of the species in the total aboveground DW per m^2, analysed across 115 relevées. Best soil predictors are shown.

In general, the results of this study imply that a stronger correlation between vegetation establishment and soil constraints is found for single pioneer species, and then for the subsequent assemblages created around these edificatory species just a couple of years later. We recognize that our keystone species act as "nuclei" to facilitate further colonization. This is principally in accordance with the baseline findings of Felinks & Wiegand (2008), that facilitation processes influence spatial patterns of early primary succession only on short-term temporal and very fine spatial scales. Moreover, of the 115 samples examined, we never found any other species but the five aforementioned keystone species to appear in a share of more than 10% in the biomass per m^2 (what is five time less than the share of these five "greats" in their respective assemblages). We believe that the extremely harsh abiotic filtering, imposed by drastic alteration by pollution deposition (for details on soil constrains see Nikolic et al., 2014, 2016, 2018), is responsible for a clear response patterns obtained (Figs. 3 and 4), what can be expected in early primary succession on man-made land (Walker & delMoral, 2003).

CONCLUSION

Very early stages of primary succession are difficult to predict. Yet, we could demonstrate that the establishment of keystone pioneer species, which facilitate further vegetation development, is closely related to the micro-scale variability of soil constraints, and thus not random. Our results should, in a long run, contribute to improving the linkage of ecological theory with restoration practice.

REFERENCES

Bradshaw, A. 1997. Restoration of mined lands—using natural processes. Ecological Engineering, 8(4), pp. 255-269. doi:10.1016/s0925-8574(97)00022-0

Buma, B., Bisbing, S. M., Wiles, G., & Bidlack, A. L. 2019. 100 yr of primary succession highlights stochasticity and competition driving community establishment and stability. Ecology, 100(12). doi:10.1002/ecy.2885

Felinks, B., & Wiegand, T. 2008. Exploring spatiotemporal patterns in early stages of primary succession on former lignite mining sites. Journal of Vegetation Science, 19(2), pp. 267-276. doi:10.3170/2008-8-18369

Néel, C., Bril, H., Courtin-Nomade, A., & Dutreuil, J. 2003. Factors affecting natural development of soil on 35-year-old sulphide-rich mine tailings. Geoderma, 111(1-2), pp. 1-20. doi:10.1016/s0016-7061(02)00237-9

Nikolic, N., & Nikolic, M. 2012. Gradient analysis reveals a copper paradox on floodplain soils under long-term pollution by mining waste. Science of The Total Environment, 425, pp. 146-154. doi:10.1016/j.scitotenv.2012.02.076

Nikolic, N., Böcker, R., Kostic-Kravljanac, L., & Nikolic, M. 2014. Assembly Processes under Severe Abiotic Filtering: Adaptation Mechanisms of Weed Vegetation to the Gradient of Soil Constraints. PLoS ONE, 9(12). doi:10.1371/journal.pone.0114290

Nikolic, N. 2014. Ecology of alluvial arable land polluted by copper mine tailings. Saarbruecken: SVH.

Nikolic, N., Böcker, R., & Nikolic, M. 2016. Long-term passive restoration following fluvial deposition of sulphidic copper tailings: Nature filters out the solutions. Environmental Science and Pollution Research, 23(14), pp. 13672-13680. doi:10.1007/s11356-015-5205-0

Nikolic, N., Kostic, L., & Nikolic, M. 2018. To dam, or not to dam? Abolishment of further flooding impedes the natural revegetation processes after long-term fluvial deposition of copper tailings. Land Degradation and Development, 29(6), pp. 1915-1924. doi:10.1002/ldr.2921

Smartt, P. F. M. 1978. Sampling for Vegetation Survey: A Flexible Systematic Model for Sample Location. Journal of Biogeography, 5(1). doi:10.2307/3038106

Tischew, S., & Kirmer, A. 2007. Implementation of Basic Studies in the Ecological Restoration of Surface-Mined Land. Restoration Ecology, 15(2), pp. 321-325. doi:10.1111/j.1526-100x.2007.00217.x

Prach, K., & Walker, L. R. 2011. Four opportunities for studies of ecological succession. Trends in Ecology and Evolution, 26(3), pp. 119-123. doi:10.1016/j.tree.2010.12.007

Walker, L. R. (ed.) 1999. Ecosystems of disturbed ground. Ecosystems of the world, Amsterdam: Elsevier., 16.

Walker, L. R., & del Moral, R. 2003. Primary Succession and Ecosystem Rehabilitation. Cambridge: Cambridge University Press (CUP). doi:10.1017/cbo9780511615078

Wiegleb, G., & Felinks, B. 2001. Predictability of early stages of primary succession in post-mining landscapes of Lower Lusatia, Germany. Applied Vegetation Science, 4(1), pp. 5-18. doi:10.1111/j.1654-109x.2001.tb00229.

UNIVERSITY THOUGHT
Publication in Natural Sciences, Vol. 10, No. 1, 2020, pp. 6-12.
DOI: https://doi.org/10.5937/univtho10-24338
Original Scientific Paper

RURAL SPRING GEOMETER MOTHS (LEPIDOPTERA, GEOMETROIDEA LEACH, 1815) IN KOSOVO AND METOHIA (SERBIA)

NEBOJŠA V. ŽIVIĆ[1*], PREDRAG N. JAKŠIĆ[1]

[1]Faculty of Natural Sciences and Mathematics, University of Priština - Kosovska Mitrovica, Serbia

ABSTRACT

This paper shows the presence of the rural geometer moths in 15 localities of Kosovo and Metohia (Serbia). A review of existing data regarding the area of Kosovo and Metohia is given. Through research, the presence of 48 species was revealed. Between them, five species are reported as new for the fauna of Kosovo and Metohia: *Plagodis pulveraria* (Linnaeus, 1758), *Scotopteryx luridata* (Hufnagel, 1767), *Catarhoe cuculata* (Hufnagel, 1767), *Anticlea badiata* (Denis & Schiffermüller, 1775) and *Anticlea derivata* (Denis & Schiffermüller, 1775).

Keywords: Lepidoptera, Geometridae, Kosovo and Metohia (Serbia).

INTRODUCTION

The order Lepidoptera Linnaeus1758, with 45 superfamilies, represents one of the larger order of insects. Among them, the superfamily of geometer moths (Geometroidea Leach, 1815), with 999 species in Europe, belongs to the number of species in the more significant group of Lepidoptera (Nieukerken et al., 2011). In Serbia, this group of insects is represented by more than 350 species (Dodok, 2006). With this in mind, it is clear that the fauna of this group is insufficiently explored in Serbia.

The first faunistic data on the geometer moths in Kosovo and Metohia are found in the work of Rebel (1917). At that time, during the First World War, part of Metohija was connected to Montenegro ("Neumontenegro").The area of Žljeb Mt., Novo Selo (north of Peć) and the surroundings of Peć, Ribarić and Čečevo Brdo were investigated. The presence of 95 species was established and this result represents a pioneering contribution of the author.

Vukčević (1954) published next data on the geometer moths in Kosovo and Metohia. Among the identified species of plant diseases and pests, the author also lists the winter moths specie *Operophtera brumata* L. and *Erannis defoliaria* (Clerck, 1759). Đorđije Đorović, from the Forestry Institute in Peć, specialized in studying the defoliators of oak. Among the numerous representatives of defoliators, Đorović identified 25 species of Geometridae (Đorović, 1974, 1976, 1979, 1980 and 1992).

After this period, practically no one specialized in the study of geometer moths in Kosovo and Metohia. In the period from 1972 to 1999, Predrag Jakšić collected specimens of this group. Some of the data are published (Jakšić, 2016; Jakšić & Ristić (1999) 2001). (Tomić et al., 2002). One part of his data, comprising 80 species, is included in a study of the family of this group in Serbia (Tomić et al., 2002). In addition, several other authors have contributed to the knowledge of this group, as indicated in the References.

Some of rural and urban Geometridae species were primarily known for melanism, an example of a well-investigated species of the genus *Biston* (Bishop, 1972; Ford, 1955). Therefore, they can be indicators of the quality of the environment. Considering Rebel's (1917) research is already 100 years old, it was interesting to compare his results with ours.

As can be seen from this review, the fauna of this group of Lepidoptera is still insufficiently studied in Serbia. Likewise, the fauna of urban and rural areas, which usually contains synanthropic species, has remained under-researched. In addition, previous research was carried out for the most part during the summer period.

Bearing these facts in mind, we thought it would be important to study the urban and rural spring fauna of geometer moths in a few localities of Kosovo and Metohia.

MATERIALS AND METHODS

Specimens of the studied species were collected in the territory of Kosovo and Metohia in a period from 1974 to 2019. Collection was carried out at the following sites (Tab. 1).

Altitude and site coordinates are determined according to Google Earth, available on the Internet.

Collection was carried out at night, using a 160 W bulb (Mercury vapour Lamp, 160 W, BB Link Lighting). Preparation of the collected material and the production of permanent microscope slides of the genital armatures were carried out by standard procedure. Genital armatures were recorded as needed on a Nikon binocular microscope using a digital Nikon camera with an AF-S Micro Nikkor Lens.

Species determination was based on wing parameters and analysis of genital armatures, if necessary. The literature given in

* Corresponding author: nebojsa.zivic@pr.ac.rs

the References was used for determination based on the wing parameters.

The classification of Lepidoptera at the levels of order, superfamily and family is according to Nieukerken et al. (2011). Taxonomy and nomenclature of examined species was done according to Müller et al. (2019). Species ID numbers and systematic order are done according to Karsholt & Razowski (1996). Species determination was carried out on the basis of contemporary literary sources.

Abbreviations: m – Male, f – Female; K & M – Kosovo & Metohia (Косово и Метохија, Србија).

Tabela 1. List of examined places.

LOCALITY	ELEVATION (m)	COORDINATES	
		Latitude φ (N)	Longitude λ (E)
Bostane (Novo Brdo)	860	42° 36' 47"	21° 25' 33"
Gornje Kusca (Gnjilane)	556	42° 29' 48"	21° 28' 56"
Leposavić	508	43° 06' 10"	20° 48' 30"
Parteš (Gnjilane)	490	42° 24' 07"	21° 26' 01"
Pasjane (Gnjilane)	500	42° 24' 25"	21° 29' 44"
Pridvorica	580	42° 55' 22"	20° 41' 21"
Priština, Gazimestan	630	42° 41' 20"	21° 07' 46"
Priština, Grmija	700	42° 40' 30"	21° 11' 57"
Sevce (Šar-Planina)	1060	42° 12' 48"	20° 56' 22"
Stanišor (Gnjilane)	548	42° 29' 30"	21° 27' 43"
Štrpce (Šar-Planina)	890	42° 14' 19"	21° 01' 45"
Velji Breg (Zubin Potok)	630	42° 55' 54"	20° 40' 41"
Vrbeštica (Šar-Planina)	1011	42° 14' 34"	20° 58' 32"
Zubin Potok	567	42° 54' 52"	20° 41' 23"
Zvečan	583	42° 54' 24"	20° 50' 35"

RESULTS: LIST OF EXAMINED SPECIES

Superfam. Geometroidea Leach, 1815

Fam. Geometridae Leach, 1815

7530 *Ligdia adustata* ([Denis & Schiffermüller], 1775): Pridvorica, 5. May 2018, 1m; Velji Breg, 13. April 2018., 1m; Zubin Potok, 16. April 2018., 1m. New species for Serbia.

7540 *Macaria alternata* ([Denis & Schiffermüller], 1775): Gornje Kusce, 16. May 2018., 1m; Štrpce, 24. June 2018., 1f.

7581 *Neognopharmia stevenaria* (Boisduval, 1840): Pasjane, 19. April 2018., 1m.

7606 *Plagodis pulveraria* (Linnaeus, 1758): Gornje Kusce, 4. May 2018., 1f.

7613 *Opisthograptis luteolata* (Linnaeus, 1758): Štrpce, 20. May 2018., 1m.

7618 *Therapis flavicaria* ([Denis & Schiffermüller], 1775): Pridvorica, 5. May 2018., 1m.

7622 *Eilicrinia cordiaria* (Hübner, 1790): Gnjilane, Gornje Kusce, 7. May 2018., Genitalia checked, slide SR-3120 (Fig. 1).

Figure 1. *E. cordiaria* (Hübner, 1790): Gnjilane, Gornje Kusce, 7. May 2018., Male genitalia.

7636 *Ennomos erosaria* ([Denis & Schiffermüller], 1775): Leposavić, 26. May 2018., 1m Genitalia checked, slide SR–3135 (Figs. 2a & 2b).

7642 *Selenia lunularia* (Hübner, [1788]): Gornje Kusce, 8. April, 2018., 1m; Pasjane, 4. April 2018., 1f.

7650 *Dasycorsa modesta* (Staudinger, 1879): Gnjilane, Gornje Kusce, 15. Mart 2018., 1m; 30. Mart 2018., 1m; 10.-16.

April 2018., 3m; Gnjilane, Stanišor, 5.–22. April 2018., 3m, Genitalia checked. (Figs. 3a & 3b).

Figure 2a. *E. erosaria* ([Denis & Schiffermüller], 1775): Leposavić, 26. May 2018., Male adult.

Figure 2b. *E. erosaria* ([Denis & Schiffermüller], 1775): Leposavić, 26. May 2018., Male genitalia.

Figure 3a. *D. modesta* (Staudinger, 1879): Gnjilane, Gornje Kusce, 16. April 2018. Male, adult.

Figure 3b. *D. modesta* (Staudinger, 1879): Gnjilane, Gornje Kusce, 30. Mart 2018. Male, genitalia.

7661 *Asovia maeoticaria* (Alphéraky, 1876): Gnjilane, Gornje Kusce, 13. April 2018., 1f. So far, for Serbia this species reported Djuric & Hric (2013) and Beshkov (2015). New species for K & M.

7663 *Colotois pennaria* (Linnaeus, [1760]): Sevce, 20. October, 1m; Štrpce, 18. October 2018., 1f. So far, Đorović (1976, 1992) reported this species for K & M.

7671 *Apocheima hispidaria* ([Denis & Schiffermüller], 1775): Gornje Kusce, 2. February 2018, 1 m; 17. February 2018., 1m; 15. March 2018., 1m. Đorović (1976 & 1979) reported this species for K & M.

7672 *Phigalia pilosaria* ([Denis & Schiffermüller], 1775): Vrbeštica, 1. March 2018., 4m. Genitalia checked, slide SR-3125 (Figs.4a & 4b). Đorović (1976, 1979, 1992) reported this species for K & M.

Figure 4a. *P. pilosaria* ([Denis & Schiffermüller], 1775). Šar-Planina, Vrbeštica, 1011m, 1. Mart, 2019. Male adult.

Figure 4b. *P. pilosaria* ([Denis & Schiffermüller], 1775). Šar-Planina, Vrbeštica, 1011m, 1. Mart, 2019. Male genitalia.

7674 *Lycia hirtaria* (Clerck, 1759): Štrpce, 29. April 2018., 1m.

7676 *Lycia graecarius* (Staudinger, 1861): Gornje Kusce, 19. March 2018, 1m; Velji Breg, 30. March 2018, 1m. Jakšić (2016; 2018) and Jakšić & Ristić (1999) reported this species for K & M.

7685 *Biston strataria* (Hufnagel, 1767): Gornje Kusce, 5. March 2018., 1m; 29. March 2018., 1m.

7694 *Agriopis bajaria* ([Denis & Schiffermüller], 1775): Štrpce, 25. October 2018., 1m. This is the second data for this species on K & M, so far Đorović (1979) reported it for Dulje and Birač.

7695. *Agriopis aurantiaria* (Hübner, 1799): Stanišor, 31. September 2018., 1m.; Štrpce, 25. October 2018., 1m.

7696 *Agriopis marginaria* (Fabricius, [1777]): Vrbeštica, 1. March 2018., 2m; Štrpce, 29. April 2018., 1m; Priština, Grmija, 6. March 1979., 1m; 20. March 1980., 1m. Genitalia checked, slides SR-3124 & SR-3126.

7699 *Erannis defoliaria* (Clerck, 1759): Zvečan, 26. October 2018., 1m; Bostane (Novo Brdo), 27. November 1982., 1m; 10. December 1982., 1m. Genitalia checked, slides SR-3128 and SR-3129. (Fig. 5).

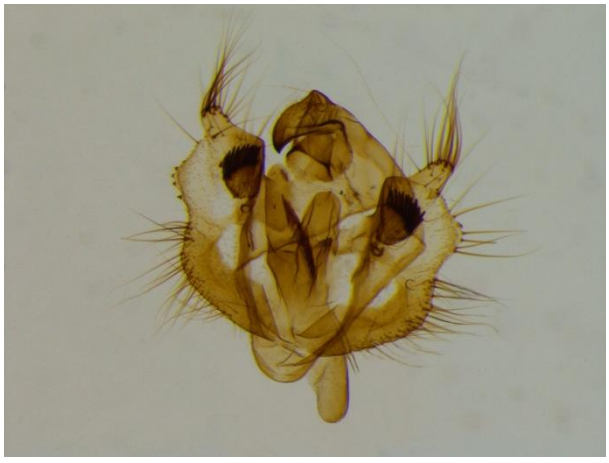

Figure 5. *E. defoliaria* (Clerck, 1759), Bostane (Novo Brdo), 10. December 1982. Male genitalia.

7804 *Ematurga atomaria* (Linnaeus, 1758): Velji Breg, 9. May 2018., 1m.

7824 *Cabera pusaria* (Linnaeus, 1758): Parteš, 12. May 2018., 1f.

7826 *Cabera exanthemata* (Scopoli, 1763): Štrpce, 20 May 2018., 1m.

7831a *Aleucis orientalis* (Staudinger, 1892): Priština, Gazimestan, 9. April 1974., 1f.; Štrpce, 29.April 2018., 1m.

7916 *Siona lineata* (Scopoli, 1763): Gornje Kusce, 7. May 2018., 1m; Zubin Potok, 15. May 2018., 1f.

7953 *Alsophila aescularia* ([Denis & Schiffermüller], 1775): Gornje Kusce, 17. March 2018., 2m; Štrpce, 29. April 2018., 3m; Vrbeštica 1. March 2018., 5m.

7971 *Comibaena bajularia* ([Denis & Schiffermüller], 1775): Leposavić, 24. May 2018., 1m Genitalia checked, slide SR-3136 (Figs. 6a & 6b).

Figure 6a. *C. bajularia* ([Denis & Schiffermüller], 1775): Leposavić, 24. May 2018., Male adult.

Figure 6b. *C. bajularia* ([Denis & Schiffermüller], 1775): Leposavić, 24. May 2018., Male genitalia.

8000 *Hemistola chrysoprasaria* (Esper, 1795): Gornje Kusce, 20. May 2018., 1f.

8020 *Cyclophora quercimontaria* (Bastelberger, 1897): Pridvorica, 7. May 2018., 1m and 1f.

8024 *Cyclophora linearia* (Hübner, [1799]): Pridvorica, 5. May, 2018., 1m; Zubin Potok, 15. May 2018, 1f.

8028 *Timandra comae* A. Schmidt, 1931: Pridvorica, 5. May 2018, 1m & 7. May 2018., 1m.

8036 *Scopula immorata* (Linnaeus, 1758): Parteš, 10 May 2018., 1f.

8045 *Scopula ornata* (Scopoli, 1763): Šar-Planina Mt., Štrpce, 20. May 2019., 1m. Genitalia checked, slide SR-3116 (Fig. 7).

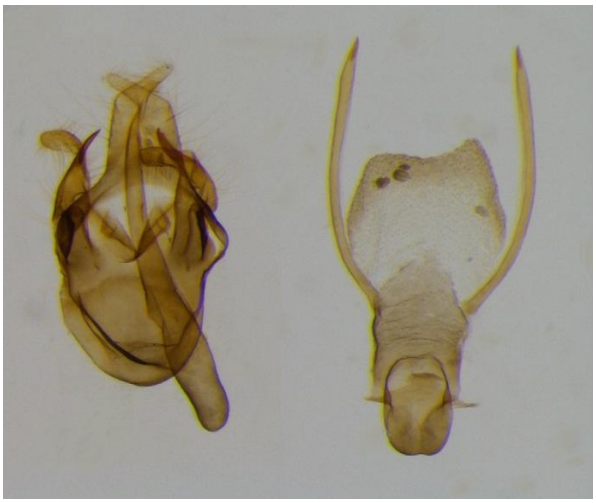

Figure 7. *S. ornata* (Scopoli, 1763): Šar-Planina Mt., Štrpce, 20. May 2019. Male genitalia.

8051 *Scopula decorata* ([Denis & Schiffermüller], 1775): Pasjane, 6. June 2018., 1f. (Fig. 8). Genitalia checked, slide SR-3117.

Figure 8. *S. decorata* ([Denis & Schiffermüller], 1775): Pasjane, 6. June 2018., Female, adult.

8059 *Scopula marginepunctata* (Goeze, 1781): Pridvorica, 9. May 2018., 1m. Genitalia checked, slide SR-3121.; Šar-Planina, Štrpce, 20. May 2019.

8062 *Scopula imitaria* (Hübner, [1799]): Pridvorica, 13. May 2018., 1f. Rebel was (1917) first who reported this species for Metohia.

8241 *Scotopteryx luridata* (Hufnagel, 1767): Pasjane, 22. April 2018., 1f.

8269 *Catarhoe cuculata* (Hufnagel, 1767): Pridvorica, 7. May 2018., 1f.

8309 *Earophila badiata* ([Denis & Schiffermüller], 1775): Štrpce, 29. April 2019., 8m.

8310 *Anticlea derivata* ([Denis & Schiffermüller], 1775): Pridvorica, 15. April 2018.,1f.

8335 *Gandaritis pyraliata* ([Denis & Schiffermüller], 1775): Gornje Kusce, 13. June 2018., 1f.

8338 *Ecliptopera silaceata* ([Denis & Schiffermüller], 1775): Štrpce, 20. May 2019., 1m.

8341 *Chloroclysta siterata* (Hufnagel, 1767): Šar-Planina, Štrpce, 890 m, 20. May 2019., 1f. Genitalia checked, slide SR-3123.

8400 *Horisme vitalbata* ([Denis & Schiffermüller], 1775): Pridvorica, 10. May 2018., 1m; Štrpce, 20. May, 1m.

8411 *Melanthia procellata* ([Denis & Schiffermüller], 1775): Pridvorica, 5-10. May 2018., 3m; 20. May – 6. June 2018., 6m; Šar-Planina, Štrpce, 20. May 2019. (Fig. 9).

Figure 9. *M. procellata* ([Denis & Schiffermüller], 1775) Šar-Planina, Štrpce, 890 m, 20. May 2019., Female.

8447 *Operophtera brumata* (Linnaeus, 1758): Vrbeštica, 23 December 2018., 7m.

8622 *Aplocera efformata* (Guené, [1858]): Štrpce, 9. June 2018., 1f.

DISCUSSION AND CONCLUSION

Presented here are the 48 species of the Geometridae Leach, 1815 family recorded in Kosovo and Metohia. The specimens were collected from 15 localities during winter and spring in 1979., 1980., 1982., 2018. and 2019.

Five species are reported as new for the fauna of Kosovo and Metohia: *Plagodis pulveraria* (Linnaeus, 1758), *Scotopteryx luridata* (Hufnagel, 1767), *Catarhoe cuculata* (Hufnagel, 1767), *Earophila badiata* (Denis&Schiffermüller, 1775) and *Anticlea derivata* (Denis & Schiffermüller, 1775).

Special attention was paid to the genus *Scopula* Schrank, 1802. Sihvonen (2005) treated the *drenowskii* Sterneck, 1941 taxon as a subspecies of *decorata* ([Denis & Schiffermüller], 1775). However, Can (2009) proved that this taxon is a valid

species (bona species). Alphéraky (1876) described the *orientalis*, which has recently been found in Romania by Dinca & Szekely (2018). Since the original description was given in Russian, we kindly asked Dr Konstantin Efetov (Simferopol, Russia) to provide us with a translation which we present here:

« – *Decorata* Brkh. Specimens from Taganrog are strongly lighter than German ones; transverse lines crossing middle of wings are slightly visible; lace-shaped pattern near outer margin is much more pale and does not rich upper angle of forewing. Size of specimens from Taganrog is similar to those of Northern Iran: 27–29mm, while German specimens: 20–23mm. According to my information specimens of this species are larger and lighter in the East than type from Western Europe and I propose to name the eastern form for example as varietas *Orientalis*. Moth is not rare; flying from end of May till September.»

Among the specimens examined in Kosovo and Metohia, 5 species of the *Scopula* Schrank, 1802 genus were found, but not the two aforementioned species.

Members of the Geometridae family are particularly sensitive to industrial pollution. This is why melanistic forms occur. Among the specimens collected, we found no melanistic forms. This serves to show that the environment is relatively well preserved.

ACKNOWLEGMENTS

We would like to thank to all colleagues who kindly provided the material for this study: Janićijević, Tanja (Gnjilane), Makić Mirjana (Gnjilane), Maksimović Milica (Gnjilane), Mladenović, Ilija (Štrpce), Orlović, Aleksandar (Štrpce), Raćićević Tijana (Brezovica), Timotijević Mirjana (Leposavić) and Živković, Mirjana (Zubin Potok).

We would like to express our gratitude to Dr. Peder Skou (Ollerup, Denmark), Dr Konstantin Efetov (Simferopol, Crimea) and Dr Stoyan Beshkov (Sofia, Bulgaria) for his valuable contributions.

REFERENCES

Alphéraky, S. 1875. Cheshuekrylyya (Lepidoptera) okrestnostei Taganroga / The Butterflies (Lepidoptera) of the environs of Taganrog. Russkago Entomologicheskago obshchestva, 8: 150-226 (1875); 10: 35–53 (1876); 11: 45-50 (1878).

Beshkov, S. 2015. Eight new and some rare for Serbia nocturnal Lepidoptera species collected at light. Entomologist's Rec. J. Var., 127, pp. 212-227; Pl. 10.

Bishop, J. A. 1972. An Experimental Study of the Cline of Industrial Melanism in *Biston betularia* (L.) (Lepidoptera) between Urban Liverpool and Rural North Wales. The Journal of Animal Ecology, 41(1). doi:10.2307/3513

Can, F. 2009. DNA barcoding confirms species rank for a cryptic geometrid species from Turkey and Bulgaria (Lepidoptera: Geometridae: Sterrhinae). Zootaxa, 2314(1), pp. 63-68. doi:10.11646/zootaxa.2314.1.4

De Prins, W. 2016. Catalogue of the Lepidoptera of Belgium: Vlaamse Vereniging voor Entomologie. In Entomobrochure. 9, 1278.

Dincă, V., & Székely, L. 2018. First record of *Scopula orientalis* (Alphéraky, 1876) (Lepidoptera, Geometridae) in Romania, at the northern limit of the BalkanS. Nota Lepidopterologica, 41(2), pp. 189-197. doi:10.3897/nl.41.24316

Djurić, M., & Hric, B. 2013. On distribution area of *Asovia maeoticaria* (Alphéraky, 1876) (Insecta: Lepidoptera: Geometridae). ZooNotes, 49, pp. 1-2.

Dodok, I. 2006. The fauna of Geometridae (Lepidoptera) in the region of Užice in Western Serbia. Acta entomologica serbica, 11(1/2), pp. 61-75.

Đorović, Đ. 1974. Defolijatori hrasta iz reda Lepidoptera na Kosovu. Beograd: Šumarski fakultet. Magistarski rad.

Đorović, Đ. 1976. Results of observations on the occurrence and morphological characteristics of harmful caterpillars from fam. Geometridae in the oak forests of the Province Kosovo. Šumarski list, 100, pp. 495-501.

Djorović, Dj., 1979. Fauna leptira (Lepidoptera) Metohije za period 1977-1978. god. – Report (unpublished), pp. 1-17. Peć.

Đorović, Đ. 1980. Karakteristike i struktura biocenotskog kompleksa defolijatora iz reda Lepidoptera u hrastovim šumama Kosova. Beograd: Šumarski fakultet. Doktorska disertacija.

Đorović, Đ. 1992. Biocenotički kompleks gusenica hrasta (Biocoenotis's complex of Oak's tree caterpillars). Nauka i društvo 1-191; 27 tabsl 67 figs.

Erlacher, S-I. 1998. Die phylogenetischen Beziehungen innerhalb des Taxon *Dyscia* Hübner, (Lepidoptera: Geometridae). Jena: Friedrich-Schiller-Universität, Jena Biologisch-Pharmazeutische Fakultät, Institut für Spezielle Zoologie und Evolutionsbiologie mit Phyletischem Museum. 1-105. Diplomarbeit.

Ford, E.B. 1955. Moths. London: Collins.

Jakšić, P. 2016. New contributions to the knowledge of Lepidortera fauna of Kosovo and Metohia (Republic of Serbia). The University Thought - Publication in Natural Sciences, 6(2), pp. 1-4. doi:10.5937/univtho6-12528

Jakšić, P., & Ristić, G. 1999. 2001. New and rare species of Lepidoptera in Yugoslavia. Acta entomologica serbica, Beograd, 4(1/2), pp. 63-74.

Karsholt, O., & Razowski, J. 1996. The Lepidoptera of Europe. Apollo Books.

Müller, B., Erlacher, S., Hausmann, A., Rajaei, H., Sihvonen, P., Skou, P., 2019. The Geometrid Moths of Europe, 6(1&2), Leiden; Boston: Brill.

Van Nieukerken, E., et al., 2011. Order Lepidoptera. In Z. Zhi-Qiang Ed., Animal biodiversity: An outline of higher-level classification and survey of taxonomic richness: Zootaxa. 3148, pp. 1-237.

Pinker, R. 1968. Die Lepidopterenfauna Mazedoniens. III. Geometridae. Prirodonaučen Muzej Skopje, 4, pp. 1-72.

Rebel, H. 1917. Lepidopteren aus Neumontenegro. Mathematisch-naturwissenschaftliche Klasse, 126: 765-813; Abteilung 1; Kaiserliche Akademie der Wissenschaften in Wien.

Ristić, G. 1997. Contribution to Knowledge of Distribution of Species Genus *Aplocera* Stephens, 1827 in Serbia

(Lepidoptera, Geometridae). University Thought, Nat. Sci., III: 41-43; 3 figs.

Sihvonen, P. 2005. Phylogeny and classification of the Scopulini moths (Lepidoptera: Geometridae, Sterrhinae). Zoological Journal of the Linnean Society, 143(4), pp. 473-530. doi:10.1111/j.1096-3642.2005.00153.x

Stojanović, A., Jovanović, M., & Marković, Č. 2018. Interesting species of the Family Geometridae (Lepidoptera) recently collected in Serbia, including some that are new to the country's fauna. Acta entomologica serbica: Color tabs., 23(2): 27-41; 8 color tabs.

Tomić, D., Zečević, M., Mihajlović, Lj., & Glavendekić, M. 2002. Fauna zemljomerki (Lepidoptera, Geometridae) Srbije. In Zbornik radova o fauni Srbije. Beograd: SANU. Knjiga VI: 73-164.

Urbahn, E. 1966. Ergebnisse der Albanien-Expedition 1961 des Deutschen Entomologischen Institutes. 51. Beitrag Lepidoptera: Geometridae. Beiträge zur Entomologie, 16(3/4), pp. 407-446.

Vukčević, R. 1954. Biljne štetočine i bolesti utvrđene na Kosmetu od 1949-1954 godine. Zaštita bilja, 26, pp. 56-106.

UNIVERSITY THOUGHT
Publication in Natural Sciences, Vol. 10, No. 1, 2020, pp. 13-19.
DOI: https://doi.org/10.5937/univtho10-21042
Original Scientific Paper

EFFECT OF DETERGENTS ON *ALKALINE INVERTASE* AND *ALKALINE PHOSPHATASE* ACTIVITY OF FUNGI *MUCOR PLUMBEUS* Bonord, 1864, *ASPERGILLUS NIGER* Tiegh, 1867 AND *TRICHODERMA HARZIANUM* Rifai, 1969

IVANA MATOVIĆ-PURIĆ[1*], TATJANA JAKŠIĆ[2], TATJANA MIHAJILOV-KRSTEV[3], PREDRAG VASIĆ[2]

[1]Medical School, Čačak, Serbia
[2]Department of Biology, Faculty of Sciences and Mathematics, University of Priština, Kosovska Mitrovica, Serbia
[3]Faculty of Sciences and Mathematics, University of Niš, Niš, Serbia

ABSTRACT

Due to their diverse metabolic potential, many filamentous fungi have a great ability for degradation of different waste substances. The present research was aimed to investigate ability of fungi *Mucor plumbeus, Aspergillus niger* and *Trichoderma harzianum,* isolated from sewer and industrial waste water, to conduct degradation of high concentrations of commercial detergent (0.3%). Within enzyme extracts of samples taken during period of 3–16 days, activity of *alkaline invertase* and *alkaline phosphatase* was followed spectrophotometrically at room temperature. Obtained results proved that all examined fungi affected degradation of detergent. Quality (inhibition/stimulation) and quantity of action of detergent on activity of investigated enzymes depended on fungal species and incubation period. The highest inhibiting effect of detergent was recorded on 9th day of incubation in samples of *T. harzianum* and *A. niger,* while its most obvious stimulating effect was noticed on 3rd day of incubation in samples of *T. harzianum* and *M. plumbeus*. Investigated fungi can be used for purification of waste water containing high concentrations of detergent.

Keywords: *Aspergillus niger*, *Mucor plumbeus*, *Trichoderma harzianum*, Waste waters, Detergent, *Alkaline invertase*, *Alkaline phosphatase*.

INTRODUCTION

Increased use of detergents in households led to their accumulation in waste water and natural water ecosystems. It also caused numerous unfavorable consequences for microbiological community and hydro-bionics (Kumar et al., 2007; Chaturvedi & Kumar, 2010; Abu-Zreig et al., 2003). As pollutants, detergents and their products of degradation, reach environment through industrial and sewer waste water, usage of pesticides and disposal of waste active mud (Cavalli, 2004; Ying, 2006).

Literature includes very few data related to degradation of commercial detergents under effect of fungi (Ojo & Oso, 2008). It is known that products with high level of SASs (Surface Active Supstance) such as detergents, in water ecosystems can cause numerous harmful effects: they inhibite growth of one-cell seaweed, decelerate process of water purification by creation of foam, which delays dissolution of oxygen important for breathing and photosynthesis, and causes eutrophication. Many studies showed that tensides modify conformation of proteins and in such way enzyme activity, stability and specifity (Kamiya et al., 2000; Buvaneswari et al., 2013). Recent researches showed that filamentous fungi *Myceliophthora thermophila*, *Geomyces* sp., *Alternaria alternata*, *Verticillium alboatrum*, *Aspergillus flavus*, *Trichoderma* sp., *Aspergillus oryzae,* isolated from river mud are able to degrade different synthetic detergents of anion type (Ojo & Oso, 2008). These fungi have specific apical growth, which provides ingrowth of hyphae into various substrates and excretion of extracellular enzymes. Under effect of these enzymes, complex organic compounds of substrates degrade into simplified compounds which can be absorbed by fungi through hyphae and used for growth (Raimbault, 1998; Saucedo-Castañeda et al., 1992; Raimbault, 1981). Filamentous fungus *Mucor plumbeus* produces different enzymes such as *invertase*, *alkaline phosphatase*, *proteinase* and *lipase* which are variously applied in biotechnology. Genus *Aspergillus* includes more than 180 species of fungi which present main decomposers of plant polysaccharides (Brookman & Denning, 2000). Especially important species in biodegradation is *Aspergillus niger* which is commonly used due to its ability to produce different extracellular enzymes. *Trichoderma* spp. are saprophytic fungi which are located in soil and roots of plants but also highly metabolically valued (Saucedo-Castañeda et al., 1992). *Trichoderma harzianum* can decompose different compounds such as following: dichlorodipheniltrichloroethan (DDT), dieldrine, endosulphan, pentachloro-nitrobenzene (PCNB) and pentachlorophenol (PCP) (Brookman & Denning, 2000). Species of *Trichoderma* have an important role in bioremediation of soil which is contaminated by pesticides, herbicides and insecticides (Brookman & Denning, 2000).

* Corresponding author: matovic.puric.ivana@gmail.com

Invertases are enzymes which hydrolize disaharide sucrose to glucose and fructose. Invertases are isolated and defined in many filamentous fungi of species *Penicillium, Neurospora, Aspergillus*, etc. (Poonawalla et al., 1965; Ashok Kumar et al., 2001; Guimaraes et al., 2009). Most of fungi synthesize intracelullar and extracellular *invertases* (Gillespie et al., 1952; Crewther & Lennox, 1953), which differ in the position within a cell (cell wall, vacuoles or cytoplasm), solubility (soluble or insoluble in buffer of a small ionic strength), optimum pH (acid or neutral/alkaline) and isoelectric point (pI).

The aim of this research was to investigate ability of filamentous species *Mucor plumbeus, Aspergillus niger* and *Trichoderma harzianum* isolated from sewer and industrial waste water for degradation of high concentrations of commercial detergent (0.3%) and to estimate their potentials for waste water purification.

MATERIAL AND METHODS

Isolation of fungi from waste water

Samples of waste water were collected using sterile glass bottles from three different localities (Sport Center 'Mladost', Industrial zone in Čačak and village Stančići) on the territory of the municipality of Čačak, during the end of May in 2013. After transport at temperature of 4 °C, collected samples were sown in Petri dishes on *Maltose agar* (MA, Sigma Aldrich) which included streptomycin (0,5 mg/ml) for purpose of inhibition of bacteria growth. Sown samples were incubated at the room temperature during 5 days. After that, isolation of fungi into clean cultures was conducted on sterilized *Potato Dextrose Agar* (PDA, Sigma Aldrich) without streptomycin. Isolated individual species are identified on the base of macroscopic and microscopic morphology at Department for Biology and Ecology at the Faculty of Science University of Kragujevac, Serbia. All isolated fungi were cultivated until sporulation on tilted PDA at room temperature during 5–7 days. After that, isolated fungi were used for preparation of suspensions of spores in 10 ml of sterile distilled water. Spores were counted under the microscope using *Noebauer* chamber in three repetition cycles, and their final concentration in inoculum was set on 10^6 spores ml^{-1} (Stojanović et al., 2010).

Enzymes extracts preparation

Prepared suspension (1 ml) of each investigated fungus was sown into two sterile Erlenmeyer flasks each containing 200 ml of modified sterile *Czapek Dox* broth (CDB, pH value adjusted to 4.7 using 1 mol l^{-1} HCl; Stojanović et al., 2010). After that, detergent (D) was added into one of two Erlenmeyer flasks to reach the final concentration 0.3% (w/w). The second Erlenmeyer flask was used as a control (K). Both Erlenmeyer flasks with samples were incubated during 16 days at the room temperature on electric shaker (Kinetor, Ljubljana, Slovenia) on 250 rpm. For further analysis samples were taken after 3, 6, 9, 12 and 16 days of incubation. The liquid in amount of 10 ml was taken from each Erlenmeyer flask. This liquid was filtered through Whatman filter paper in order to remove traces of mycelia. After that, liquids were centrifuged for 10 min at 10,000 rpm, at the temperature of +4 °C (Stojanović et al., 2010). Obtained supernatants were used as a raw enzyme extracts for defining of activity of enzymes of *alkaline invertase* and *alkaline phosphatase*. The experiment was conducted in three repetitions.

Determination of alkaline invertase activity

Invertase enzyme activity was determined by Sumner & Howell method (1935). Firstly, reactive mixture was developed in two tubes. This mixture included following components: 0.5 ml of raw enzyme extract, 0.5 ml 0.02 mol l^{-1} of phosphate buffer (pH 8.0) and 1 ml 1% (w/w) of sucrose. One tube (trial one) was incubated in water bathroom at 37 °C for 15 min and the second one (control) was placed on ice during the same period. After that, 1 ml of mixture from each of tube was transferred into new tubes and 2 ml of dinitrosalicylic reagent was added into each of them. Both tubes were then incubated at 100 °C for 5 min. After cooling to the room temperature, the amount of reducing sugars was determined spectrophotometrically at absorbance of 540 nm. The standard line was constructed using six tubes which contained 0.05, 0.10, 0.20, 0.30, 0.40 and 0.50 ml of standard solution of glucose (1 mg ml^{-1} of solution of 5.56×10^{-3} mol^{-1} glucose standard – Sigma Aldrich) in distilled water which was used as a base line. All tubes were incubated at 55 °C for 20 min. The results were presented as a mean value of three repetitions.

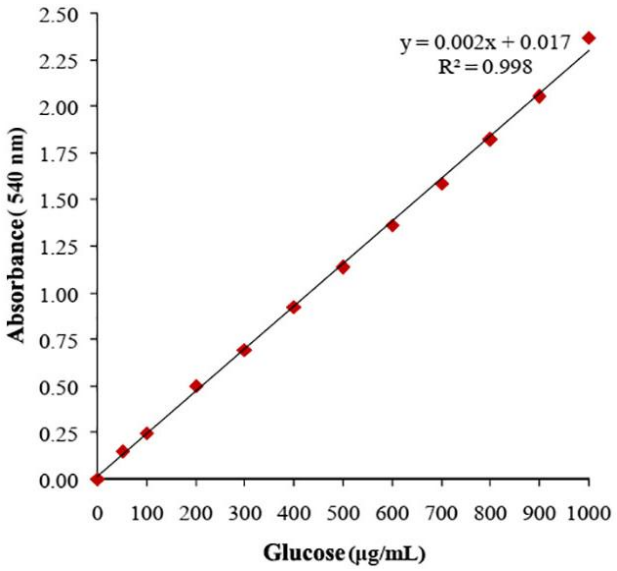

Figure 1. Standard line for glucose.

Determination of alkaline phosphatase activity

Enzyme activity of *alkaline phosphatase* was determined using the certain amount of inorganic phosphorus by Allen method according to Stojanović (2007). Enzyme activity was

measured in reaction mixture prepared of 1 ml of enzyme extract, 1 ml of glycol buffer (pH 9.0) with Mg^{2+} and 1 ml of *β*-glycerophosphate (substrate). Tubes with reactive mixture were incubated at 37 ºC for 30 min, after which the enzyme reaction is stopped by adding 3 ml of 10% trihydroxyuric acid (TCA). After that, tubes were held on ice for 15 min, after which their content was filtrated and the filtrate was collected. Control tubes were prepared in the same way except the incubation process. The phosphorus concentration in samples was determined through Allen reaction. The amount of 1 ml of filtrate for trial and 1 ml of filtrate for control were measured in two tubes each. After that, 0.4 ml of amido (Sigma Aldrich), 0.4 ml of 60% TCA (Sigma Aldrich), 0.2 ml of ammonium molybdate and 3 ml of distilled water were added to each of tubes. Tubes were incubated at the room temperature for 11 min. In order to construct standard line for phosphorus, the series of phosphorus standard solutions with lowered concentration were prepared and the described procedure was repeated. The measurement of absorbance was conducted at 720 nm. The results were expressed as a mean value of three repetitions (Heinonen & Lahti, 1981).

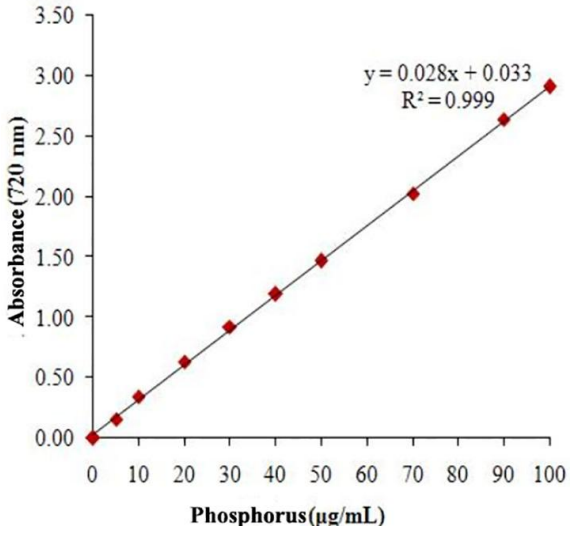

Figure 2. Standard line for phosphorus.

Statistical analysis

All experiments were performed in triplicate and results were expressed as means ± standard error of mean. For statistical analysis, the following tests were used: Mann-Whitney and Kruskal-Wallis Tests. Values of $p < 0.05$ were considered statistically significant.

RESULTS AND DISCUSSION

Results of many researches confirmed that activity of *invertases* depends on kind of surface and phase of development of fungi. Vainstein & Peberdy (1991) proven that *Aspergillus nidulans* produces extracellular invertases when grown on medium containing sucrose or raffinose, and their enzyme maximum can be achieved after 15 h of incubation at 28 °C. Poonawalla et al. (1965) concluded that *Penicillium chrysogenum* and *Sascharomyces cerevisiae* grown on medium with 30 g l^{-1} sucrose in submerged fermentation produce intra- and extracellular invertase with maximum activity of enzymes achieved between 72 and 96 h.

In the present study we investigated activity of *alkaline invertase* and *alkaline phosphatase* in control medium (which included sucrose in the first case) and in the medium containing detergent. Summary results of the experiment are presented in the Table 1.

With the exception of *alkaline phosphatase* activity in *T. harzianum*, Mann-Whitney U Test indicated that the activity of both enzymes was significantly higher ($p < 0.05$) in detergent containing media than in control media (Table 2). Also, Kruskal-Wallis Test showed statistically significant difference between enzymes activity in different fungi both on control media and detergent containing media (Table 3).

Activity of *alkaline invertase* of *M. plumbeus* (Table 1) in control medium was negligible on the 3rd day of the experiment while it was almost totally inhibited on the 6th day (0.0082 IU ml^{-1}). Sudden increasing of enzyme activity was recorded in a period from the 9th to 16th day, when it reached maximum value of 0.0883 IU ml^{-1}. In case of medium containing 0.3% of detergent, the significantly higher activity of *alkaline invertase* was recorded. It did not change much during investigated time period and its enzyme maximum was reached on the 16th day of the experiment (0.1607 IU ml^{-1}) when the mycelium of fungus was totally developed.

Activity of *alkaline invertase* of *A. niger* (Table 1) in control medium was changeable. The maximum activity was recorded on the 3rd day of incubation, after which its slope was recorded. It reached its minimum value on the 9th day of the experiment (0.0680 IU ml^{-1}). Activity of *alkaline invertase* in medium containing detergent was expressed during the entire period of mycelium growth, from the 3rd to 9th day, while maximum activity was measured at the 3rd day of the experiment (3.7673 IU ml^{-1}).

Activity of *alkaline invertase* of *T. harzianum* (Table 1) in control medium was negligible till 9th day of experiment, when it reached sudden increase of enzymes activity to their maximum value (0.8097 IU ml^{-1}). In surface with detergent, the enzymes activity was the smallest on the 3rd day of the experiment (0.1620 IU ml^{-1}), while on the 6th day it had sudden increase to its maximum value (3.4257 IU ml^{-1}), which was measure on the 16th day.

Phosphatases hydrolize esters and anhydrides of phosphoric acid. These enzymes are involved in various biological processes such as cell cycle, differentiation of cells and other cell processes. Optimum value of pH beeing 9 is needed for effect of alkaline phosphatase, while numerous researches showed that enzyme is active in wide range of pH being 3–9. Characteristics of acid and alkaline phosphatase in nutritive medium (extracellular enzymes) and mycelium extracts (citoplasmatic

and cellular bonded enzymes) were investigated in different fungi grown in stationary conditions on liquid mineral medium (Raper & Fennell, 1965). Many *alkaline phosphatases* have speciffic effects on substrate. Production of phosphatase of *A. awamor*i var. *kawachii* was investigated in media with small or large concentration of phosphate. This fungus has maximum of phosphatase activity in medium with small concentration of phosphate, such as bake yeast, *Escherichia coli* and *Neurospora crassa* (Schmidt et al., 1956). On the other hand, in medium with high concentration of phosphate, phosphatase activity was weak but still higher with β-glycerosphate as substrate than with glucose-6-phosphate. Researche conducted by Koffi et al. (2010) showed that SDS detergent displays strong inhibitory effect (cca 98%) on phosphatase activity.

Table 1. Activity of *alkaline invertase* and *alkaline phosphatase* (IU ml^{-1}) in fungi *M. plumbeus*, *A. niger* and *T. harzianum* followed period of 3–16 days*.

Sample	*Alkaline invertase* (IU ml^{-1})			*Alkaline phosphatase* (IU ml^{-1})		
	M. plumbeus	*A. niger*	*T. harzianum*	*M. plumbeus*	*A. niger*	*T. harzianum*
K-3	0.0273±0.0198	3.5337±0.0024	0.0410±0.0295	0.1373±0.0033	0.1043±0.0024	0.4673±0.0050
K-6	0.0082±0.0057	0.1967±0.0038	0.0623±0.0023	0.3640±0.0026	0.0317±0.0023	0.0023±0.0009
K-9	0.0220±0.0026	0.0680±0.0029	0.8097±0.0052	0.5130±0.0087	0.0857±0.0035	1.8213±0.0064
K-12	0.0430±0.0023	0.3363±0.0033	0.2870±0.0023	0.0051±0.0004	0.1343±0.0041	0.4557±0.0091
K-16	0.0883±0.0043	0.9167±0.0035	0.3340±0.0017	0.6760±0.0061	0.1733±0.0050	0.7120±0.0040
D-3	0.1543±0.0024	3.7673±0.0055	0.1620±0.0032	2.1987±0.0034	0.2507±0.0018	1.4467±0.2467
D-6	0.1487±0.0043	3.6140±0.0032	0.9563±0.0041	1.0943±0.0029	0.3577±0.0029	0.7607±0.0015
D-9	0.1527±0.0026	3.6777±0.0032	0.5767±0.0043	1.2490±0.0032	0.0710±0.0017	0.0061±0.0005
D-12	0.1570±0.0021	2.3010±0.0032	0.8937±0.0041	0.3510±0.0038	0.7627±0.0020	0.3170±0.0026
D-16	0.1607±0.0035	2.7010±0.0044	3.4257±0.0041	1.5840±0.0021	0.4683±0.0033	0.2613±0.0032

*K – control samples without detergent (K3–K16); D – samples with addition of 0.3% (w/w) detergent (D3–D16); results were expressed as means ± standard error of mean

Table 2. Mann-Whitney U Test for comparison of *alkaline invertase* and *alkaline phosphatase* activity between control samples and samples with addition of detergent.

	Ranks				Test Statistics		
	Group	N	Means (IU ml^{-1})	Sum of Ranks	Mann-Whitney U	Z	p-level*
Alkaline invertase activity	*M. plumbeus*						
	Control	15	0.0378	120.00	0.00	-4.66628	0.000003
	Detergent	15	0.1547	345.00			
	A. niger						
	Control	15	1.0103	138.00	18.00	-3.91968	0.000089
	Detergent	15	3.2122	327.00			
	T. harzianum						
	Control	15	0.3068	156.00	36.00	-3.17307	0.001508
	Detergent	15	1.2029	309.00			
Alkaline phosphatase activity	*M. plumbeus*						
	Control	15	0.3391	147.00	27.00	-3.54637	0.000391
	Detergent	15	1.2954	318.00			
	A. niger						
	Control	15	0.1059	156.00	36.00	-3.17307	0.001508
	Detergent	15	0.3821	309.00			
	T. harzianum						
	Control	15	0.6917	243.00	102.00	0.435520	0.663186
	Detergent	15	0.5584	222.00			

*Values of $p < 0.05$ were considered statistically significant

Activity of *alkaline phosphatase* of investigated fungi in control medium and in medium containing detergent is also presented in Table 1. In control medium, activity of alkaline phosphatase of *M. plumbeus* (Table 1) was significantly increased in period of mycelium growth (3rd to 9th day) after which its sudden decrease appeared to negligible value (0.0051 IU ml^{-1}) measured on the 12th day. In medium with detergent enzyme activity varied from maximum value on the 3rd day of the experiment (2.1987 IU ml^{-1}) to minimum value on the 12th day of experiment (0.3510 IU ml^{-1}) after which it increased till 16th day of the experiment (1.5840 IU ml^{-1}).

Activity of *alkaline phosphatase* of *A. niger* in control medium decreased from the 3rd to 6th day. It was totally inhibited by 6th day. Enzyme maximum of *A. niger* in control medium was reached on the last day of the experiment (0.1733 IU ml^{-1}). In medium with detergent, the enzyme activity has been increased during development of fungi mycelium. Significant decreasing of enzyme activity was recorded on 9th day (0.0710 IU ml^{-1}), while the highest increase in activity was recorded on the 12th day (0.7627 IU ml^{-1}). Presence of detergent in medium stimulated activity of *alkaline phosphatase* compared to control nutritive medium.

Table 3. Kruskal-Wallis ANOVA by Ranks for comparison of *alkaline invertase* and *alkaline phosphatase* activity among fungi *M. plumbeus, A. niger* and *T. Harzianum.*

	Ranks				Test Statistics		
	Group	N	Means (IU ml^{-1})	Sum of Ranks	H(2)	Total N	p-level*
Alkaline invertase activity	Control samples						
	M. plumbeus	15	0.0378	164.00	21.24720	45	0.0000
	A. niger	15	1.0103	489.50			
	T. harzianum	15	0.3068	381.50			
	Samples with addition of detergent						
	M. plumbeus	15	0.1547	126.50	35.07609	45	0.0000
	A. niger	15	3.2122	552.00			
	T. harzianum	15	1.2029	356.50			
Alkaline phosphatase activity	Control samples						
	M. plumbeus	15	0.3391	369.00	9.857391	45	0.0072
	A. niger	15	0.1059	222.00			
	T. harzianum	15	0.6917	444.00			
	Samples with addition of detergent						
	M. plumbeus	15	1.2954	511.50	16.16232	45	0.0003
	A. niger	15	0.3821	251.00			
	T. harzianum	15	0.5584	272.50			

*Values of $p < 0.05$ were considered statistically significant

Activity of *alkaline phosphatase* of *T. harzianum* in control medium was totally inhibited on the 6th day, after which an increase was recorded. Maximum of enzyme activity was measured on the 9th day (1.8213 IU ml^{-1}). However, in the stage of autolysis (12th day), the activity was near to the value recorded on the 3rd day (0.4673 IU ml^{-1}). In medium with detergent, the enzyme activity was changeable. Enzyme maximum was recorded on the 3rd day (1.4461 IU ml^{-1}), after which a decrease of enzyme activity was recorded. It was inhibited on the 9th day and reached its minimum value (0.0061 IU ml^{-1}).

CONCLUSION

Effect of detergent on *alkaline invertase* and *alkaline phosphatase* activity of *Mucor plumbeus*, *Aspergillus niger* and *Trichoderma harzianum* was significantly different during experimental period of 16 days. In control medium, the lowest activity of *alkaline invertase* was recorded in *M. plumbeus* during the entire experimental period while maximum of enzyme activity was reached in *A. niger* (3rd day) and *T. harzianum* (16th day). In the medium containing detergent, activity of *alkaline invertase* was stimulated or inhibited depending on fungal species. The highest stimulating effect of detergent was related to activity of *alkaline invertase* of *A. niger* (3rd day) and *T. harzianum* (16th day). Inhibitory effect of detergent was recorded for enzyme activity of *M. plumbeus* (during the entire experiment period) and *T. harzianum* (3rd day). In control medium, the activity of *alkaline phosphatase* was the lowest in *T. harzianum* (6th day), but the same fungus reached the highest enzyme activity on 9th day. Detergent had stimulatory or inhibitory effect on this enzyme, mostly depending on fungal species. The strongest inhibitory effect of detergent was recorded in enzyme activity of *T. harzianum* (9th day) and *A. niger* (9th day). Stimulatory effect of detergent was recorded for enzyme activity of *M. plumbeus* (3rd day) and *T. harzianum* (3rd day).

Obtained results are important for possible practical application of mentioned fungus species in processes of waste

water purification and production of enzymes for use in chemical industry. Based on comparison of enzyme activity of different fungi in detergent containing media we can recommend *M. plumbeus* for waste water treatment due to high *alkaline phosphatase* activity as well as *A. niger* due to high *alkaline invertase* activity.

REFERENCES

Abu-Zreig, M., Rudra, R. P., & Dickinson, W. T. 2003. Effect of Application of Surfactants on Hydraulic Properties of Soils. Biosystems Engineering, 84(3), pp. 363-372. doi:10.1016/s1537-5110(02)00244-1

Ashokkumar, B., Kayalvizhi, N., & Gunasekaran, P. 2001. Optimization of media for β-fructofuranosidase production by Aspergillus niger in submerged and solid state fermentation. Process Biochemistry, 37(4), pp. 331-338. doi:10.1016/s0032-9592(01)00204-7

Brookman, J. L., & Denning, D. W. 2000. Molecular genetics in Aspergillus fumigatus. Current Opinion in Microbiology, 3(5), pp. 468-474. doi:10.1016/s1369-5274(00)00124-7

Buvaneswari, S., Damodarkumar, S., & Murugesan, S. 2013. Bioremediation studies on sugar-mill effluent by selected fungal species. International Journal of Current Microbiology and Applied Sciences, 2, pp. 50-58.

Cavalli, L. 2004. Environmental impact, surfactant science series. Part B. In U. Zoller Ed., Handbook of Detergents. New York: Marcel Dekker, 121, pp. 373-427.

Chaturvedi, V., & Kumar, A. 2010. Toxicity of sodium dodecyl sulfates in fishes and animals. International Journal of Applied Biology and Pharmaceutical Technology, 1, pp. 630-633.

Crewther, W., & Lennox, F. 1953. Enzymes of Aspergillus Oryzae III. The Sequence of Appearance and Some Properties of the Enzymes Liberated During Growth. Australian Journal of Biological Sciences, 6(3), p. 410. doi:10.1071/bi9530410

Gillespie, J. M., Jermyn, M. A., & Woods, E. F. 1952. Multiple Nature of the Enzymes of Aspergillus Oryzæ and of Horse-Radish: Enzymes of Aspergillus oryzae. Nature, 169(4299), pp. 487-488. doi:10.1038/169487a0

Guimarães, L. H. S., Somera, A. F., Terenzi, H. F., Polizeli, M. d. T. d., & Jorge, J. A. 2009. Production of β-fructofuranosidases by Aspergillus niveus using agroindustrial residues as carbon sources: Characterization of an intracellular enzyme accumulated in the presence of glucose. Process Biochemistry, 44(2), pp. 237-241. doi:10.1016/j.procbio.2008.10.011

Heinonen, J. K., & Lahti, R. J. 1981. A new and convenient colorimetric determination of inorganic orthophosphate and its application to the assay of inorganic pyrophosphatase. Analytical Biochemistry, 113(2), pp. 313-317. doi:10.1016/0003-2697(81)90082-8

Kamiya, M., Judson, H., Okazaki, Y., Kusakabe, M., Muramatsu, M., Takada, S., Takagi, N., Arima, T., Wake, N., Kamimura, K., Satomura, K., Hermann, R., Bonthron, D. T. & Hayashizaki, Y. 2000. The cell cycle control gene ZAC/PLAGL1 is imprinted--a strong candidate gene for transient neonatal diabetes. Human Molecular Genetics, 9(3), pp. 453-460. doi:10.1093/hmg/9.3.453

Koffi, D., Faule, B., Gonnety, J., Bédikou, M., Kouamé, L., Zoro, I., & Niamké, S. 2010. Biochemical characterization of phosphatase, β-galactosidase and α-mannosidase activities of seeds of an oleaginous cucurbit: Lagenaria siceraria (Molina) Standl blocky-fruited cultivar. Sciences and Nature, 7(2). doi:10.4314/scinat.v7i2.59966

Kumar, M., Trivedi, S. P., Misra, A., & Sharma, S. 2007. Histopathological changes in testis of the freshwater fish Heteropneustes fossilis (Bloch) expos to linear alkyl benzene sulphonate (LAS). Journal of Environmental Bioogy, 28, pp. 679-684.

Ojo, O. A., & Oso, B. A. 2008. Isolation and characterization of synthetic detergent-degraders from waste water. African Journal of Biotechnology, 7, pp. 3753-3760.

Poonawalla, F. M., Patel, K. L., & Iyengar, M. R. S. 1965. Invertase production by Penicillium chrysogenum and other fungi in submerged fermentation. Applied and Environmental Microbiology, 13, pp. 749-754.

Raimbault, M. 1981. Fermentation en milieu solide: Croissance de champignons filamenteux sur substrats amylacés. Paris: Orstom. Série Travaux et Documents.

Raimbault, M. 1998. General and microbiological aspects of solid substrate fermentation. Electronic Journal of Biotechnology, 1(2), pp. 174-188. doi:10.2225/vol1-issue3-fulltext-9

Raper, K. B., & Fennell, D. I. 1965. The genus Aspergillus. Baltimore: William and Wilkins.

Saucedo-Castañeda, G., Lonsane, B. K., Navarro, J. M., Rogssos, S., & Raimbault, M. 1992. Potential of using a simple fermenter for biomass built up, starch hydrolysis and ethanol production: Solid state fermentation system involving Schwanniomyces castellii. Applied Biochemistry and Biotechnology, 36(1), pp. 47-61. doi:10.1007/bf02950774

Saucedo-Castaneda, G., Lonsane, B. K., Krishnaiah, M. M., Navarro, J. M., Roussos, S., & M. Raimbault, 1992. Maintenance of heat and water balances as a scale-up criterion for the production of ethanol by schwanniomyces castellii in a solid state fermentation system. Process Biochemistry, 27(2), pp. 97-107. doi:10.1016/0032-9592(92)80016-v

Schmidt, G., Seraidarian, K., Greenbaum, L. M., Hickey, M. D., & Thannhauser, S. J. 1956. The effects of certain nutritional conditions on the formation of purines and of ribonucleic acid in baker's yeast. Biochimica et Biophysica Acta, 20, pp. 135-149. doi:10.1016/0006-3002(56)90272-4

Stojanović, J. 2007. Praktikum iz biohemije. Kragujevac: Prirodno-matematički fakultet.

Stojanović, J., Jakovljević, V., Matović, I., Mijušković, Z., & Nedeljković, T. 2010. The influence of detergents, sodium tripoly-phosphates and ethoxyled oleyl-cetyl alcohol on metabolism of the fungi Penicillium verrucosum peyronel. Acta veterinaria, 60(1), pp. 67-77. doi:10.2298/avb1001067s

Sumner, J. B., & Howell, S. F. 1935. A method for determination of saccharase activity. The Journal of Biological Chemistry, 108, pp. 51-54.

Vainstein, M. H., & Peberdy, J. F. 1991. Regulation of invertase in Aspergillus nidulans: effect of different carbon sources. Journal of General Microbiology, 137(2), pp. 315-321. doi:10.1099/00221287-137-2-315

Ying, G. 2006. Fate, behavior and effects of surfactants and their degradation products in the environment. Environment International, 32(3), pp. 417-431. doi:10.1016/j.envint.2005.07.004

UNIVERSITY THOUGHT
Publication in Natural Sciences, Vol. 10, No. 1, 2020, pp. 20-25.
DOI: https://doi.org/10.5937/univtho10-25574
Original Scientific Paper

PHENOLIC AND FLAVONOID CONTENT AND ANTIOXIDANT EVALUATION OF HAWTHORN (*Crataegus monogyna* Jacq.) FRUITS AND LEAVES EXTRACTS

VIDOSLAV DEKIĆ[1*], NOVICA RISTIĆ[1], BILJANA DEKIĆ[1], MILENKO RISTIĆ[1]

[1]Faculty of Science and Mathematics, University of Priština, Kosovska Mitrovica, Serbia

ABSTRACT

Considering the facts that phenolic compounds have many pharmacological effects, as well that antioxidant effect of phenolic compounds has been proven in various experimental systems, aim of this research was to determine the content of total phenols and flavonoids and evaluation of antioxidant activity in ethanol, ethyl acetate and chloroform extracts of fruits and leaves of the plant species *Crataegus monogya* Jacq., which is known as common hawthorn. The content of total phenolic compounds was determined by the spectrophotometric method using Folin-Ciocalteu reagent and the content of flavonoids was determined using aluminum chloride. *In vitro* evaluation of the antioxidant activity of tested extracts was performed using the DPPH method. The amount of total phenolics was varied in fruits and leaves extracts and ranged from 38.05 ± 0.18 to 365.11 ± 0.32 mg GAE/g dw. Ethyl acetate extract of hawthorn leaves showed the highest content of phenolic compounds (365.11 ± 0.32 mg GAE/g dw). The flavonoid content was different in the fruits and leaves of hawthorn and ranged from 21.11 ± 0.11 to 122.98 ± 0.21 mg RU/g dw, whereby the highest content of flavonoids was found in ethyl acetate extract of leaves (122.98 ± 0.21 mg RU/g dw). Antioxidant activity of the tested extracts was expressed as IC_{50} values and ranged from 5.53 ± 0.08 to 293.51 ± 0.28 μg/ml. Ethyl acetate extract of hawthorn leaves showed considerable antioxidant potential (IC_{50} = 5.53 ± 0.08 μg/ml). Based on the obtained results, a significant correlation was found between the antioxidant activity and the content of total phenolics and flavonoids compounds in hawthorn fruits and leaves extracts.

Keywords: Phenolics, Flavonoids, *Crataegus monogyna*, Extracts, Antioxidant activity.

INTRODUCTION

The connection between man and plants dates back thousands of years ago. Throughout history, plants have gained increasing importance as a source of biologically active substances. It is known that the use of medicinal herbs is a significant factor that improves the general health of people, and the study of its positive impact is more and more the subject of current research. This property is explained primarily by the presence of secondary metabolites in plants, which can exhibit different biological activities. Phenolic compounds are widespread products of secondary metabolism and the antioxidant activity of plant extracts is mainly related to their presence (Kaur & Kapoor, 2008). The most common phenolic compounds are phenolic acids (benzoic and cinnamic acid derivatives), flavonoids, stilbenes, lignans, coumarins and tannins. Due to their pronounced antioxidant activity, phenolic compounds have the ability to directly bind ("catch") free radicals (Kancheva, 2009; Rice-Evans et al., 1996; Kirakosyan et al., 2003).

The genus *Crataegus*, commonly known as hawthorn, comprises about 200 species (Dönmez, 2004). It is widely distributed in the temperate and subtropical regions of the Northern hemisphere, most in North America and somewhat less in Europe and Asia. This genus is characterized by deciduous, usually thorny shrubs or low trees about 5-15m high. The lifespan of hawthorn can be over 200 years. Today more than 20 species of hawthorn are used in folk medicine and some of them are found in the pharmacopeias of many countries (Chang et al., 2002). Leaves, flowers, and fruits are used as an herbal drug. The flowers are collected early in the spring when are completely developed, leaves are collected during the summer, and the fruits when are ripe, mid in the fall. Hawthorn flower and leaf contain, as active principles, complexes of flavonoid heterosides in the amount of 1-2%. The fruits contain less flavonoids (about 0.1%) but there are more sugars, organic acids, carotenoids, and vitamin C. Hawthorn is considered one of the most valuable and effective cardio protector plants for the heart. It has been observed that extracts of fruits, leaves, and flowers of hawthorn have a beneficial effect on coronary artery flow, contraction of the heart muscle and following this they are used as powerful cardiotonic, hypotensive and antiaritmic agents (Alirezalu et al., 2018; Long et al., 2006; Degenring et al., 2003). In some nations, certain species of the genus *Crataegus* are used in the treatment of digestive problems, dyspnea and kidney stones (Rigelsky & Sweet, 2002). Hawthorn extracts also show a wide range of antioxidant, antimicrobial, antifungal, anti-inflammatory and antiviral activities (García-Mateos et al., 2013; Orhan et al., 2007; Tadić et al., 2008; Benli et al., 2008).

Crataegus monogyna Jacq. (common hawthorn) is a deciduous shrub or low tree up to 10 m high. This species is most

* Corresponding author: vidoslav.dekic@pr.ac.rs

abundant in the zone of a deciduous forest at 900-1200 m above sea level. In many nations of the world, common hawthorn has a very wide and varied use. Thus, hawthorn fruits are used in culinary, mostly for making jams and drinks (Chang et al., 2002). Fruits and leaves of hawthorn have a mild diuretic, antispasmodic and cardiotonic effect (Barros et al., 2011; Edwards et al., 2012; Nabavi et al., 2015; Fakir et al., 2009). Hawthorn extracts have proved to be beneficial to the nervous system and are used against migraines, memory loss and calming, thus on that way improving overall condition of the organism (Elango & Devaraj, 2010; Zhang et al., 2004; Novais et al., 2004). Due to the presence of different types of bioactive components, the extracts of leaves, flowers, and fruits of this plant species exhibit extraordinary antioxidant activity (Keser et al., 2014; Konyalioglu et al., 2017; Özcan et al., 2005).

In light of our previous work (Radulović et al., 2020; Živić et al., 2019; Dekić et al., 2019) which is regarding to the pharmacological and antioxidant effects of many plant species from area of Serbia, the aim of this study was to determine the content of phenols and flavonoids and evaluate the antioxidant activity of fruits and leaves extracts of plant species *Crataegus monogyna* Jacq.

EXPERIMENTAL

Materials and methods

Chemicals and reagents

The solvents (HPLC grade) used in the experimental work were purchased from J.T. Baker (USA) and Merk (Germany) while gallic acid, rutin, and ascorbic acid were purchased from Acros Organics (Belgium). Also, 2,2-diphenyl-1-picrylhydrazyl (DPPH), potassium acetate (CH_3COOK) and Folin-Ciocalteu reagent were purchased from Sigma-Aldrich (USA). All other chemicals used in this research were from Merck (Germany) and Fisher Scientific (USA).

UV-Vis spectroscopy.

All absorbance was measured using a LLG UniSPEC 2 spectrophotometer

Plant material

The fruits and leaves of the plant species *Crataegus monogyna* Jacq. were collected from the area of Šara mountain at 1150 m above sea level, in september 2018. After 12 days of drying in the shade, the plant material was packed in dark glass bottles and stored in a dry and dark place until analyzed.

Extraction

About 8 g of dried and well grind fruits and leaves of hawthorn were extracted in a Soxhlet apparatus, whereby used 100 ml of solvents with different polarity: ethanol, ethyl acetate and chloroform. The extraction was performed for 6 hours at the boiling point of the solvent. After the expiration of the estimated period time, the extracts were evaporated to dryness on a rotary vacuum evaporator at a temperature of 35 °C. The dry extracts were then packed in vials and kept in the refrigerator at 5 ºC until use.

Determination of total phenolic content

The total phenolic content of the tested hawthorn fruits and leaf extracts was determined spectrophotometrically with Folin-Ciocalteu reagent according to the previously described method (Singleton et al., 1999), with slight modifications. The dry extracts were dissolved in methanol (1000 μg/ml) and used during the analysis. Briefly, 1.5 ml of Folin-Ciocalteu reagent (diluted 10 times with distilled water) was added to a test tube with 0.5 ml of extracts and then was shaking. After 2 minutes, 2 ml of 7.5% Na_2CO_3 solution was added, test tubes were slightly shaken and then incubated at 32 °C for 90 minutes in a dark place. The same procedure was repeated for gallic acid, which was used to construct the calibration curve, and it was constructed based on different concentrations of gallic acid solution (1.95-250 μg/ml). The absorbance was measured at 765 nm relative to the blank (1.5 ml of Folin-Ciocalteu reagent and 2 ml of 7.5% Na_2CO_3 was added in 0.5 ml of methanol) on LLG UniSPEC 2 spectrophotometer. The total phenolic content of the samples was calculated from the calibration curve equation and results were presented as mg of gallic acid equivalents per g of dried weight extracts (mg GAE/g dw).

Determination of total flavonoid content

The total flavonoid content of extracts was determined spectrophotometrically, using a method based on the formation of complexes between the flavonoids and aluminum (Chang et al., 2002). In 0.5 ml of extracts (1000 μg/ml) was gradually added 1 ml of methanol, 80 μl of 10% $AlCl_3$ solution, 80 μl of 1 M CH_3COOK solution and 2.5 mL of distilled water. The same procedure was repeated for the standard solution of rutin (3.91-125 μg/ml). After incubation at room temperature for 50 minutes, the absorbance was measured at 415 nm on a spectrophotometer. The blank contained all reagents, except tested extracts, which were replaced with 0.5 ml of methanol. The total flavonoid content was calculated from the calibration curve equation and is expressed as mg of rutin equivalents per g of dried weight extract (mg RU/g dw).

DPPH assay

For the determination of the antioxidant activity of tested extracts the DPPH (2,2-diphenyl-1-picrylhydrazyl) test was used, according to the previously described method (Braca et al., 2001) with small modifications. The procedure was as follows: 0.8 ml of methanolic solution of extracts (3.91-1000 μg/ml) was placed in a test tube and mixed with 2 ml of 0.004% DPPH methanolic solution. The test tubes were allowed to stand for 45 minutes in a dark place and at room temperature. The blank contained 0.8 ml

of methanol instead of extracts. The same procedure was repeated for the standard solution of ascorbic acid (1.96-125 μg/ml), which in our case was used as a measure of comparison of efficacy with the tested extracts (positive control). The absorbance was measured at 517 nm on a spectrophotometer. The inhibition of DPPH radicals in the presence of tested samples is calculated by the formula and expressed as a percentage of inhibition (%): inhibition (%)= ((Ab-As)/Ab)·100, Ab-absorbance of blank (2 ml of DPPH and 0.8 ml of methanol), As-absorbance of the methanolic extracts solution (2 ml of DPPH and 0.8 ml of extracts solution). The results are expressed as IC_{50} values in μg/mL (IC_{50} value represents the concentration of tested extracts and/or standard antioxidant which inhibited 50% of the initial concentration of DPPH molecules).

Statistical analysis

Statistical and numerical analyzes were performed using GraphPad Prism ver. 7.00 and MS Office Excel (2016) software package. All results are presented as the mean of three repetitions (n = 3 ± standard deviation).

RESULTS AND DISCUSSION

Yields (%), total phenolics and total flavonoids content

Based on the obtained results (Table 1) the yields of isolated hawthorn fruits extracts ranged from 2.03 to 24.51%, while for leaves extracts ranged from 5.15 to 40.69% (results are expressed in percentages and refer to 100 g of dry plant material).

Ethanol (ethanolic hawthorn leaf extract) was given the highest yield during the extraction of plant material as the most polar solvent (40.69%), while the yield of a chloroform extract (chloroform hawthorn fruit extract) was the lowest (2.03%).

Table 1. Percentage yields (%) of *Crataegus monogyna* Jacq. fruits and leaves extracts.

Extract	Percentage yield % (w/w)	
	Fruits	Leaves
Ethanol	24.51	40.69
Ethyl acetate	4.32	9.02
Chloroform	2.03	5.15

The concentration of total phenolics compounds in the tested extracts was determined spectrophotometrically (the method is based on the measurement of the reducing capacity of phenolics compounds) and the values were calculated based on the equation obtained from the calibration curve. The total phenolics content of hawthorn fruits and leaves extracts ranged from 38.05 ± 0.18 to 152.87 ± 0.11 mg GAE/g dw for fruits and from 83.36 ± 0.21 to 365.11 ± 0.32 mg GAE/g dw for leaves extracts (Table 2). Based on the obtained results it can be concluded that the total content of phenolics compounds is higher for hawthorn leaves extracts than for fruits extracts. Ethyl acetate extract of leaves showed the highest concentration of phenolics compounds with a value of 365.11 ± 0.32 mg GAE/g dw, while the lowest concentration of phenolics showed chloroform extract of fruits (38.05 ± 0.18 mg GAE/g dw). In the ethanol extracts of fruits and leaves the content of phenolics compounds was 101.01 ± 0.12 mg GAE/g dw and 188.21 ± 0.18 mg GAE/g dw, respectively.

Table 2. Content of total phenolics and flavonoids compounds of *Crataegus monogyna* Jacq. fruits and leaves extracts.

Extract	Total phenolics (mg GAE/g dw)		Total flavonoids (mg RU/g dw)	
	Fruits	Leaves	Fruits	Leaves
Ethanol	101.01 ± 0.12	188.21 ± 0.18	48.27 ± 0.26	89.78 ± 0.13
Ethyl acetate	152.87 ± 0.11	365.11 ± 0.32	58.81 ± 0.12	122.98 ± 0.21
Chloroform	38.05 ± 0.18	83.36 ± 0.21	21.11 ± 0.11	36.01 ± 0.16

According to numerous studies, the total phenolics content of many plant species depends on the type of extraction as well as the polarity of the used solvents (Mohsen & Ammar, 2008; Zhou &Yu, 2004). The content of phenolics compounds, in our case, was highest in ethyl acetate extracts of fruits and leaves and the lowest in chloroform extracts. Base on that the content of phenolics compounds decreases in the order: ethyl acetate > ethanol > chloroform extracts. External factors such as light, temperature, and presence of nutrients in the soil have a significant impact on the composition and amount of phenolics compounds.

Determination of total flavonoids content is based on the property of flavonoids to give a complex with metal ions (such as Al^{3+}) whereby chelates are formed and occur a displacement of absorption bands by about 50 nm toward higher wavelengths - bathochromic displacement (Silva et al., 2015). The concentration of total flavonoids in the tested hawthorn fruits extracts ranged from 21.11 ± 0.11 to 58.81 ± 0.12 mg RU/g dw and in leaves extracts from 36.01 ± 0.16 to 122.98 ± 0.21 mg RU/g dw (Table 2). Hawthorn a leaf extracts contains higher amounts of flavonoids than fruit extracts. The highest concentration of flavonoids was in ethyl acetate hawthorn leaves and fruits extracts (122.98 ± 0.21 and 58.81 ± 0.12 mg RU/g dw, respectively), while chloroform leaves and fruits extracts showed

lowest amount of flavonoids (36.01 ± 0.16 and 21.11 ± 0.11 mg RU/g dw, respectively) Based on the obtained results the flavonoids content decreases in the order: ethyl acetate > ethanol > chloroform extracts. All tested hawthorn fruit and leaf extracts contain a significantly lower amount of flavonoids than the phenolics compounds.

DPPH assay

The antioxidant activity of the extracts obtained from hawthorn fruits and leaves was determined by the DPPH assay, and the results of the analyzes were expressed as IC_{50} values in μg/mL, (Figure 1). The lower IC_{50} values correspond to the stronger antioxidant activity of the extracts.

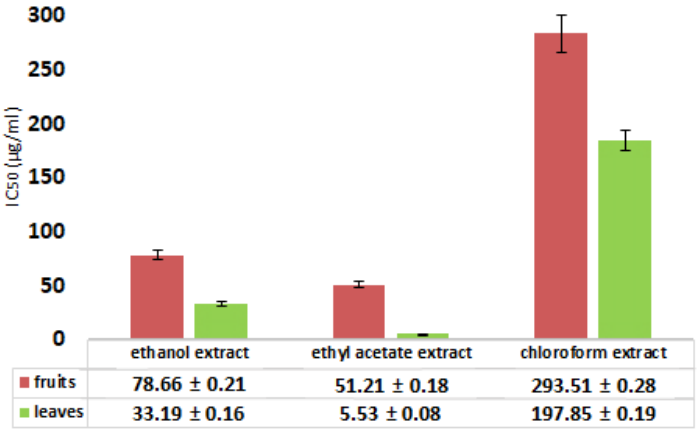

Figure 1. Free radical scavenging activity of *Crataegus monogyna* Jacq. fruit and leaf extracts expressed as IC_{50} values (μg/ml) measured by DPPH method. Ascorbic acid was used as positive control (IC_{50} = 3.12 ± 0.14 μg/ml).

All tested extracts showed strong and significant antioxidant activity. Hawthorn leaves extracts showed stronger antioxidant activity compared to hawthorn fruit extracts. Ethyl acetate extracts of fruits and leaves which neutralize 50% of DPPH radicals at concentrations of 51.21 ± 0.18 μg/ml and 5.53 ± 0.08 μg/ml, respectively, showed the highest antioxidant activity. Also, ethanol extracts (IC_{50} = 78.66 ± 0.21 μg/ml for fruits and IC_{50} = 33.19 ± 0.16 μg/ml for leaves extracts) showed a significant and stronger inhibition of DPPH radicals compared to chloroform extracts, which showed lower antioxidant activity (IC_{50} = 293.51 ± 0.28 μg/ml for fruits and IC_{50} = 197.85 ± 0.19 μg/ml for leaves extracts). The strong antioxidant activity of all tested extracts is associated with the high content of phenolics and flavonoids compounds and indicates that these compounds contribute to the antioxidant activity of hawthorn fruits and leaves extracts.

Correlation analysis

The correlation between the antioxidant activity of the hawthorn fruits and leaves extracts and the content of total phenolics and total flavonoids compounds is showed on Figures 2 and 3. Based on the obtained results, a significant degree of correlation between total phenolics content and antioxidant activity ($r = -0.934$ for fruit extracts and $r = -0.859$ for leaves extracts) indicates that the antioxidant properties of the tested extracts originate from the presence of phenolics compounds in the extracts, especially in the case of hawthorn fruits.

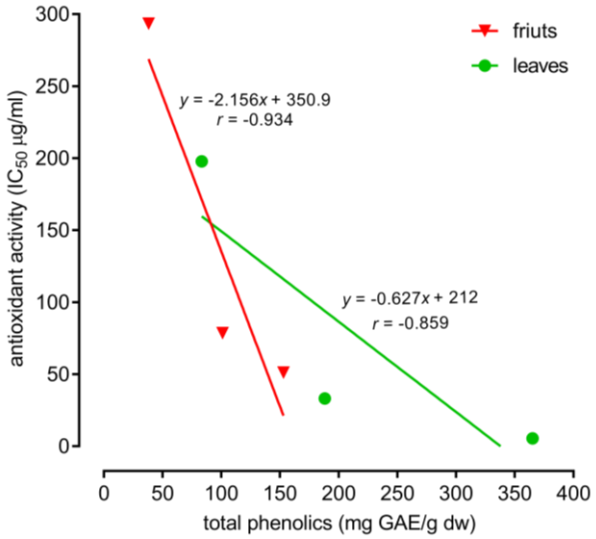

Figure 2. Linear correlation of total phenolics compounds and antioxidant activity of hawthorn fruits and leaves extracts.

An even better and more significant correlation was found between the antioxidant activities of hawthorn fruits and leaves extracts and total flavonoids content. A high degree of correlation in fruit extracts (r = -0.968) and leaves (r = -0.987) indicates that the presence of flavonoids compounds is crucial for the pronounced antioxidant activity of the tested extracts.

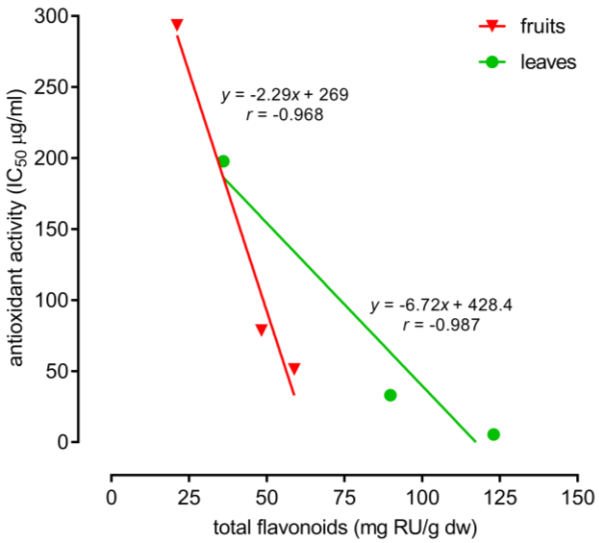

Figure 3. Linear correlation of total flavonoids compounds and antioxidant activity of hawthorn fruits and leaves extracts.

Since a lower IC_{50} value indicates a higher antioxidant activity, it can be concluded that as the content of phenolics and

flavonoids increases, the IC_{50} value decreases. Therefore, the linear correlation is negative and strong, and in our case is particularly pronounced between antioxidant activity and total flavonoids content in all tested extracts.

CONCLUSION

Hawthorn, as a plant species that has been long used in traditional medicine as well for medical purposes, also widely used in the process of preparing food and many drinks. The presented research showed that hawthorn extracts (*Crataegus monogyna* Jacq.) have a high content of phenolics and flavonoids compounds, which is directly reflected in their remarkable antioxidant potential. This is confirmed by a significant correlation between the total content of phenolics and flavonoids compounds and antioxidant activity. The results obtained in this study will influence on ethnopharmacological use of fruits and leaves of the plant species *Crataegus monogyna* Jacq., as well as their potential use in some branches of the pharmaceutical and food industry. This research further shows and classifies hawthorn as a natural source of antioxidants and enhances the picture about the use of hawthorn in traditional medicine for the treatment of many diseases.

ACKNOWLEDGMENTS

This research was financially supported by the Ministry of Education, Science and Technological Development of Serbia [Project No. 172061 and 45022].

REFERENCES

Alirezalu, A., Salehi, P., Ahmadi, N., Sonboli, A., Aceto, S., Maleki, H. H., & Ayyari, M. 2018. Flavonoids profile and antioxidant activity in flowers and leaves of hawthorn species (Crataegus spp.) from different regions of Iran. International Journal of Food Properties, 21(1), pp. 452-470. doi: 10.1080/10942912.2018.1446146

Barros, L., Carvalho, A. M., & Ferreira, I. C. 2011. Comparing the composition and bioactivity of Crataegus monogyn flowers and fruits used in folk medicine. Phytochemical Analysis, 22(2), pp.181–188. doi: 10.1002/pca.1267

Benli M., Yiğit, N., Geven, F., Güney, K., & Bingöl, Ü. 2008. Antimicrobial activity of endemic Crataegus tanacetifolia (Lam.) Pers and observation of the inhibition effect on bacterial cells. Cell Biochemistry and Function, 26(8), pp. 844-851. doi: 10.1002/cbf.1515

Braca, A., Tommasi, N. D., Bari, L. D., Pizza, C., Politi, M., & Morelli, I. 2001. Antioxidant Principles from Bauhinia terapotensis. Journal of Natural Products, 64(7), pp. 892-895. doi: 10.1021/np0100845

Chang, C., Yang, M., Wen, H., & Chern, J. 2002. Estimation of Total Flavonoid Content in Propolis by Two Complementary Colorimetric Methods. Journal of Food and Drug Analysis, 10(3), pp. 178-182.

Chang, Q., Zuo, Z., Harrison, F., & Chow, M. S. 2002. Hawthorn. The Journal of Clinical Pharmacology, 42(6), pp. 605-612. doi: 10.1177/00970002042006003

Degenring, F. H., Suter, A., Weber, M., & Saller, R. 2003. A randomised double blind placebo controlled clinical trial of a standardised extract of fresh Crataegus berries (Crataegisan®) in the treatment of patients with congestive heart failure NYHA II. Phytomedicine, 10(5), pp. 363-369. doi: 10.1078/0944-7113-00312

Dekić, B. R., Ristić, M. N., Mladenović, M. Z., Dekić, V. S., Ristić, N. R., Ranđelović, V., & Radulović, N. S. 2019. Diethyl-Ether Flower Washings of Dianthus cruentus Griseb. (Caryophyllaceae): Derivatization Reactions Leading to the Identification of New Wax Constituents. Chemistry & Biodiversity, 16(7): e1900153. doi: 10.1002/cbdv.201900153

Dönmez, A. 2004. The Genus Crataegus L. (Rosaceae) with Special Reference to Hybridisation and Biodiversity in Turkey. Turkish Journal of Botany, 28(1), pp. 29-37.

Edwards, J. E., Brown, P. N., Talent, N., Dickinson, T. A., & Shipley, P. R. 2012. A review of the chemistry of the genus Crataegus. Phytochemistry, 79, pp. 5–26. doi: 10.1016/j.phytochem.2012.04.006

Elango, C., & Devaraj, S. N. 2010. Immunomodulatory effect of Hawthorn extract in an experimental stroke model. Journal of Neuroinflammation, 7(1): 97. doi: 10.1186/1742-2094-7-97

Fakir, H., Korkmaz, M., & Güller, B. 2009. Medicinal plant diversity of western Mediterrenean region in Turkey. Journal of Applied Biological. Science, 3(2), pp. 30–40.

García-Mateos, R., Ibarra-Estrada, E., & Nieto-Ángel, R. 2013. Antioxidant compounds in hawthorn fruits (Crataegus spp.) of Mexico. Revista Mexicana de Biodiversidad, 84(4), pp. 1298-1304. doi: 10.7550/rmb.35675

Kancheva, V. D. 2009. Phenolic antioxidants - radical-scavenging and chain-breaking activity: A comparative study. European Journal of Lipid Science and Technology, 111, pp. 1072- 1089. doi: 10.1002/ejlt.200900005

Kaur, C., & Kapoor, H. C. 2008. Antioxidants in fruits and vegetables-the millennium's health. International Journal of Food Science & Technology, 36(7), pp. 703-725. doi: 10.1111/j.1365-2621.2001.00513.x

Keser, S., Celik, S., Turkoglu, S., Yilmaz, Ö., & Turkoglu, I. 2014. The investigation of some bioactive compounds and antioxidant properties of hawthorn (Crataegus monogyna subsp. monogyna Jacq). Journal of Intercultural Ethnopharmacology, 3(2), pp. 51-55. doi:10.5455/jice.20140120103320

Kirakosyan, A., Seymour, E., Kaufman, P. B., Warber, S., Bolling, S., & Chang, S. C. 2003. Antioxidant Capacity of Polyphenolic Extracts from Leaves of Crataegus laevigata and Crataegus monogyna (Hawthorn) Subjected to Drought and Cold Stress. Journal of Agricultural and Food Chemistry, 51, pp. 3973-3976. doi: 10.1021/jf030096r

Konyalioglu, S., Cebe, E. G., & Aktar, S. 2017. P 113 - Antioxidant activity of Crataegus Monogyna L flowers. Free Radical Biology and Medicine, 108(1), S56. doi: 10.1016/j.freeradbiomed.2017.04.198.

Long, S. R., Carey, R. A., Crofoot, K. M., Proteau, P. J., & Filtz, T. M. 2006. Effect of hawthorn (Crataegus oxycantha) crude extract and chromatographic fractions on multiple activities

in a cultured cardiomyocyte assay. Phytomedicine, 13(9-10), pp. 643-650. doi: 10.1016/j.phymed.2006.01.005

Mohsen, S. M., & Ammar, A. S. M. 2008. Total phenolic contents and antioxidant activity of corn tassel extracts. Food Chemistry, 112(3), pp. 595-598. doi: 10.1016/j.foodchem.2008.06.014

Nabavi, S. F., Habtemariam, S., Ahmed, T., Sureda, A., Daglia, M., Sobarzo-Sánchez, E., & Nabavi, S. M. 2015. Polyphenolic Composition of Crataegus monogyna Jacq.: From Chemistry to Medical Applications. Nutrients, 7(9), pp. 7708-7728. doi: 10.3390/nu7095361.

Novais M. H., Santos, I., Mendes, S., & Pinto-Gomes, C. 2004. Studies on pharmaceutical ethnobotany in Arrabida Natural Park (Portugal). Journal of Ethnopharmacology, 93(2-3), pp.183-195. doi: 10.1016/j.jep.2004.02.015

Orhan, I., Özçelik, B., Kartal, M., Özdeveci, B., & Duman, H. 2007. HPLC Quantification of Vitexine-2′′-O-rhamnoside and Hyperoside in Three Crataegus Species and Their Antimicrobial and Antiviral Activities. Chromatographia, 66, pp. 153-157. doi: 10.1365/s10337-007-0283-x

Özcan, M., Hacıseferoğulları, H., Marakoglu, T., & Arslan, D. 2005. Hawthorn (Crataegus spp.) fruit: some physical and chemical properties. Journal of Food Engineering, 69 (4), pp. 409–413. doi: 10.1016/j.jfoodeng.2004.08.032

Radulović, N. S., Mladenović, M. Z., Ristić, M. N., Dekić, V. S., Dekić, B. R., & Ristić, N. R. 2020. A new longipinane ketone from Achillea abrotanoides (Vis.) Vis.: chemical transformation of the essential oil enables the identification of a minor constituent. Phytochemical Analysis, published online. doi: 10.1002/pca.2913

Rice-Evans, C. A., Miller, N. J., & Paganga, G. 1996. Structure-antioxidant activity relationship of flavonoids and phenolic acids. Free Radical Biology and Medicine, 20(7), pp. 933-956. doi: 10.1016/0891-5849(95)02227-9

Rigelsky, J. M., & Sweet, B. V. 2002. Hawthorn: Pharmacology and therapeutic uses. American Journal of Health-System Pharmcy, 59(5), pp. 417-422. doi: 10.1093/ajhp/59.5.417

Singleton, V. L., Orthofer, R., & Lamuela-Raventos, R. M. 1999. Analysis of total phenols and other oxidation substrates and antioxidants by means of Folin-Ciocalteu reagent. Methods in Enzymology, 299, pp. 152-178. doi: 10.1016/S0076-6879(99)99017-1

Tadić, V. M., Dobrić, S., Marković, G. M., Đorđević, S. M., Arsić, I. A., Menković, N. R., & Stević, T. 2008. Anti-inflammatory, Gastroprotective, Free-Radical-Scavenging, and Antimicrobial Activities of Hawthorn Berries Ethanol Extract. Journal of Agriculture and Food Chemistry, 56(17), pp. 7700–7709. doi: 10.1021/jf801668c

Zhang, D. L., Zhang, Y. T., Yin, J. J., & Zhao, B. L. 2004. Oral administration of Crataegus flavonoids protects against ischemia/reperfusion brain damage in gerbils. Journal of Neurochemistry, 90(1), pp. 211–219. doi: 10.1111/j.1471-4159.2004.02480.x

Zhou, K., & Yu, L. 2004. Effects of extraction solvent on wheat bran antioxidant activity estimation. LWT – Food Science and Technology, 37(7), pp. 717-721. doi: 10.1016/j.lwt.2004.02.008

Živić, N., Milošević, S., Dekić, V., Dekić, B., Ristić, N., Ristić, M., & Sretić, Lj. 2019. Phytochemical and antioxidant screening of some extracts of Juniperus communis L. and Juniperus oxycedrus L. Czech Journal of Food Sciences, 37(5), pp. 351-358. doi: 10.17221/28/2019-CJFS

UNIVERSITY THOUGHT
Publication in Natural Sciences, Vol. 10, No. 1, 2020, pp. 26-30.
DOI: https://doi.org/10.5937/univtho10-25898
Original Scientific Paper

SYNTHESIS AND SPECTROSCOPIC CHARACTERIZATION OF POLYNUCLEAR SILVER(I) COMPLEX WITH 2,2'-BIQUINOLINE

DEJAN M. GUREŠIĆ[1*], SONJA Ž. ĐURIĆ[2], TINA P. ANDREJEVIĆ[2], MIRJANA M. POPSAVIN[3], BILJANA Đ. GLIŠIĆ[2]

[1]Faculty of Technical Sciences, University of Priština, Kosovska Mitrovica, Serbia
[2]Department of Chemistry, Faculty of Science, University of Kragujevac, Kragujevac, Serbia
[3]Department of Chemistry, Biochemistry and Environmental Protection, Faculty of Sciences, University of Novi Sad, Novi Sad, Serbia

ABSTRACT

Polynuclear silver(I) complex, $[Ag(NO_3\text{-}O)(2,2'\text{-bq-}N,N')]_n$, was synthesized by the reaction of equimolar amount of silver(I) nitrate and 2,2'-biquinoline (2,2'-bq) in ethanol at room temperature. The characterization of the complex was established on the basis of elemental microanalysis, IR, NMR (^{1}H and ^{13}C) and UV-Vis spectroscopic techniques. The results of spectroscopic analyses revealed that in $[Ag(NO_3\text{-}O)(2,2'\text{-bq-}N,N')]_n$ complex, 2,2'-bq ligand behaves as a chelate, while the remaining coordination sites are occupied by the oxygen atoms of two nitrates.

Keywords: Silver(I) complexes, *N*-Heterocycles, Polynuclear complexes, Spectroscopy.

INTRODUCTION

Silver(I) complexes with aromatic nitrogen-containing heterocycles (*N*-heterocycles) have attracted a considerable attention in the field of pharmaceutical and supramolecular chemistry (Khlobystov et al., 2001; Medici et al., 2019). Thus, various silver(I) complexes with this type of ligands are known to exhibit remarkable antimicrobial activity against different Gram-positive and Gram-negative bacteria and fungal species, which are causative agents of many microbial infections (Nomiya et al., 2000; Rowan et al., 2006; Kalinowska-Lis et al., 2014; Kalinowska-Lis et al., 2015; Pettinari et al., 2011; Savić et al., 2016; Glišić et al., 2016; Savić et al., 2018; Andrejević et al., 2018; Pavić et al., 2019). Furthermore, silver(I) complexes with aromatic *N*-heterocycles have shown significant antiproliferative activity against different human tumor cell lines, being, in some cases, superior to the clinically used platinum(II) complexes (Banti et al., 2013).

The second important reason for investigation of silver(I) chemistry with aromatic *N*-heterocycles stems from the findings that the Ag(I) ion coordinated by these ligands is a favorable building block for coordination polymers, having potential applications for design of innovative materials, including liquid crystals (Khlobystov et al., 2001; Yeşilel et al., 2010; Pucci et al., 2011). In coordination polymers, Ag(I) ion can have coordination numbers between two and six, adopting various geometries, such as linear, bent, trigonal, T-shaped, tetrahedral, trigonal pyramidal and octahedral. Moreover, weak contacts, such as argentophilic Ag···Ag, Ag···π and Ag···solvent/counterion interactions, have significant influence on the structural properties of silver(I) coordination polymers in the solid state (Khlobystov et al., 2001; Fik et al., 2014).

In the design of silver(I) coordination polymers, various bridging and chelating aromatic *N*-heterocycles have been used. Among them, 2,2'-bipyridine (2,2'-bipy) and its derivatives have been a subject of research due to their coordination versatility which allowed the tuning of the topology, the supramolecular architectures and other features in a series of silver(I) complexes (Pucci et al., 2011; Bellusci et al., 2008; Bowmaker et al., 2005). Herein, 2,2'-biquinoline (2,2'-bq), which is a larger and more rigid π system than 2,2'-bipy, was used as a ligand for complexation to Ag(I) ion. This ligand has two nitrogen-donors and the two flexible quinoline moiety linked together by a single C–C bond, which allow its different coordination behaviour towards metal ions (Pucci et al., 2011). Considering this, the reaction of silver(I) nitrate with an equimolar amount of 2,2'-biquinoline (2,2'-bq) was performed and polynuclear silver(I) complex, $[Ag(NO_3\text{-}O)(2,2'\text{-bq-}N,N')]_n$, was isolated and characterized by spectroscopy (IR, ^{1}H and ^{13}C NMR and UV-Vis).

EXPERIMENTAL

Reagents

Silver(I) nitrate, 2,2'-biquinoline (2,2'-bq), ethanol, dimethylformamide (DMF) and deuterated dimethylformamide (DMF-d_7) were purchased from the Sigma-Aldrich Chemical Co. All the employed chemicals were of analytical reagent grade and used without further purification.

Measurements

Elemental microanalysis of the silver(I) complex for carbon, hydrogen and nitrogen was performed by the

*Corresponding author: dejan.guresic@pr.ac.rs

Microanalytical Laboratory, Faculty of Chemistry, University of Belgrade. All NMR spectra were recorded at 25 °C on a Bruker Avance III 400 MHz spectrometer (^{1}H at 400 MHz, ^{13}C at 101 MHz). 5 mg of 2,2'-bq and its silver(I) complex was dissolved in 0.6 mL of DMF-d_7 and transferred into a 5 mm NMR tube. Chemical shifts are expressed in ppm (δ / ppm) and scalar couplings are reported in Hertz (J / Hz). Chemical shifts were calibrated relative to those of the solvent. The IR spectra were recorded as KBr pellets on a Perkin-Elmer Spectrum One FT-IR spectrometer over the wavenumber range 4000 – 450 cm^{-1}. The UV-Vis spectra were recorded over the wavelenth range of 900 – 200 nm on a Shimadzu UV-1800 spectrophotometer after dissolving 2,2'-bq and its silver(I) complex in DMF. The concentration was $1.9 \cdot 10^{-5}$ M.

Synthesis of [Ag(NO$_3$-O)(2,2'-bq-N,N')]$_n$ complex

5.0 mL of ethanolic solution of $AgNO_3$ (1.0 mmol, 169.9 mg) was added dropwise to ethanolic solution (5.0 mL) of 2,2'-bq (1.0 mmol, 256.3 mg) with stirring at room temperature. The stirring was continued for 3 h in the dark at room temperature, and after that time, the final solution was left to slowly evaporate. After a while, the pale-yellow crystals of silver(I) complex were obtained. These crystals were filtered off and dried in the dark at room temperature. The yield was 73% (311.1 mg).

[Ag(NO$_3$-O)(2,2'-bq-N,N')]$_n$. Anal. Calcd. for $C_{18}H_{12}AgN_3O_3$ (MW 426.18): C, 50.73; H, 2.84; N, 9.86%. Found: C, 50.92; H, 2.89; N, 9.74%. ^{1}H NMR (400 MHz, DMF-d_7): δ = 7.56 - 7.66 (*m*, 4 H, H-6 and H-7), 8.09 (*dd*, 2 H, $J_{5,6}$ = 7.7 Hz, $J_{5,7}$ = 1.6 Hz, H-5), 8.16 (*dd*, 2 H, $J_{7,8}$ = 8.3 Hz, $J_{6,8}$ = 1.1 Hz, H-8), 8.83 (*d*, 2 H, $J_{3,4}$ = 8.7 Hz, H-4), 8.89 (*d*, 2 H, $J_{3,4}$ = 8.7 Hz, H-3). ^{13}C NMR (101 MHz, DMF-d_7): δ = 121.75 (C-3), 129.29 (C-5), 129.60 (C-6), 130.36 (C-4a), 130.93 (C-8), 132.70 (C-7), 141.06 (C-4), 147.43 (C-8a), 153.40 (C-2). IR (KBr, cm^{-1}): ~3000*w* (ν(C$_{ar}$–H)), 1594*m*, 1505*m* (ν(C$_{ar}$=C$_{ar}$) and ν(C$_{ar}$=N)), 1384*vs*, 1302*s* (ν_{as}(NO$_3$)), 1326 (ν(C–N)), 812*m*, 745*m* (γ(Car–H)). UV-Vis (DMF, λ_{max}, nm): 315.0 ($\varepsilon = 2.5 \cdot 10^4$ M^{-1}cm^{-1}), 326.0 ($\varepsilon = 2.9 \cdot 10^4$ M^{-1}cm^{-1}), 339.0 ($\varepsilon = 2.5 \cdot 10^4$ M^{-1}cm^{-1}), 355.0 ($\varepsilon = 3.8 \cdot 10^3$ M^{-1}cm^{-1}).

2,2'-bq (data given for comparative purposes). MW = 256.30. ^{1}H NMR (400 MHz, DMF-d_7): δ = 7.54 (*ddd*, 2 H, $J_{5,6}$ = 8.1 Hz, $J_{6,7}$ = 6.9 Hz, $J_{6,8}$ = 1.2 Hz, H-6), 7.72 (*ddd*, 2 H, $J_{7,8}$ = 8.4 Hz, $J_{6,7}$ = 6.9 Hz, $J_{5,7}$ = 1.4 Hz, H-7), 7.94 (*dd*, 2 H, $J_{5,6}$ = 8.1 Hz, $J_{5,7}$ = 1.1 Hz, H-5), 8.07 (*bd*, 2 H, $J_{7,8}$ = 8.4 Hz, H-8), 8.46 (*d*, 2 H, $J_{3,4}$ = 8.6 Hz, H-4), 8.73 (*d*, 2 H, $J_{3,4}$ = 8.6 Hz, H-3). ^{13}C NMR (101 MHz, DMF-d_7): δ = 119.83 (C-3), 128.29 (C-6), 128.99 (C-5), 129.53 (C-4a), 130.55 (C-8), 130.98 (C-7), 138.12 (C-4), 148.69 (C-8a), 156.72 (C-2). IR (KBr, cm^{-1}): ~3000*w* (ν(C$_{ar}$–H)), 1594*s*, 1497*m* (ν(C$_{ar}$=C$_{ar}$) and ν(C$_{ar}$=N)), 1327 (ν(C–N)), 829*vs*, 738*vs* (γ(Car–H)). UV-Vis (DMF, λ_{max}, nm): 315.0 ($\varepsilon = 3.6 \cdot 10^4$ M^{-1}cm^{-1}), 326.0 ($\varepsilon = 4.2 \cdot 10^4$ M^{-1}cm^{-1}), 339.0 ($\varepsilon = 3.3 \cdot 10^4$ M^{-1}cm^{-1}).

RESULTS AND DISCUSSION

Synthesis and structural features of [Ag(NO$_3$-O)(2,2'-bq-N,N')]$_n$ complex

Silver(I) complex with 2,2'-biquinoline (2,2'-bq) was synthesized according to the route presented in Figure 1. The reaction of $AgNO_3$ and 2,2'-bq in 1 : 1 mole ratio in ethanol at room temperature yielded polynuclear [Ag(NO$_3$-*O*)(2,2'-bq-*N,N'*)]$_n$ complex. The composition and structural formula of this silver(I) complex was consistent with elemental analysis, IR, solution NMR (^{1}H and ^{13}C) and UV-Vis spectroscopic results. We isolated the crystals of the complex suitable for X-ray analysis, however, the crystallographic results indicated that the crystal structure of [Ag(NO$_3$-*O*)(2,2'-bq-*N,N'*)]$_n$ was very similar to that for the complex obtained in the reaction of $AgNO_3$ and 2,2'-bq in acetonitrile (Bowmaker et al., 2005). Considering this, the crystal structure of polynuclear [Ag(NO$_3$-*O*)(2,2'-bq-*N,N'*)]$_n$ complex will not be discussed herein.

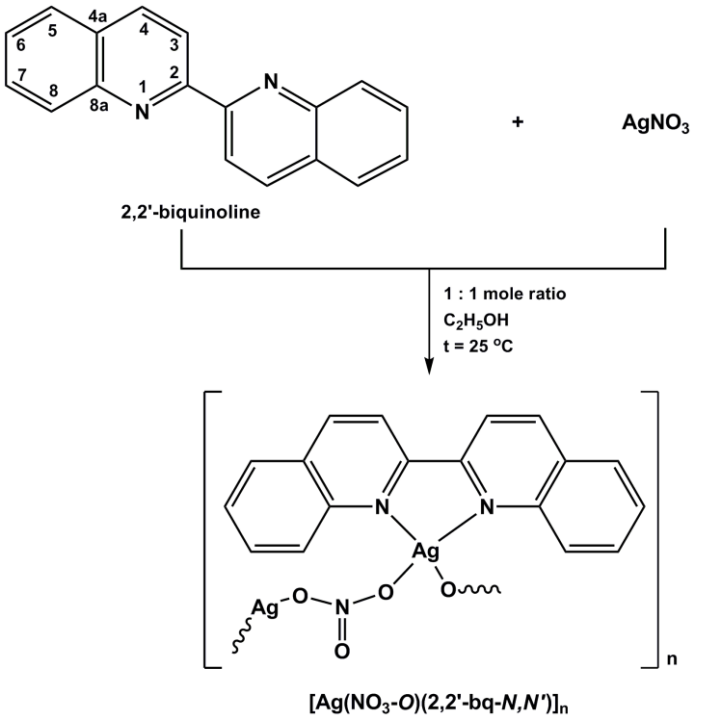

Figure 1. Schematic presentation of the synthesis of [Ag(NO$_3$-*O*)(2,2'-bq-*N,N'*)]$_n$ complex. Numbering scheme of carbon and nitrogen atoms in 2,2'-bq is in agreement with IUPAC recommendations for fused ring systems.

Spectroscopic characterization

The IR, NMR (^{1}H and ^{13}C), and UV-Vis spectroscopic data for 2,2'-bq and [Ag(NO$_3$-*O*)(2,2'-bq-*N,N'*)]$_n$ complex are listed in the Experimental section. In the IR spectrum of [Ag(NO$_3$-*O*)(2,2'-bq-*N,N'*)]$_n$ complex, two strong bands at 1384 and 1302 cm^{-1} due to the nitrate asymmetric stretching vibrations are observed (Table 1), indicating that nitrate is coordinated to Ag(I) ion (Potapov et al., 2015). The splitting of the nitrate asymmetric

stretching vibrations in the IR spectrum of $[Ag(NO_3\text{-}O)(2,2'\text{-bq-}N,N')]_n$ is in accordance with that observed in the spectra of polynuclear $[Ag(NO_3\text{-}O)(qz)]_n$ (qz is quinazoline) (Savić et al., 2016) and $[Ag(NO_3\text{-}O)(L\text{-}N4)_2]_n$ complexes, L is 1-benzyl-1*H*-tetrazole (bntz), 1-benzyl-1*H*-tetrazol-5-amine (bntza) and 1-(4-methoxybenzyl)-1*H*-tetrazol-5-amine (mbntza) (Andrejević et al., 2018), all containing nitrate as a bridging ligand between two Ag(I) ions (Table 1).

Table 1. IR asymmetric nitrate stretching frequencies (ν, cm^{-1}) of polynuclear silver(I) complexes containing nitrate as a bridging ligand

Silver(I) complex	$\nu_{asym}(NO_3^-)$	Ref.
$[Ag(NO_3\text{-}O)(2,2'\text{-bq-}N,N')]_n$	1384, 1302	This work
$[Ag(NO_3\text{-}O)(qz)]_n$	1377, 1352	Savić et al., 2016.
$[Ag(NO_3\text{-}O)(bntz\text{-}N4)_2]_n$	1384, 1354	Andrejević et al., 2018.
$[Ag(NO_3\text{-}O)(bntza\text{-}N4)_2]_n$	1384, 1364	Andrejević et al., 2018.
$[Ag(NO_3\text{-}O)(mbntza\text{-}N4)_2]_n$	1384, 1306	Andrejević et al., 2018.

Solution state ^1H and ^{13}C NMR spectra were measured in deuterated DMF in order to confirm the bidentate coordination of 2,2'-bq to the Ag(I) ion. The spectra of the $[Ag(NO_3\text{-}O)(2,2'\text{-bq-}N,N')]_n$ complex were compared with those for the corresponding ligand. Numbering scheme of carbon atoms in 2,2'-bq is presented in Figure 1. In the ^1H NMR spectrum of the silver(I) complex, there are noticeable downfield shifts (+0.16 and +0.37 ppm) for the H-3 and H-4 protons of the pyridyl moiety of 2,2'-bq in respect to those for these protons of the free ligand (Figure 2). The shifting of the resonance due to the H-3 proton is thought to be a consequence of a change of 2,2'-bq configuration upon its coordination from preferred transoid form to a cisoid one (Starosta et al., 2013). Furthermore, the resonances of the H-5 – H-8 protons are slightly shifted compared to those of the uncoordinated 2,2'-bq. The small coordination shifts observed for these protons in $[Ag(NO_3\text{-}O)(2,2'\text{-bq-}N,N')]_n$ complex are in agreement with the spectroscopic features of silver(I) complexes with aromatic nitrogen-containing heterocyclic ligands, due to the fast ligand exchange phenomenon on the NMR timescale (Kalinowska-Lis et al., 2015). For the presently investigated silver(I) complex, the order of ^1H resonances is in accordance with those for the mononuclear $[Ag(tsac\text{-}S)(2,2'\text{-bq-}N,N')]\cdot CH_3CN$ complex, which spectrum is recorded in DMSO-d_6 (tsac is thiosaccharinate anion) (Burrow et al., 2016). The latter complex was previously obtained in the reaction of hexameric $[Ag_6(tsac)_6]$ complex with 2,2'-bq in acetonitrile as solvent (Burrow et al., 2016).

The ^{13}C NMR spectrum of $[Ag(NO_3\text{-}O)(2,2'\text{-bq-}N,N')]_n$ in DMF-d_7 displays nine signals differently positioned from those of the uncoordinated ligand. Within the 2,2'-biquinoline, the nitrogen-adjacent C-atoms, *i.e.* C-2 and C-8a are shielded (-3.32 ppm for C2 and -1.26 ppm for C8a), while the more far-distant ring carbons are deshielded (up to +2.94 ppm for C4).

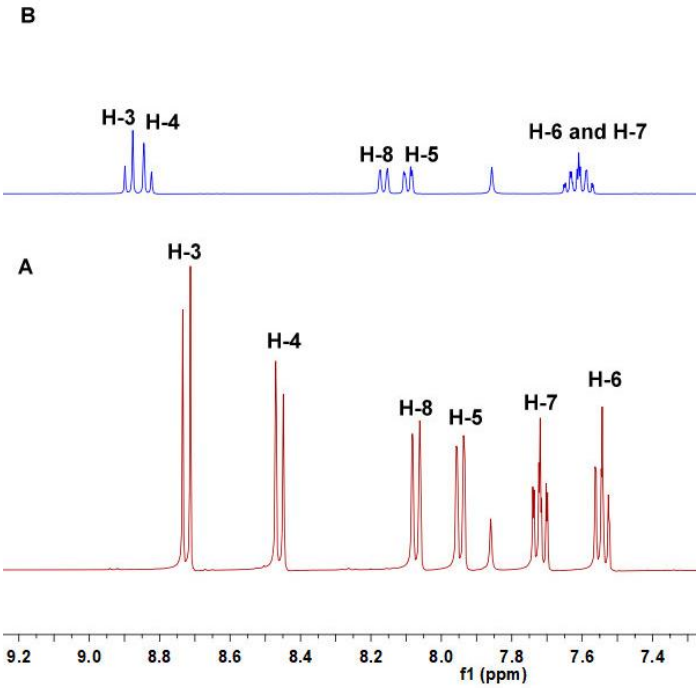

Figure 2. ^1H NMR spectra of 2,2'-bq (**A**) and $[Ag(NO_3\text{-}O)(2,2'\text{-bq-}N,N')]_n$ complex (**B**) measured in DMF-d_7 (400 MHz).

The UV-Vis spectrum of $[Ag(NO_3\text{-}O)(2,2'\text{-bq-}N,N')]_n$ complex recorded in DMF at room temperature shows three bands with absorption maxima at λ = 315.0, 326.0 and 339.0 nm and lower intensity shoulder at λ = 355.0 nm (Figure 3).

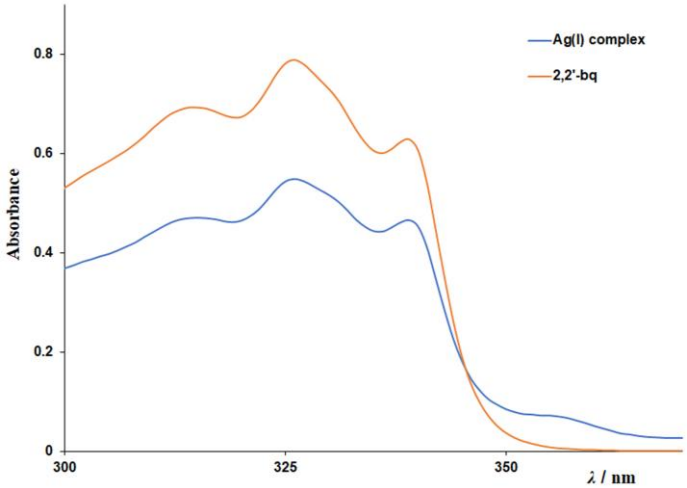

Figure 3. UV-Vis spectra of 2,2'-bq and $[Ag(NO_3\text{-}O)(2,2'\text{-bq-}N,N')]_n$ complex measured in DMF ($c = 1.9\cdot10^{-5}$ M).

As can be seen, the spectral features of this complex are similar with those of the 2,2'-bq, differing only in the appearance of a shoulder in the spectrum of the complex. Considering this

and the fact that the d^{10} metal coordination does not influence the electronic transitions already active in the ligand, the three bands at $\lambda = 315.0$, 326.0 and 339.0 nm can be attributed to the $\pi \rightarrow \pi^*$ transitions of the aromatic rings of the 2,2'-bq and originate from an intraligand charge transfer (ILCT) (Pucci et al., 2011). On the other hand, the appearance of a shoulder at $\lambda = 355.0$ nm in the spectrum of the complex is attributed to the complexation process and can be assigned to the charge transfer processes between silver(I) ion and 2,2'-bq ligand (Tailor et al., 2015; Rusu et al., 2016; Kharat et al., 2011). No $d \rightarrow d$ transitions are expected for a complex of d^{10} metal ion.

CONCLUSION

We have shown that the reaction between $AgNO_3$ and 2,2'-biquinoline (2,2'-bq) in 1 : 1 mole ratio in ethanol leads to the formation of polynuclear silver(I) complex, $[Ag(NO_3\text{-}O)(2,2'\text{-bq-}N,N')]_n$. In this complex, Ag(I) ion is bidentately coordinated by 2,2'-biquinoline and by the oxygen atoms of two nitrate ions. The present results are in contrast to those previously reported for the silver(I) complexes obtained in the reactions of $AgClO_4$, $AgCF_3SO_3$ and $[Ag_6(tsac)_6]$ with 2,2'-biquinoline, all leading to the formation of discrete mononuclear $[Ag(ClO_4\text{-}O,O')(2,2'\text{-bq-}N,N')]$, $[Ag(CF_3SO_3\text{-}O)(2,2'\text{-bq-}N,N')(H_2O)]$ and $[Ag(tsac\text{-}S)(2,2'\text{-bq-}N,N')]\cdot CH_3CN$ species, respectively (Bowmaker et al., 2005; Pucci et al., 2011; Burrow et al., 2016). This study confirms that the constitution of the silver(I) complexes with aromatic *N*-heterocyclic ligands strongly depends on the reaction conditions, such as starting silver(I) compound and solvent. All these together should be carefully considered during preparation of new silver(I) complexes for different applications in medicinal and supramolecular chemistry.

ACKNOWLEGMENTS

This research has been financially supported by the Ministry of Education, Science and Technological Development of the Republic of Serbia (Agreement No. 451-03-68/2020-14/200042). The authors wish to thank Dr. Hubert Wadepohl (Institute of Inorganic Chemistry, Heidelberg University) for performing single-crystal X-ray diffraction analysis.

REFERENCES

Andrejević, T. P., Nikolić, A. M., Glišić, B. Đ., Wadepohl, H., Vojnovic, S., Zlatović, M., Petković, M., Nikodinovic-Runic, J., Opsenica, I. M., & Djuran, M. I. 2018. Synthesis, structural characterization and antimicrobial activity of silver(I) complexes with 1-benzyl-1H-tetrazoles. Polyhedron, 154, pp. 325-333. doi.10.1016/j.poly.2018.08.001

Banti, C. N., & Hadjikakou S. K. 2013. Anti-proliferative and anti-tumor activity of silver(I) compounds. Metallomics, 5, pp. 569-596. doi.10.1039/C3MT00046J

Bellusci, A., Crispini, A., Pucci, D., Szerb, E. I., & Ghedini, M. 2008. Structural variations in bipyridine silver(I) complexes: Role of the substituents and counterions. Crystal Growth and Design, 8, pp. 3114-3122. doi.10.1021/cg8003323

Bowmaker, G. A., Effendy, Marfuah, S., Skelton, B. W., & White, A. H. 2005. Syntheses, structures and vibrational spectroscopy of some 1:1 and 1:2 adducts of silver(I) oxyanion salts with 2,2′-bis(pyridine) chelates. Inorganica Chimica Acta, 358, pp. 4371-4388. doi.10.1016/j.ica.2005.04.001

Burrow, R. A., Belmonte, G. Z., Dorn, V., & Dennehy, M. 2016. Three new Ag(I) thiosaccharinate complexes: Synthesis, structural studies, spectral characterization and theoretical analysis. Inorganica Chimica Acta, 450, pp. 39-49. doi.10.1016/j.ica.2016.05.004

Fik, M. A., Gorczyński, A., Kubicki, M., Hnatejko, Z., Fedoruk-Wyszomirska, A., Wyszko, E., Giel-Pietraszuk, M., & Patroniak, V. 2014. 6,6″-Dimethyl-2,2′:6′,2″-terpyridine revisited: New fluorescent silver(I) helicates with in vitro antiproliferative activity via selective nucleoli targeting. European Journal of Medicinal Chemistry, 86, pp. 456-468. doi.10.1016/j.ejmech.2014.09.004

Glišić, B. Đ., Senerovic, L., Comba, P., Wadepohl, H., Veselinovic, A., Milivojevic, D. R., Djuran, M. I., & Nikodinovic-Runic, J. 2016. Silver(I) complexes with phthalazine and quinazoline as effective agents against pathogenic Pseudomonas aeruginosa strains. Journal of Inorganic Biochemistry, 155, pp. 115-128. doi.10.1016/j.jinorgbio.2015.11.026

Kalinowska-Lis, U., Felczak, A., Chęcińska, L., Lisowska, K., & Ochocki, J. 2014. Synthesis, characterization and antimicrobial activity of silver(I) complexes of hydroxymethyl derivatives of pyridine and benzimidazole. Journal of Organometallic Chemistry, 749, pp. 394-399. doi.10.1016/j.jorganchem.2013.10.035

Kalinowska-Lis, U., Felczak, A., Chęcińska, L., Zawadzka, K., Patyna, E., Lisowska, K., & Ochocki, J. 2015. Synthesis, characterization and antimicrobial activity of water-soluble silver(I) complexes of metronidazole drug and selected counter-ions. Dalton Transactions, 44, pp. 8178-8189. doi.10.1039/C5DT00403A

Kharat, A. N., Bakhoda, A., Foroutannejad, S., & Foroutannejad, C. 2011. Molecular structure and antimicrobial activity of a luminescent dinuclear silver(I) complex of phenyl- bis(2- pyridyl)phosphine. Zeitschrift für Anorganische und Allgemeine Chemie, 637, pp. 2260-2264. doi.10.1002/zaac.201100235

Khlobystov, A. N., Blake, A. J., Champness, N. R., Lemenovskii, D. A., Majouga, A. G., Zyk, N. V., & Schröder, M. 2001. Supramolecular design of one-dimensional coordination polymers based on silver(I) complexes of aromatic nitrogen-donor ligands. Coordination Chemistry Reviews, 222, pp. 155-192. doi.10.1016/S0010-8545(01)00370-8

Medici, S., Peana, M., Nurchi, V. M., & Zoroddu, M. A. 2019. Medical uses of silver: History, myths, and scientific evidence. Journal of Medicinal Chemistry, 62, pp. 5923-5943. doi.10.1021/acs.jmedchem.8b01439

Nomiya, K., Takahashi, S., Noguchi, R., Nemoto, S., Takayama, T., & Oda, M. 2000. Synthesis and characterization of water-

soluble silver(I) complexes with L-histidine (H_2his) and (S)-(−)-2-pyrrolidone-5-carboxylic acid (H_2pyrrld) showing a wide spectrum of effective antibacterial and antifungal activities. Crystal structures of chiral helical polymers $[Ag(Hhis)]_n$ and $\{[Ag(Hpyrrld)]_2\}_n$ in the solid state. Inorganic Chemistry, 39, pp. 3301-3311. doi.10.1021/ic990526o

Pavić, A., Savić, N. D., Glišić, B. Đ., Crochet, A., Vojnovic, S., Kurutos, A., Stanković, D. M., Fromm, K. M., Nikodinovic-Runic, J., & Djuran, M. I. 2019. Silver(I) complexes with 4,7-phenanthroline efficient in rescuing the zebrafish embryos of lethal Candida albicans infection. Journal of Inorganic Biochemistry, 195, pp. 149-163. doi.10.1016/j.jinorgbio.2019.03.017

Pettinari, C., Marchetti, F., Lupidi, G., Quassinti, L., Bramucci, M., Petrelli, D., Vitali, L. A., da Silva, M. F. C. G., Martins, L. M. D. R. S., Smoleński, P., & Pombeiro, A. J. L. 2011. Synthesis, antimicrobial and antiproliferative activity of novel silver(I) tris(pyrazolyl)methanesulfonate and 1,3,5-triaza-7-phosphadamantane complexes. Inorganic Chemistry, 50, pp. 11173-11183. doi.10.1021/ic201714c

Potapov, A. S., Nudnova, E. A., Khlebnikov, A. I., Ogorodnikov, V. D., & Petrenko, T. V. 2015. Synthesis, crystal structure and electrocatalytic activity of discrete and polymeric copper(II) complexes with bitopic bis(pyrazol-1-yl)methane ligands. Inorganic Chemistry Communications, 53, pp. 72-75. doi.10.1016/j.inoche.2015.01.024

Pucci, D., Crispini, A., Ghedini, M., Szerb, E. I., & La Deda, M. 2011. 2,2′-Biquinolines as test pilots for tuning the colour emission of luminescent mesomorphic silver(I) complexes. Dalton Transactions, 40, pp. 4614-4622. doi.10.1039/C0DT01842B

Rowan, R., Tallon, T., Sheahan, A. M., Curran, R., McCann, M., Kavanagh, K., Devereux, M., & McKee, V. 2006. 'Silver bullets' in antimicrobial chemotherapy: Synthesis, characterisation and biological screening of some new Ag(I)-containing imidazole complexes. Polyhedron, 25, pp. 1771-1778. doi.10.1016/j.poly.2005.11.021

Rusu, A., Hancu, G., Tóth, G., Vancea, S., Toma, F., Mare, A. D., Man, A., Nițulescu, G. M., & Uivarosi, V. 2016. New silver complexes with levofloxacin: Synthesis, characterization and microbiological studies. Journal of Molecular Structure, 1123, pp. 384-393. doi.10.1016/j.molstruc.2016.07.035

Savić, N. D., Glišić, B. Đ., Wadepohl, H., Pavic, A., Senerovic, L., Nikodinovic-Runic, J., & Djuran, M. I. 2016. Silver(I) complexes with quinazoline and phthalazine: Synthesis, structural characterization and evaluation of biological activities. MedChemComm, 7, pp. 282-291. doi.10.1039/C5MD00494B

Savić, N. D., Vojnovic, S., Glišić, B. Đ., Crochet, A., Pavic, A., Janjić, G. V., Pekmezović, M., Opsenica, I. M., Fromm, K. M., Nikodinovic-Runic, J., & Djuran, M. I. 2018. Mononuclear silver(I) complexes with 1,7-phenanthroline as potent inhibitors of Candida growth. European Journal of Medicinal Chemistry, 156, pp. 760-773. doi.10.1016/j.ejmech.2018.07.049

Starosta, R., Brzuszkiewicz, A., Bykowska, A., Komarnicka, U. K., Bażanów, B., Florek, M., Gadzała, Ł., Jackulak, N., Król, J., & Marycz, K. 2013. A novel copper(I) complex, [CuI(2,2′-biquinoline)$P(CH_2N(CH_2CH_2)_2O)_3$] – Synthesis, characterisation and comparative studies on biological activity. Polyhedron, 50, pp. 481-489. doi.10.1016/j.poly.2012.11.033

Tailor, S. M., & Patel. U. H. 2015. Synthesis, spectroscopic characterization, antimicrobial activity and crystal structure of silver and copper complexes of sulfamethazine. Journal of Coordination Chemistry, 68, pp. 2192-2207. doi.10.1080/00958972.2015.1055258

Yeşilel, O. Z., Kaştaş, G., Darcan, C., İlker, İ., Paşaoğlu, H., & Büyükgüngör, O. 2010. Syntheses, thermal analyses, crystal structures and antimicrobial properties of silver(I)-saccharinate complexes with diverse diamine ligands. Inorganica Chimica Acta, 363, pp. 1849-1858. doi.10.1016/j.ica.2010.02.013

UNIVERSITY THOUGHT
Publication in Natural Sciences, Vol. 10, No. 1, 2020, pp. 31-36.
DOI: https://doi.org/10.5937/univtho10-24790
Original Scientific Paper

ANALYSIS OF AIR TEMPERATURE TRENDS: CITY OF PODGORICA (MONTENEGRO)

NIKOLA BAČEVIĆ[1*], ALEKSANDAR VALJAREVIĆ[1], DUŠAN KIĆOVIĆ[2], NIKOLA MILENTIJEVIĆ[1], MARKO IVANOVIĆ[1], MELIHA MUJEVIĆ[1]

[1]Faculty of Natural Sciences and Mathematics, University of Priština, Kosovska Mitrovica, Serbia
[2]The College of Tourism, Academy of Applied Studies, Belgrade, Serbia

ABSTRACT

This paper presents the results of the analyzed trends for three categories of parameters: average annual air temperature (YT), average maximum air temperature (YTx) and average minimum air temperature (YTn) for the Podgorica Meteorological Station in the Republic of Montenegro. The aim of this paper is to present possible climate changes based on the results obtained from the analyzed air temperature trends. The methodology is based on the application of: a) linear trend equations, b) trend magnitudes and c) Mann-Kendall trend test. The data from the respectable meteorological station in Podgorica for the period from 1947 to 2018 were used in order to estimate the trend. The obtained results indicate a statistically significant positive trend for all analyzed time series. Analyzing the trend test hypotheses, it was concluded that in all three cases the Ha hypothesis prevails. Average annual air temperature in Podgorica increased by 1.4°C, average maximum air temperature increased by 2.5°C and average minimum air temperature increased by 0.6°C. In accordance with the trends analyzed, the increase in air temperature is dominant in the capital of the Republic of Montenegro.

Keywords: Climate changes, Air temperature, Mann-Kendall test, Podgorica, Montenegro.

INTRODUCTION

The trend of increasing average annual air temperature has been identified worldwide. However, the spatio-temporal distribution of the increase in global air temperature is not uniform on Earth. The rise in air temperature varies by region. A higher rise in air temperature was observed in the northern hemisphere. Regional differences in terms of increasing average global air temperature are in the range of 0.65°C 1.06°C. This is indicated by various reports given by the International Panel on Climate Change (IPCC, 2007; IPCC, 2014; IPCC, 2018). Also, in Europe there is a statistical trend of increasing average annual air temperature. The data obtained from various meteorological stations across Europe, (Klein et al., 2002) indicated an upward trend. The same rising trend in Europe has been observed with average seasonal air temperatures (Brázdil et al., 1996; Brunetti et al., 2004; Feidas et al., 2004; Brunet et al., 2007). Therefore, trends in the increase of air temperatures in the greatest part of Europe were recorded during the 20th century. They were most pronounced during the 1990s (Kovats et al., 2014). A similar trend continued in the next century, so the four warmest years since instrumental measurements were recorded in the second decade of the 21st century - 2015, 2016, 2017 and 2018 (WMO, 2019). Previous research into climate change in the wider region and in Southeast Europe has addressed similar issues (Jovanović et al., 2002; Unkašević & Tošić, 2013; Tosić et al., 2016; Trbić et al., 2017; Gavrilov et al., 2015; Gavrilov et al., 2016; Gavrilov et al., 2018; Ivanović et al., 2016; Popov et al., 2017; Popov et al., 2018; Vukoičić et al., 2018; Papić et al., 2019) and aridity as an indicator of climate change (Hrnjak et al., 2014; Bačević et al., 2017; Radaković et al., 2017; Milentijević et al., 2018). A statistically significant upward trend in the average annual air temperature was also observed in the urban area (Savić et al, 2013; Bačević et al., 2018). This paper analyzes recent trends for average, average maximum and average minimum air temperatures in the urban area of Podgorica. The problem of climate in the study area was addressed by numerous authors (Vujević, 1953; Radinović, 1981; Burić et al., 2007; Burić et al., 2011; Burić et al., 2013; Burić et al., 2014; Burić et al., 2015; Burić et al., 2018; Burić et al., 2019).

MATERIAL AND METHODS

Study area

In geomorphotectonic sense, the area of Podgorica is part of the mid-Montenegrin valley. The valley is an area that extends from the Gatačko Field in Herzegovina to Lake Skadar, while the river Bojana opens to the Adriatic Sea. The valley consists of: Golija and Duga (800 to 1000 m of a.h.), Niksic Field (600 to 660 meters), Bjelopavlić plain (40 to 56 meters) and Podgorica-Skadar Valley (6 to 67 meters). North of Skadar Lake (as part of the Podgorica-Skadar basin) is the Zeta plain. It covers the lower course of the Morača River. This is the largest continental lowland of Montenegro, measuring about 240 km². The plain is low in altitude (except for limestone mounds) and is slightly sloping from northeast to southwest and south. In its northern part is Podgorica. The administrative center and capital of Podgorica is located in the central part of the Republic of

* Corresponding author: nikola.bacevic@pr.ac.rs

Montenegro. The urban area covers an area of about 1500 km², which represents 10.5% of the total territory. In the north and northwest, the municipalities of Podgorica are bordered by the municipalities of Kolašin, Andrijevica and Danilovgrad, and in the south and southwest by the municipalities of Bar, Ulcinj and Cetinje. To the east, the municipality borders with the Republic of Albania. Podgorica Weather Station is located in Golubovci, 10 km from the city center (Burić et al., 2007). According to Kepen's climate classification, Podgorica and its surroundings belong to the *Csa* subtype. It is characterized by warm and dry summers and moderate and rainy winters. The average temperature of the coldest month is between -3℃ and 18℃. Summer is the warmest period of the year, with the warmest monthly temperature > 22℃(Burić et al., 2014).

Data

This paper uses data for average annual, average maximum and average minimum air temperatures, published in the Meteorological Yearbooks of the Republic Hydrometeorological Institute of the Republic of Montenegro from the meteorological station in Podgorica, for the period from 1947 to 2018 (http://www.meteo.co.me/). Coordinates of defined study area are: φ=42°26′00″ N, λ=19°17′00″ E and 49 m of altitude. The geographical location of the Podgorica meteorological station is shown in Map 1. The technical and critical control of these measurements was realized by the Republic Hydrometeorological Institute of the Republic of Montenegro. Long time climate series used for analyses are influenced by inhomogenieties. They are caused by few factors: a) relocation of the meteorological station, b) the replacement of instruments or/and observers, c) changes in observation rules, d) changes in the environment of the meteorological station, etc. planting or/and uprooting of trees and grass, e) human errors in data processing. Many authors presented different homogeneity test: a) standard normal homogeneity test (SNHT; Alexandersson, 1986; Alexandersson & Moberg, 1997); b) Pettitt's test (Pettitt, 1979); c) Von Neumann ratio test (Von Neumann, 1941). If these inhomogenieties are not detected and treated adequately, results of climate analyses will be inaccurate. In paper Savić et al. (2012) homogenisation test provided relatively low break point magnitudes and adjustment values (from ±0.03 to ±0.26°C), probably caused by small territory of Vojvodina Province, not too large distance among weather stations and the geographical area with a gentle relief, so generally, the climate is free from orographic effects. Furthermore, these stations are a group of higher-rank stations (main stations) which probably resulted in higher quality of observations. Homogenisation process show relatively low differences of mean monthly (from 0°C to 0.12°C) and trend (from 0°C to 0.001°C/per year) air temperature values between raw and homogenised time series. Similarly, here are dominantly factors as small territory of Podgorica Municipality, plain relief, one main station in study area. For this reasons, in this paper weren't applied none of mentioned homogeneity tests.

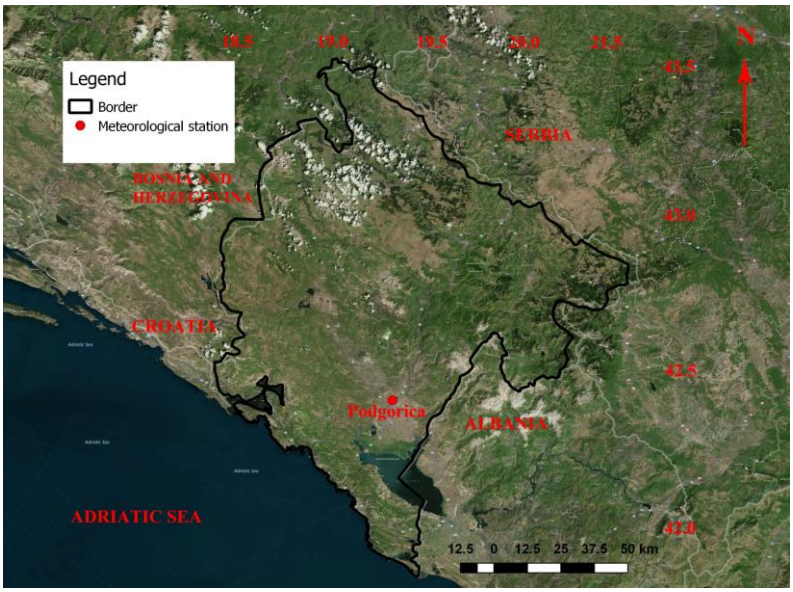

Figure 1. Physical-geographical map of the Republic of Montenegro and the geographical location of the capital Podgorica, marked in red.

Method

The paper uses three statistical approaches in order to analyze air temperature trends. The trend equation is the first statistical approach, which is of utmost importance for the analysis, evaluation and distribution of short-term climate change. Another statistical approach consists in determining the magnitude of the trend (Mann, 1945; Kendall, 1938). Whereas, the third statistical approach is to test the MK trend test, for each time series separately (Gavrilov et al., 2016). Air temperature trends were determined using EXCEL, which is part of the MICROSOFT OFFICE XLSTAT software package, used to

calculate value levels, *p*, and to test hypotheses (https://www.xlstat.com/en).

The trend equation

The linear trend is a statistical procedure, which is of great importance in the analysis and evaluation of changes in air temperatures (Hrnjak et al., 2014). The equation takes the following form:

$$y=ax+b \quad (1)$$

where *y* represents the air temperatures in ℃ and *a* is the magnitude of the slope, *x* is the time series, while *b* is the temperature at the beginning of the period. The value of the trend of air temperature is in function of the slope size. There are three possible scenarios: a) the slope size is greater than zero - the trend is positive; b) equal to zero - no trend; v) less than zero - the trend is negative.

Trend Magnitude

Trend magnitude is determined according to the trend equation (Gavrilov et al, 2015), i.e.:

$$\Delta y=y(1948) - y(2018) \quad (2)$$

where Δy represents the trend magnitude expressed in ℃, *y* (1948) in the equation is the value of the variable at the beginning of the period and *y* (2018) represents its value at the end of the period. When it comes to trend magnitude, there are three possible scenarios here: a) when it is greater than zero - the trend is negative; b) when Δy is less than zero - the trend is positive; c) when equal to zero – there is no trend.

RESULTS AND DISCUSSION

Trend parameters

The results are presented as average annual air temperatures (P-YT), as average annual maximum air temperatures (P-YTx) and as average annual minimum air temperatures (P-YTn). The MK trend test analysis is presented for a total of three time series for the Podgorica meteorological station. Figure 2 show the average annual, average maximum and average minimum air temperatures, trend test equations and linear trend for the Podgorica Meteorological Station for the observed period from 1947 to 2018. Trend magnitudes, Δy (℃) and trend probability *p*, for each of the three time series are presented in Tables 1 and 2.

Table 1. The trend equation y, the trend magnitude Δy, and probability *p* of the confidences for 3 time series.

Time series	Trend equation	Δy (℃)	*p (%)*
P-YT	*y=0.0196x+15.044*	1.4	< 0.0001
P-YTx	*y=0.035x+25.757*	2.5	< 0.0001
P-YTn	*y=0.0087x+5.0861*	0.6	0.0176

Table 2. The main results of the analysis of temperature trends for 3 time series.

Time series	Trend equation	Classical MK test
P-YT	*positive trend*	*positive significant trend*
P-YTx	*positive trend*	*positive significant trend*
P-YTn	*positive trend*	*positive significant trend*

Trend evaluation

The obtained MK trend test results for average air temperatures in Podgorica are shown in Table 2 for the observed period from 1947 to 2018. Of the three time series, in all cases the MK trend test analyzes showed a statistically significant positive trend. Also, a positive statistical trend is shown by all numerical parameters and graphical representations (Figure 2).

For the P-YT and P-YTx time series for Podgorica Meteorological Station, the *p* value is <0.0001. For both time series above, the same values of the Mk trend test analysis apply. As the computed *p*-value is lower than the significance level alpha =0.05, they should reject the null hypothesis H0, and accept the alternative hypothesis Ha. The risk to reject the null hypothesis is Ha, while it is true is lower than 0.01%.

For the P-YTn time series for the Podgorica Meteorological Station, the *p* value is 0.0176. As the computed p-value is lower than the significance level alpha = 0.05, one should reject the null hypothesis H0, and accept the alternative hypothesis Ha. The risk to reject the null hypothesis Ha while it is true is lower than 1.77%.

Individually observed in Podgorica, the highest temperature increase of 2.5°C was noticed in the P-YTx time series. This is followed by an average air temperature increase of 1.4°C for the P-YT time series. Whereas, the least average temperature increase of 0.6°C was observed for the P-YTn time series. In all three cases, a statistically positive trend was observed, where the Ha hypothesis prevails. According to the IPCC (2018) report on a global average annual average, the average maximum and minimum air temperatures of 0.6°C to 1.8°C are significantly more pronounced in the Montenegrin capital. Similar results were observed in Bosnia and Herzegovina (Mostar and Bileća). In Mostar, the average annual temperature rose by 0.9 °C and in Bileća by 1.7°C. Average maximum temperatures in Mostar and Bileća increased by 1.9°C and 1.3°C, respectively, and average minimum temperatures increased by 1.4°C and 0.7°C (Papić et al., 2019). Also, a positive trend of increasing air temperature is noticed in Vojvodina (Gavrilov et al., 2015), Novi Sad as an urban environment (Savić et al., 2013), and Kosovo and Metohija region (Gavrilov et al., 2018). The average air temperature increased by 1.2°C. Such results confirm that there are tendencies that suggest an increase in average air temperature on regional and national levels.

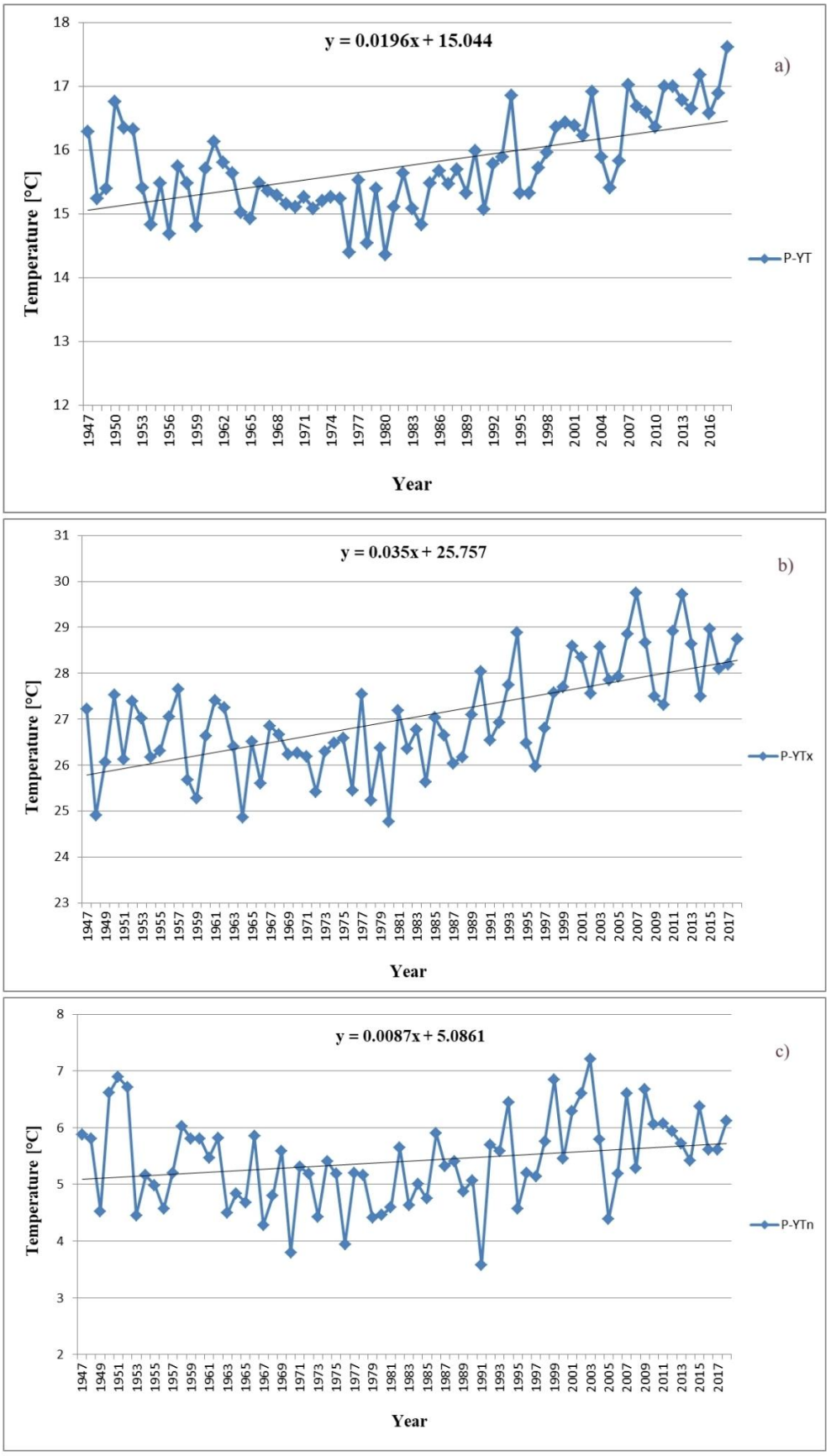

Figure 2. Graphical representation of a) average annual, b) average maximum, c) average minimum air temperature, trend equation and linear trend for the observed period from 1947 to 2018 in Podgorica.

CONCLUSION

Analyzing the trend equation, trend magnitude and MK trend test for average annual, average annual maximum and average annual minimum air temperature in Podgorica, a significant increase in air temperature was observed in all time series. Hypothesis Ha is prevalent, with a very low risk of rejecting the hypothesis. Positive trends for the Podgorica Meteorological Station represent a manifested pattern of climate change globally in line with the conclusions of the International Panel on Climate Change (IPCC, 2018). Unfortunately, this global problem has not, in scientific terms, been given much attention in the Republic of Montenegro. Future research should be focused on monitoring and analyzing climate extremes in the future. Also, it should be borne in mind that the analysis of trends was carried out on the basis of the parameters from the only station in the city territory. The presented results, due to the large heterogeneity of the space, show the general state of the selected parameters. There are many factors that influence the existence of microclimate differences in the area: degree of urbanization, terrain hypsometry, hydrographic objects, vegetation. For these reasons, monitoring of the required parameters through automatic weather stations would be necessary. This is possible if an AMS network is organized in the city. Climate change leads to numerous socio-economic consequences such as extreme climate events (aridity, drought - an unfavorable circumstance in agriculture), consequences for human health, reduction or even the disappearance of terrestrial and marine ecosystems.

REFERENCES

Alexandersson, H. 1986. A homogeneity test applied to precipitation data. Journal of Climatology. 6, pp. 661-675.

Alexandersson, H., & Moberg, A. 1997. Homogenization of Swedish temperature data. Part I: homogeneity test for linear trends. International Journal of Climatology. 17, pp. 25-34.

Bačević, R. N, Vukoičić, Z. D., Nikolić, M., Janc, N., Milentijević, N., & Gavrilov B. M. 2017. Aridity in Kosovo and Metohija, Serbia. Carpathian Journal of Earth and Environmental Sciences. 12(2), pp. 563-570.

Bačević, R. N., Pavlović, M., & Rašljanin, I. 2018. Trend Assessing Using Mann-Kendall's Test for Priština Meteorological Station Temperature and Precipitation Data, Kosovo and Metohija, Serbia. The University Thought - Publication in Natural Sciences, (8)2, pp. 39-43. doi:10.5937/univtho8-19513

Burić, D., Ivanović, R. & Mitrović, L. 2007. Klima Podgorice. Hidrometeorološki zavod Crne Gore, Podgorica.

Burić, D., Ducić, V. & Luković, J. 2011. Kolebanje klime u Crnoj Gori u drugoj polovini XX i početkom XXI vijeka. Posebna izdanja Crnogorske akademije nauka i umjetnosti, knjiga 36, pp. 6-261. Podgorica, IVPE Cetinje.

Burić, D., Ducić, V., & Mihajlović, J. 2013. The climate of Montenegro: Modificators and types - part one. Glasnik Srpskog Geografskog Društva, 93(4), pp. 83-102. doi.org/10.2298/GSGD1304083B

Burić, D., Ducić, V., & Mihajlović, J. 2014. The climate of Montenegro: Modificators and types - part two. Glasnik Srpskog Geografskog Društva. 94(1), pp. 73-90. doi:10.2298/GSGD1401073B

Burić, D., Ducić, V., Mihajlović, J., Luković, J., & Dragojlović, J. 2015. Recent extreme air temperature changes in Montenegro. Glasnik Srpskog Geografskog Društva, 95(4), pp. 53-46. doi.org/10.2298/GSGD140626002B

Burić, B. D., Dragojlović, M. J., Milenković, M., Popović, Z. Lj. & Doderović, M. M. 2018. Influence of variability of the East Atlantic Oscillation on the air temperature in Montenegro. Thermal Science, 22(1), pp. 759-766. doi.org/10.2298/TSCI170710211B

Burić, D., Milenković, M., & Ducić, V. 2019. The specificities of the climate of Danilovgrad (Montenegro). Glasnik Srpskog Geografskog Društva, 99(1), pp. 19-28. doi.org/10.2298/GSGD1901019B

Brázdil, R., Budíková, M., Auer, I., Böhm, R., Cegnar, T., Faško, P., Lapin, M., Gajić-Čapka, M., Zaninović, K., Koleva, E., Niedźwiedź, T., Ustrnul, Z., Szalai, S. & Weber, R. O. 1996. Trends of maximum and minimum daily temperatures in central and southeastern Europe. International Journal of Climatology, 16(7), Manhattan. doi: 10.1002/(SICI)1097-0088(199607)

Brunet, M., Jones, P. D., Sigro, J., Saladie, O., Aguilar, E., Moberg, A., Della-Marta, P. M., Lister, D., Walther, A. & López, D. 2007: Temporal and spatial temperature variability and change over Spain during 1850-2005. Journal of Geophysical Research: Atmospheres 112. Manhattan. doi: 10.1029/2006JD008249

Brunetti, M., Buffoni L., Mangianti, F., Maugeri, M. & Nanni, T. 2004. Temperature, precipitation and extreme events during the last century in Italy. Global and Planetary Change, 40(1/2). New York, Amsterdam, London. doi: 10.1016/S0921-8181(03)00104-8

Feidas, H., Makrogiannis, T., & Bora-Senta, E. 2004. Trend analysis of air temperature time series in Greece and their relationship with circulation using surface and satellite data: 1955-2001. Theoretical and Applied Climatology, 79(3-4), pp. 185-208. doi:10.1007/s00704-004-0064-5

Gavrilov, M. B., Marković, S. B., Jarad, A. & Korać, V. M. 2015. The analysis of temperature trends in Vojvodina (Serbia) from 1949 to 2006. Thermal Science, 19(2), pp. 339-350. doi.org/10.2298/TSCI150207062G

Gavrilov, M. B., Tošić, I., Marković, S. B., Unkašević, M. & Petrović, P. 2016. The analysis of annual and seasonal temperature trends using the Mann-Kendall test in Vojvodina, Serbia. IDŐJÁRÁS, 122(2), pp. 203-216. doi:10.28974/idojaras.2018.2.6

Gavrilov, M. B., Marković, S. B., Janc, N., Nikolić, M., Valjarević, A., Komac, B., Zorn, M., Punišić, M. & Bačević, N. 2018. Assessing average annual air temperature trends using the Mann–Kendall test in Kosovo. Acta geographica Slovenica, 58(1), 8-25. doi:10.3986/ags.1309

Hrnjak, I., Lukić, T., Gavrilov, M. B., Marković, S. B., Unkašević, M. & Tošić, I. 2014. Aridity in Vojvodina,

Serbia. Theoretical and Applied Climatology, 115, pp. 323-332. doi 10.1007/s00704-013-0893-1

IPCC. 2007. Intergovernmental Panel Climate Change. The physical science basis. In: Solomon, S., Qin. D., Manning, M., Chen, Z., Marquis, M., Averyt, K. B., Tignor, M., Miller, H. L. (eds.). Contribution of Working Group I to the Fourth Assessment Report of the Intergovernmental Panel on Climate Change. Cambridge University Press, Cambridge

IPCC. 2014. Climate Change 2014: Synthesis Report. Contribution of Working Groups I, II and III to the Fifth Assessment Report of the Intergovernmental Panel on Climate Change [Core Writing Team, R.K. Pachauri and L.A. Meyer (eds.)]. IPCC, Geneva, Switzerland, pp. 151.

IPCC. 2018. Summary for Policymakers. In: Global warming of 1.5°C. An IPCC Special Report on the impacts of global warming of 1.5°C above pre-industrial levels and related global greenhouse gas emission pathways, in the context of strengthening the global response to the threat of climate change, sustainable development, and efforts to eradicate poverty [V. Masson-Delmotte, P. Zhai, H. O. Pörtner, D. Roberts, J. Skea, P. R. Shukla, A. Pirani, W. Moufouma-Okia, C. Péan, R. Pidcock, S. Connors, J. B. R. Matthews, Y. Chen, X. Zhou, M. I. Gomis, E. Lonnoy, T. Maycock, M. Tignor, T. Waterfield (eds.)]. World Meteorological Organization, Geneva, Switzerland, 32.

Ivanovic, R., Valjarevic, A., Vukoicic, D., & Radovanovic, D. 2016. Climatic regions of Kosovo and Metohija. The University Thought - Publication in Natural Sciences, 6(1), pp. 49-54. doi:10.5937/univtho6-10409

Jovanović, G., Reljin, I. & Savić, T. 2002. NAO Influence on climate variability in FRY. 18th International conference on Carpathian meteorology, Belgrade.

Kendall, M. 1938. A new measure of rank correlation. Biometrika, 30, pp. 81–89.

Klein, T. A. M. G., Wijngaard, J. B., Können, G. P., Böhm, R., Demarée, G., Gocheva, A., & et al., 2002. Daily dataset of 20th-century surface air temperature and precipitation series for the European Climate Assessment. International Journal of Climatology, 22(12), pp. 1441-1453. doi:10.1002/joc.773

Kovats, R. S., Valentini, R., Bouwer, L. M., Georgopoulou, E., Jacob, D., Martin, E., Rounsevell, M. & Soussana, J. F. 2014. Europe. In: Barros, V. R., Field, C. B., Dokken, D. J., Mastrandrea, M. D., Mach, K. J., Bilir, T. E., Chatterjee, M., Ebi, K. L., Estrada, Y. O., Genova, R. C., Girma, B., Kissel, E. S., Levy, A.N., MacCracken, S., Mastrandrea, P. R., White, L.L.[eds.].Climate Change 2014: Impacts, Adaptation, and Vulnerability. Part B: Regional Aspects. Contribution of Working Group II to the Fifth Assessment Report of the Intergovernmental Panel on Climate Change. Cambridge University Press, Cambridge, United Kingdom and New York, NY, USA.

Mann, H. B. 1945. Non-parametric Tests Against Trend. Econometrica, 13, pp. 245-259.

Milentijević, N., Dragojlović, J., Ristić, D., Cimbaljević, M., Demirović, D. &, Valjarević, A. 2018. The assessment of aridity in Leskovac Basin, Serbia (1981-2010). Journal of the Geographical Institute "Jovan Cvijić", 68(2), pp. 249-264. doi.org/10.2298/IJGI1802249M

Papić, D., Bačević, R. N., Valjarević, A., Milentijević, N., Gavrilov, B. M., Živković, M. & Marković, B. S. 2019. Assessment of Air Temperature Trends in South and Southeast Bosnia and Herzegovina (B&H) from 1961 to 2017. IDŐJÁRÁS (ACCEPTED FOR PUBLICATION).

Pettitt, A.N. 1979. A non- parametric approach to the change- point problem. Journal of Applied Statistics. 28, pp. 126-135.

Popov, T., Gnjato, S. & Trbić, G. 2017. Trends in extreme temperatures indices in Bosnia and Herzegovina: A case study of Mostar. Herald, 21, pp. 107-132. doi: 10.7251/HER2117107P

Popov, T., Gnjato, S., Trbić, G. & Ivanišević, M. 2018. Recent Trends in Extreme Temperature Indices in Bosnia and Herzegovina. Carpathian Journal of Earth and Environmental Sciences, 13, pp. 211-224.

Radaković, G. M., Tošić, A. I., Bačević, R. N., Mađan, D., Marković, S. B. & Gavrilov, M. B. 2017. The analysis of aridity in Central Serbia from 1949-2015. Theoretical and Applied Climatology, 133(3-4) pp. 887-898. doi:10.1007/s00704-017-2220-8

Radinović, Đ. 1981. Vreme i klima Jugoslavije. Beograd: IRO "Građevinska knjiga".

Republic Hydrometeorological Service of Republika Montenegro, http://www.meteo.co.me/ (accessed 09.02.2019)

Savić, S., Milošević, D., Marković, V. & Kujundžić Dačović, R. 2012. Homogenisation of mean air temperature time series from Vojvodina (North Serbia). Geographica Pannonica. 16(2), pp. 38-43.

Savić, S., János, U., Tamás, G., Milošević, D. & Popov, Z. 2013. Urban heat island research of Novi Sad (Serbia): A review. Geographica Pannonica, 17(1), pp. 32-36.

Tošić, I., Zorn, M., Ortar, J., Unkašević, M., Gavrilov, M. B. & Marković, S. B. 2016. Annual and seasonal variability of precipitation and temperatures in Slovenia from 1961 to 2011. Atmospheric Research, 168, pp. 220-233. doi.org/10.1016/j.atmosres.2015.09.014

Trbić, G., Popov, T. & Gnjato, S. 2017. Analysis of air temperature trends in Bosnia and Herzegovina. Geographica Pannonica, 21, pp. 68–84. doi.org/10.5937/GeoPan1702068T

Unkašević, M. & Tošić, I. 2013. Trends in temperature indices over Serbia: relationships to large-scale circulation patterns. International Journal of Climatology, 33(15), pp. 3152-3161. doi:10.1002/joc.3652

Von Neumann J. 1941. Distribution of the ratio of the mean square successive difference to the variance. Annals of Mathematical Statistics. 12, pp. 367-395.

Vujević, P. 1953. Podneblje FNR Jugoslavije. Arhiv za poljoprivredne nauke, 6, pp. 3-42.

Vukoičić, Z. D., Milosavljević, A. S., Penjišević, T. I., Bačević, R. N., Nikolić, M., Ivanović, D. R., Jandziković, M. B. 2018. Spatial analysis of temperature and its impact on the sustainable development of mountain in Central and Western Serbia. Időjárás-Quarterly Journal of the Hungarian Meteorological Service. 122(3), 259-283.

WMO. 2019. Statement on the State of the Global Climate in 2018. WMO-No. 1233. World Meteorological Organization, Geneva, Switzerland.

XLSTAT, http://www.xlstat.com/en/ (accessed 10.03.2019)

UNIVERSITY THOUGHT
Publication in Natural Sciences, Vol. 10, No. 1, 2020, pp. 37-43.
DOI: https://doi.org/10.5937/univtho10-24774
Original Scientific Paper

APPLICATION OF MANN-KENDAL (MK) TEST IN TREND ANALYSIS OF AIR TEMPERATURE AND PRECIPITATION: CASE OF MAČVA DISTRICT (SERBIA)

NIKOLA MILENTIJEVIĆ[1*], NIKOLA BAČEVIĆ[1], DUŠAN RISTIĆ[1], ALEKSANDAR VALJAREVIĆ[2], MILANA PANTELIĆ[3], DUŠAN KIĆOVIĆ[4]

[1]Faculty of Sciences, University in Priština, Kosovska Mitrovica, Serbia
[2]Faculty of Geography, University of Belgrade, Belgrade, Serbia
[3]Faculty of Sciences, University of Novi Sad, Novi Sad, Serbia
[4]The College of Tourism, Academy of Applied Studies, Belgrade, Serbia

ABSTRACT

Recent climate changes cause significant natural and socio-economic consequences. They represent one of the major environmental problems of the late 20th and early 21st centuries. Changes in temperature and precipitation play a significant role in understanding climate change issues. They include numerous extreme climatic events such as heat waves, droughts, forest fires and more. Looking at regional differences in temperature and precipitation regime change, Southern Europe, including the Republic of Serbia, occupies a special place. The Mačva district (3.272 km²) is almost four times as spacious as the Mačva area. The administrative-political division of the Mačva district is comprised of eight municipalities. The paper presents trends of two climate variables: mean annual air temperature and mean annual precipitation in the study area. In methodological sense, the main statistical procedure is the non-parametric Mann-Kendall (MK) test. Data from three available meteorological stations in the Mačva district (1949-2015) were used for the analysis. The presented results of the trends in air temperature indicate that there is a statistically significant positive trend in all-time series. In trends, precipitation amounts a statistically significant positive trend was observed in two time series, while in one there is no trend. The expressed trends, especially in the case of air temperatures, lead to the possibility of drought. Mačva district and Mačva have some agricultural importance in the Republic of Serbia. For these reasons, some adaptation to climate change is needed as arid conditions lead to fluctuations in agricultural yield.

Keywords: Climate change, Air temperature trends, Precipitation trends, Mann Kendall test, Mačva district (Serbia).

INTRODUCTION

Fifth Assessment Report the Intergovernmental Panel on Climate Change (IPCC, 2014) highlights several important conclusions: a) over the past hundred years, the average temperature on Earth has increased by 0.6 °C. During this interval, two warming periods are distinguished - from 1910 to 1945 and from 1976 to the present; b) "the period from 1983 to 2012 is probably the hottest 30-year series on the northern hemisphere in the last 1400 years"; c) the past three decades have been the warmest during the instrumental period. Each decade was successively warmer than the previous one, so the first decade of the 21st century was the warmest since 1850.

Apart from the report, many authors have addressed the issue of climate change. According to Luterbacher et al. (2004) the second half of the twentieth century and the beginning of the twenty-first century (1974-2003) make up the hottest 30-year series. This is in line with the latest Intergovernmental Panel on Climate Change Report. Blunden et al. (2018) found that since instrumental measurements were made (1880–2012), the average global air temperature has shown a growth trend of 0.85 °C.

Regional differences are below or above the established limit (in the range of 0.65 to 1.06 °C). The most intense warming in recent decades has been observed in the temperate latitudes of the Northern Hemisphere (Fei et al., 2014). During the twentieth century, air temperatures rose almost throughout the whole Europe. However, regionally, the largest changes in annual and seasonal air temperatures have been identified in Northern Europe latitudes (Kovats et al., 2014). Since 1980, warming has been most intense above Scandinavia (especially in winter), while warming in the Iberian Peninsula is pronounced during the summer months (EEA, 2012). Climate change is particularly affecting the area of Southeast Europe.

There are numerous authors who have analyzed the annual trends in air temperature: in Slovenia (Milošević et al., 2013; Milošević et al., 2017), Montenegro (Burić et al., 2014a), Serbia (Unkašević & Tošić, 2013; Bajat et al., 2015; Gavrilov et al., 2015; Gavrilov et al., 2016; Gavrilov et al., 2018; Bačević et al., 2018), Greece (Mamara et al., 2016), and Bosnia and Herzegovina (Trbić et al., 2017; Popov et al., 2018a; Popov et al., 2018b).

*Corresponding author: nikola.milentijevic@pr.ac.rs

Globally, there are trends in increasing precipitation (Nguyen et al., 2018). However, regional variations in precipitation do not follow global trends. From 1900 to 2005, precipitation decreased in the Sahel, the Mediterranean, South Africa and parts of South Asia. These trends have been expressed especially since the 1980s (Spinoni et al., 2017). The exception is North Africa, northern Italy and the western part of the Iberian Peninsula where a trend of increasing precipitation has been observed (Philandras, 2011). The annual rainfall since 1960 shows a trend increase of 70 mm per decade in Northern Europe and Western Europe. A decrease in the sum of 90 mm per decade has been reported in Southern Europe (EEA, 2017).

Precipitation variability as an indicator of climate change in Southeast Europe was addressed by: in Serbia (Gocić & Trajković, 2013; Tošić et al., 2014a; Tošić & Unkašević, 2014b; Putniković & Tošić, 2018), Montenegro (Burić et al., 2014b; Burić et al., 2018a; Burić et al., 2018b), Slovenia (Tošić et al., 2016), Greece (Markonis et al., 2017); Bosnia and Herzegovina (Popov et al., 2019a; Popov et al., 2019b).

The subject of this paper is an analysis of recent trends in air temperature and precipitation in the Mačva district, from 1949 to 2015.Mačva district belongs to an important agricultural region in Serbia. One of the sectors most affected by climate change is the agricultural sector (by phenomenon as drought). Irrigation is an effective measure in the fight against drought. Using irrigation systems, in wet years, the unequal distribution of precipitation would be corrected, and in the dry conditions, the humidity deficit would be eliminated. Two important factors that make today's agricultural production unsustainable: a) obsolescence, neglect or absence of irrigation systems; b) the absence of a methodology for forecasting natural disasters, prevention and reduction of damage incurred (Armenski et al., 2014). For this reason, the presented results form the basis of further research of interaction between climate changes and agricultural production. The climate of Mačva as part of the District has been analyzed in climatic terms in several textbooks (Rakićević, 1980; Grčić & Grčić, 2002; Ducić & Radovanović, 2005). Numerous attempts at climate change in the former Yugoslavia, and within the framework of Mačva, show a strong compliance (Milutinović, 1974; Rakićević, 1980; Ducić& Radovanović, 2005; Ivanović et al., 2016). According to A. Milutinović (1974) Mačva belongs to the Cfwbx variant of moderately warm and humid climate (according to Kepen's climate classification).

T. Rakićević (1980) classified Mačva in the Kolubara-Mačva climate region. The mean temperatures of the hottest month in the annual flow of air temperature, July, are between 20-22 ℃, while the annual precipitation amounts are between 600-800 mm. Ducić & Radovanović (2005) They classify Mačva in the Climate Area A (Subarea A-1-a). These are conditions of continental climate. However, there is a serious lack of literature in the field of climate research (Ćirković, 1977; Gajić & Vujadinović, 2007). The reasons for the inadequate treatment of climate change problems are the small size of the territory and the lack of the relevant meteorological stations. A larger number of stations would result in better spatial distribution of climate parameters, which would allow for more adequate climate analysis.

THEORETICAL PART

Study area

The plain of Mačva represents a special sub-continent within the Pannonian Basin. Its borders are natural: the Sava River in the north and east, the lower course of the Drina River in the west and the Pocerina River in the south. It is dissected by a dense network of river flows belonging to the Drina, Sava and Kolubara basins.The area of Mačva is 860 km². In the administrative-political sense, the Mačva district is a far larger entity (3.272 km²). It is composed of the following municipalities: Bogatić, Vladimirci, Koceljeva, Krupanj, Loznica, Ljubovija, Mali Zvornik and Šabac (Grčić& Grčić, 2002). There is only one meteorological station in the territory of Mačva (MS Šabac). For this reason, the study area was extended to the entire district, where two more meteorological stations (MS Loznica and MS Ljubovija) were located. The area defined in this way (Figure 1), with more stations, makes it possible to represent more time series. In this way, a better analysis of the trends is obtained.

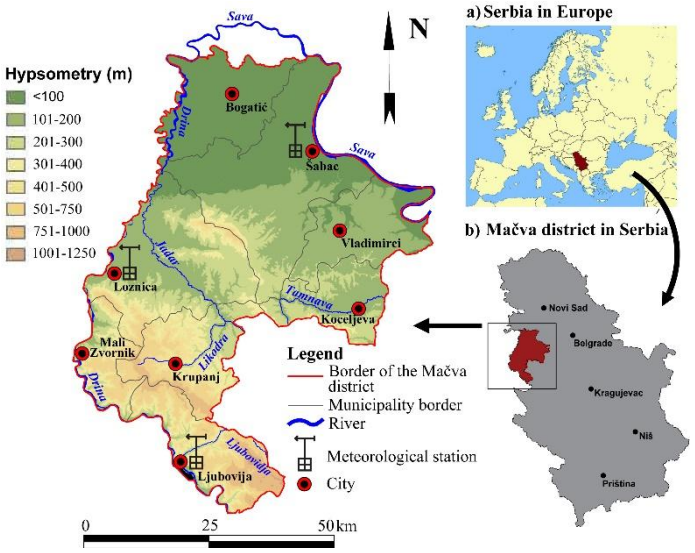

Figure 1. Map location of Mačva district in Republic of Serbia, with selected meteorological stations.

EXPERIMENTAL PART

Materials and methods

For the purposes of the paper, an analysis of selected climatic parameters was performed for a 66-year data set. Data from 3 meteorological stations, taken from the Meteorological

Yearbooks of the Republic Hydrometeorological Service of Serbia (RHSS, 2019) were used. Climate variables are categorized into two groups of data: mean annual air temperature (YT) and mean annual precipitation (YP). The analysis of selected variables by weather stations determined a total of six time series. Each of the six time series is indicated by a corresponding acronym containing the abbreviation for the year and air temperature or precipitation (Table 1).

Table 1. Acronyms for 6 time series per meteorological station based on the abbreviation for the year and selected climate variable.

Station	Year (Y)
Šabac	*Š-YT*
	Š-YP
Loznica	*L-YT*
	L-YP
Ljubovija	*Lj-YT*
	Lj-YP

Trends in air temperature and precipitation were processed using three statistical approaches: a) the trend equation was determined individually for each time series; b) the trend magnitude (Δy) is calculated based on the trend equation; v) apart from these procedures, the existence or absence of a trend was analyzed using a non-parametric Mann-Kendall (MK) test. The essence of the first statistical procedure is to determine the slope size of the selected variable in the trend equation. There are three possible scenarios here: a) the slope size is greater than zero - *the trend is positive*; b) the slope size is less than zero - *the trend is negative*; v) slope equals zero - *there is no trend*. Based on the trend equation, the magnitude (change) of the trend was determined as the difference of parameters (air temperature and/or precipitation) at the beginning and end of the period. The period means the analyzed interval, from 1949 to 2015. At trend magnitude, there are three possible scenarios: a) when Δy is greater than zero - the trend is negative; b) when Δy is less than zero - the trend is positive; v) when Δy equals zero - there is no trend. (Gavrilov et al., 2015; Gavrilov et al., 2016). The third statistical procedure is the most complex and involves the analysis of time series using the MK test (Kendall, 1975; Gilbert, 1987). This test has wide application in the interpretation of climatological time series, e.g. air temperature and precipitation (Karmeshu, 2012), extreme temperatures (Wibig & Glowicki, 2002), aridity as an indicator of climate change (Hrnjak et al., 2014; Bačević et al., 2017; Radaković et al., 2017; Milentijević et al. al., 2018). Its advantages are ease of use and manipulation of missing values. According to MK test, two hypotheses were tested: H_0 (null hypothesis) where there is no trend in time series; and the alternative hypothesis (H_a), where there is a statistically significant trend in time series, for the selected significance level (α). The probability (p) was calculated in order to determine the level of significance in the hypotheses. Microsoft Office Excell 2007 software and its XLSTAT extension (https://www.xlstat.com/en) were used to analyze the data.

Inhomogeneity in time series can cause the incorrect interpretation of climate time series (Rahman et al., 2017), and be misleading in the interpretation of tendencies in the time series. Several methods can be used to detect abrupt changes: Alexandersson's test (Alexandersson, 1986), Pettitt's test (Kocsis et al., 2019).Savić et al. (2012) applied homogeneity test on example of Vojvodina (Serbia) according to Alexandersson (1986). In this paper time time series related to air temperature values were tested. The test of homogeneity points to relatively low differences of mean monthly (from 0℃ to 0.12℃) and trend (from 0℃ to 0.001℃) air temperatures values between raw and homogenised time series. Authors Tošić et al. (2014b) analyzed wet and dry periods in Serbia, by application of the same method. Their conclusions are similar to previous research (homogeneity is determined in all time series related to precipitation). In this paper none of presented homogeneity tests wasn't applied. Main reasons can be summarised in the following statements: a) small territory of Mačva district; b) small distance between meteorological stations; c) the dataset was complete, without missing data.

RESULTS AND DISCUSSION

Trend parameters

The paper presents the results for 6 time series. For each time series, the trend equation, linear trend, and MK test analysis (from 1949-2015) were determined. The analysis was supplemented with trend magnitude (Δy) and trend probability (p) for each time series from the selected meteorological station. The results are summarized in Tables 2 and 3 and Figure 1.

Table 2. Trend equation (y), trend magnitude (Δy), and reliability probability (p) for mean annual air temperature (YT).

Time series	Trend equation	Δ*y* (℃)	*p* (%)
Š-YT	*y = 0.0138x + 10.94*	0.9	<0.0001
L-YT	*y = 0.0228x + 10.636*	1.5	<0.0001
Lj-YT	*y = 0.0202x + 10.074*	1.3	<0.0001

Table 3. Trend equation (y), trend magnitude (Δy), and reliability probability (p) for mean annual precipitation (YP).

Time series	Trend equation	Δ*y* (mm)	*p* (%)
Š-YP	*y = 0.9538x + 656.24*	62.9	0.1517
L-YP	*y = 1.3753x + 797.6*	90.8	<0.0001
Lj-YP	*y = 1.8657x + 838.73*	123.1	<0.0001

Trend assessment

The obtained MK test results for mean annual air temperatures and mean annual rainfall in the Mačva district are shown in Table 4. The analysis of selected time series identifies two key statements: *a) in five time series cases there is a statistically significant positive trend; b) only in the case of the*

time series relating to precipitation (Š-YP) there is no established trend. The results obtained in this way are confirmed by the numerical parameters presented (Table 4 and Figure 2).

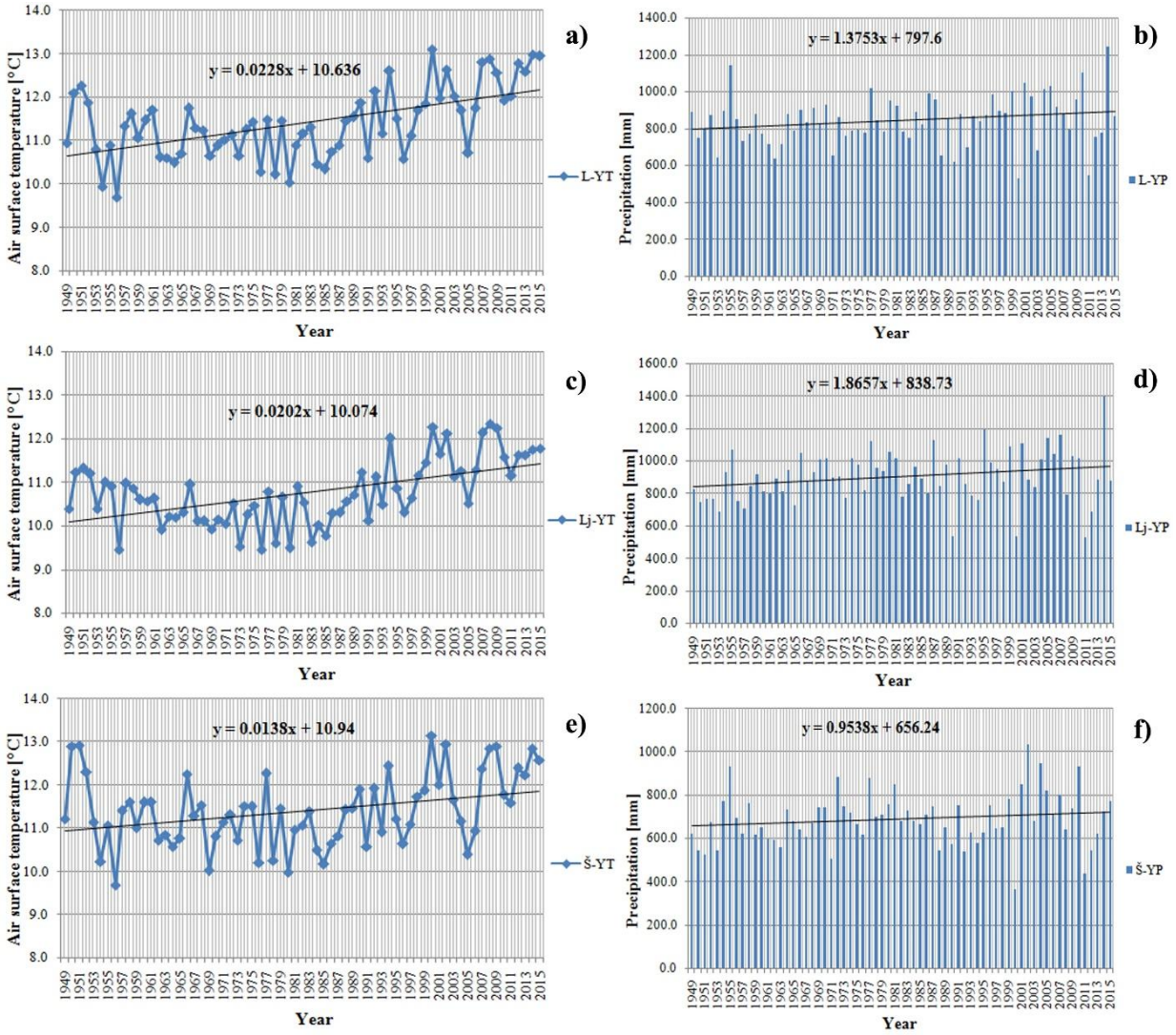

Figure 2. Linear trends: a, b) mean annual air temperatures and precipitation amount measured in Loznica meteorological station; c, d) mean annual air temperatures and precipitation for the Ljubovija meteorological station; e, f) mean annual air temperatures and precipitation for the Šabac meteorological station.

Table 4. Summary results of the trend analysis of annual air temperatures and precipitation in the Mačva district (1949-2015).

Time series	Trend equation	Standard MK test
L-YT	*Positive trend*	*Statistically significant positive trend*
Lj-YT	*Positive trend*	*Statistically significant positive trend*
Š-YT	*Positive trend*	*Statistically significant positive trend*
L-YP	*Positive trend*	*Statistically significant positive trend*
Lj-YP	*Positive trend*	*Statistically significant positive trend*
Š-YP	*No trend*	*No trend*

In the Mačva district, for time series relating to the mean annual air temperature L-YT, Lj-YT and Š-YT, the p value is the same and amounts to <0.0001. There is a statistically significant positive trend in these time series. As the computed p-value is lower than the significance level alpha = 0.05, they should reject the null hypothesis H0, and accept the alternative hypothesis Ha. The risk to reject the null hypothesis is Ha, while it is true is lower than 0.01%.

Similar results can be identified in the literature. Klein-Tank & Können (2003) have established a trend of increasing air temperature in Europe since 1979, both on an annual and seasonal basis. Milosevic et al. (2017) in Slovenia have identified a significant increase in mean annual, mean maximum and mean minimum air temperatures (per decade of 0.3-0.5 °C). By analyzing data from 52 meteorological stations in Greece,

Mamara et al. (2016) found a negative trend between 1960 and 1976. A statistically significant positive trend has been reported since 1977-2004. years. Similarly, in the near region temperature increase is dominant in Montenegro (Burić et al., 2014), Bosnia and Herzegovina (Trbić et al., 2017; Popov et al., 2018a; Popov et al., 2018b). In the territory of Serbia in the region of Vojvodina (Gavrilov et al., 2015; Gavrilov et al., 2016) and in Kosovo and Metohija (Gavrilov et al., 2018) positive trends in air temperature were also observed.

Time series in terms of mean sums of precipitation in the Mačva District show slightly different results. In two time series, L-YP and Lj-YP, a statistically significant positive trend was observed. The only time series from all analyzed in which there is no trend is W-YP. For the above time series, the p value is <0.0001. As the computed p-value is lower than the significance level alpha = 0.05, one should reject the null hypothesis H0, and accept the alternative hypothesis Ha. The risk to reject the null hypothesis Ha, while it is true is lower than 0.01 %. For time seris Š-YP, p value is 0.1517. As the computed p-value is greater than the significance level alpha=0.05, one cannot reject the null hypothesis H0. The risk to reject the null hypothesis H0 while it is true is 15.18%.

There is some agreement on increasing precipitation in the study area and globally. The Mediterranean area is exposed to a decrease in average rainfall. This scenario is expected to continue in the future, with the 20% decrease (IPCC, 2014). An example of a Mediterranean country that showed a similar scenario is Greece (Markonis, 2016). These authors have found a decrease in annual precipitation over most of the territory since 1950. However, since the 1980s, there has been a trend of increasing annual precipitation. For these reasons, it is difficult to find similar results in the literature in terms of increasing rainfall over a wider area. Decrease of rainfall is dominant in Bosnia and Herzegovina (Popov et al., 2019a), Montenegro (Burić et al., 2018a; Burić et al., 2018b), Slovenia (Milošević et al., 2013; Milošević et al., 2013). 2017). The paper by Gocić & Trajković (2013) found that there is no trend in the case of annual rainfall at most stations in Serbia. A positive trend was observed at the seasonal level, during the autumn and winter months. Analyzing precipitation trends in Vojvodina, Tošić et al. (2014) found that there are positive trends in precipitation on a yearly and seasonal basis (winter and autumn). Rainfall trends were observed during spring and winter.

CONCLUSION

Based on the results presented, it is difficult to draw general conclusions, but certain conclusions can be drawn. First, positive trends in air temperatures are dominant. These trends can be explained by the effect of global warming, which is also expressed at regional and local level (Hardy, 2006). In the case of precipitation, positive trends dominate in two time series, while one time series does not establish a trend. This is generally in line with global precipitation trends, however, in recent decades the Mediterranean has seen a decrease in precipitation. For these reasons, further research into these cases is needed in order to determine possible causes. Thus, it would be desirable to analyze other parameters (temperature extremes, air temperature and precipitation by season). That is why this paper provides a solid foundation in future climate research as it provides insights into the dynamics of climate over the past decades. Also, future projections of climate in Europe and the Mediterranean predict a higher incidence of extreme climate events, such as drought. Drought is causing a number of socio-economic changes related to nature, agriculture and available water resources. Therefore, it is necessary to implement appropriate adaptation measures (Bressers et al., 2016). Mačva district and Mačva, as a significant agricultural area, require some adaptation measures to climate change, as defined by the Report of the Republic of Serbia under the UN Framework Convention on Climate Change (Ministry of Environmental Protection, 2017).

ACKNOWLEGMENTS

This paper was created as a result of project No. III43007 funded by the Ministry of Education, Science and Technological Development of the Republic of Serbia.

REFERENCES

Alexandersson, H. 1986. A homogeneity test applied to precipitation data. Journal of Climatology, 6, pp. 661-675.

Armenski, T., Stankov, U., Dolinaj, D., Mesaroš, M., Jovanović, M., Pantelić, M., Pavić, D.,Popov, S., Popović, Lj., Frank, A., & Ćosić, Đ. 2014. Social and Economic Impact ofDrought on Stakeholders in Agriculture, Geographica Pannonica, 18(2), pp. 34-42. doi: 10.5937/GeoPan1402034A

Bačević, R. N., Vukoičić, Z. D., Nikolić, M., Janc, N., Milentijević, N., & Gavrilov, B. M. 2017. Aridity in Kosovo and Metohija, Serbia. Carpathian Journal of Earth and Environmental Sciences, 12(2), pp. 563-570.

Bačević, R. N., Pavlović, M., & Rašljanin, I. 2018. Trend Assessing Using Mann-Kendall'sTest for Priština Meteorological Station Temperature and Precipitation Data, Kosovo and Metohija, Serbia. The University Thought-Publication in Natural Sciences, (8)2, pp. 39-43. doi: 10.5937/univtho8-19513

Bajat, B., Blagojević, D., Kilibarda, M., Luković, J., & Tošić, I. 2015. Spatial Analysis of the Temperature Trends in Serbia during the Period 1961-2010. Theoretical and Applied Climatology, 121(1), pp. 289-301.

Blunden, J., Arndt, D. S., & Hartfield, G. 2018. State of the Climate in 2017, Bulletin of American Meteorogical Society, 99(8), Si-S332.

Burić, D., Luković, J., Ducić, V., Dragojlović, J., & Doderović, M. 2014a. Recent trends in daily temperature extremes over southern Montenegro (1951-2010), Natural Hazards Earth Systems. Sci., 14, pp. 67-72.

Burić, D., Ducić, V., Mihajlović, J., Luković, J., & Dragojlović, J. 2014b. Relationship between the precipitation variability in

Montenegro and the Mediterranean oscillation. Bulletin of the Serbian Geographical Society. 94(4), pp. 109-120. doi: 10.2298/GSGD1404109B

Burić, B. D., Dragojlović, M. J., Milenković, M., Popović, Z. Lj., & Doderović, M. M. 2018a. Influence of variability of the East Atlantic Oscillation on the air temperature in Montenegro. Thermal Science. 22(1B), pp. 759-766.

Burić, D., Ducić, V., & Mihajlović, J. 2018b. Relationship between mean annual temperatures and precipitation sums in Montenegro between 1951-1980 and 1981-2010 periods. Bulletin of the Serbian Geographical Society, 98(1), pp. 31-48.

Bressers, J. T. A., Bressers, N., & Larrue, C., (Ed.) 2016. Governance for Drought Resilience: Land and Water Drought Management in Europe. Springer.

Ćirković, Lj. 1977. Climate properties of Western Serbia. Collection of Papers of Geographical Institute "Jovan Cvijić", 29, pp. 105-133. (In Serbian)

Ducić, D. & Radovanović, M. 2005. Climate of Serbia. Belgrade: ZUNS. (In Serbian)

European Environment Agency (EEA), 2017. Climate change, impacts and vulnerability in Europe 2016, an indicator - based report (EEA Report No. 1/2017). European Environment Agency, Copenhagen.

Fei, J., Zhaohua, W., Jianping, H., & Chassignet, E. P. 2014. Evolution of Land Surface Air Temperature Trend. Nature Climate Change, 4, pp. 462-466.

Gajić, M., & Vujadinović, S. 2007. Thermal Regime in the area of Jadar. Collection of Papers, Faculty of Geography, LV, pp. 29-38. (In Serbian).

Gavrilov, M. B., Marković, S. B., Jarad, A., & Korać, V. M. 2015. The analysis of temperature trends in Vojvodina (Serbia) from 1949 to 2006. Thermal Science. 19(2), pp. 339-350.

Gavrilov, M. B., Tošić, I., Marković, S. B., Unkašević, M., & Petrović, P. 2016. The analysis of annual and seasonal temperature trends using the Mann-Kendall test in Vojvodina, Serbia. Időjárás. 122(2), pp. 203-216.

Gavrilov, M. B., Marković, S. B., Janc, N., Nikolić, M., Valjarević, A., Komac, B., Zorn, M., Punišić, M., & Bačević, N. 2018. Assessing average annual air temperature trends using the Mann-Kendall test in Kosovo. Acta geographica Slovenica. 58(1),pp. 8-25.

Gilbert, R. O. 1987.Statistical methods for environmental pollution monitoring. New York: Van Nostrand Reinhold.

Gocic, M., & Trajkovic, T. 2013. Analysis of precipitation and drought data in Serbia over the period 1980-2010,Journal of Hydrology, 494, pp. 32-42.

Grčić, M. & Grčić, Lj. 2002. Mačva, Posavina and Pocerina, Belgrade: Faculty of Geography. (In Serbian)

Hardy, J., T. 2006. Climate change – causes, effects and solutions. Chichester.

Hrnjak, I., Lukić, T., Gavrilov, M. B., Marković, S.B.,Unkašević, M., & Tošić, I.2014. Aridity in Vojvodina, Serbia. Theoretical and Applied Climatology, 115(1-2), pp. 323-332.

IPCC, 2014. Climate change 2014: synthesis report, in: Core Writing Team, Pachauri, R. K., Meyer, L. A., (Eds.), Contribution of Working Groups I, II and III to the Fifth Assessment Report of the Intergovernmental Panel on Climate Change. IPCC, Geneva, pp. 151.

IPCC, 2018. Summary for Policymakers. In: Masson-Delmotte V, Zhai P, Pörtner HO, Roberts D, Skea J, Shukla PR, Pirani A, Moufouma-Okia W, Péan C, Pidcock R, Connors S, Matthews JBR, Chen Y, Zhou X, Gomis MI, Lonnoy E, Maycock T, Tignor M, Waterfield T (eds.) Global warming of 1.5°C. An IPCC Special Report on the impacts of global warming of 1.5°C above pre-industrial levels and related global greenhouse gas emission pathways, in the context of strengthening the global response to the threat of climate change, sustainable development, and efforts to eradicatepoverty. World Meteorological Organization, Geneva, pp. 3-24.

Ivanović, R., Valjarević, A., Vukoičić, D., & Radovanović, D. 2016. Climatic regions of Kosovo and Metohija. The University Thought-Publication in Natural Sciences, 6(1), pp. 49-54. doi: 10.5937/univtho6-10409

Karmeshu, N. 2012. Trend detection in annual temperature & precipitation using the Mann Kendall Test – a case study to assess climate change on select states in the northeastern United States. Master's thesis, University of Pennsylvania. Philadelphia.

Kendall, M.G. 1975. Rank correlation methods

Klein Tank, A. M. G. & Können, G. P., 2003. Trends in Indices of Daily Temperature and Precipitation Extremes in Europe, 1946-99. Journal of Climate, 16(22), pp. 3665–3680.

Kocsis, T., Kovács-Székely, I., & Anda, A. 2019. Homogeneity tests and non-parametric analyses of tendencies in precipitation time series in Keszthely, Western Hungary. Theoretical and Applied Climatology.doi:10.1007/s00704-019-03014-4

Kovats, R. S., Valentini, R., Bouwer, L. M., Georgopoulou, E., Jacob, D., Martin, E., Rounsevell, M., & Soussana, J. F. 2014. Europe. In: Climate Change 2014: Impacts, Adaptation, and Vulnerability. Part B: Regional Aspects. Contribution of Working Group II to the Fifth Assessment Report of the Intergovernmental Panel on Climate Change [Barros, V.R., C.B. Field, D.J. Dokken, M.D. Mastrandrea, K.J. Mach, T.E. Bilir, M. Chatterjee, K.L. Ebi, Y.O. Estrada, R.C. Genova, B. Girma, E.S. Kissel, A.N. Levy, S. MacCracken, P.R. Mastrandrea, and L.L.White (eds.)]. Cambridge University Press, Cambridge, United Kingdom and New York, NY, USA, pp. 1267-1326.

Luterbacher, J., Dietrich, D., Xoplaki, E., Grosjean, M., & Wanner, H. 2004. European Seasonal and Annual Temperature Variability, Trends, and Extremes since 1500. Science, 303, pp. 1499-1503.

Mamara, A., Argiriou, A. A., & Anadranistakis, M. 2016. Recent Trend Analysis of Mean Air Temperature in Greece Based on Homogenized Data. Theoretical and Applied Climatology, 126(3-4), pp. 543-573.

Markonis, Y., Batelis, S. C., Dimakos, Y., Moschou, E., & Koutsoyiannis, D. 2017. Temporal and spatial variability of rainfall over Greece. Theoretical and Applied Climatology, 130, pp. 217-232.

Milentijević, N., Dragojlović, J., Ristić, D., Cimbaljević, M., Demirović, D. & Valjarević, A. 2018. The assessment of aridity in Leskovac Basin, Serbia (1981-2010), Journal of the Geographical Institute "Jovan Cvijić", 68(2), pp. 249-264.

Milutinović, A. 1974. Classification of climate of Yugoslavia according to Köppen and modification of this classification according to our climate properties, SHSS, IX Consulting of climatologist of Yugoslavia, Belgrade. (In Serbian)

Milošević, D., Savić, S. & Žiberna, I. 2013. Analysis of the Climate Change in Slovenia: Fluctuations of Meteorological Parameters for the Period 1961-2011 (Part I). Bulletin of the Serbian Geographical Society, 93(1), pp. 1-14. doi: 10.2298/GSGD1301001M

Milošević, D., Savić, S., Stankov, U., Žiberna, I., Pantelić, M., Dolinaj, D., & Leščešen, I. 2017. Maximum temperatures over Slovenia and their relationship with atmospheric circulation patterns. Geografie. 122(1), pp. 1-20.

Ministry of Environmental Protection, 2017. Second National Communication of the Republic of Serbia under the United Nations Framework Convention on Climate Change. Ministry of Environmental Protection, Belgrade.

Nguyen, P. A., Thorstensen, S., Sorooshian, K., Hsu, A., Aghakouchak, H., Ashouri, H. T., & Braithwaite, D. 2018. Global precipitation trends across spatial scales using satellite observations.Bulletin of the American Meteorological Society. 99, pp. 689-697.

Philandras, C. M., Nastos, P. T., Kapsomenakis, J., Douvis, K. C., Tselioudis, G., & Zerefos, C. S. 2011. Long term precipitation trends and variability within the Mediterranean region. Natural Hazards and Earth System Sciences. 11, pp. 3235-3250.

Popov, T., Gnjato, S., & Trbić, G. 2018a. Changes in temperature extremes in Bosnia and Herzegovina: A fixed tresholds-based index analysis. Journal of the Geographical Institute "Jovan Cvijić" SASA. 68(1), pp. 17-33.

Popov, T., Gnjato, S., Trbić, G., & Ivanišević, M. 2018b. Recent trends in extreme temperature indices in Bosnia and Herzegovina. Carpathian Journal of Earth and Environmental Sciences. 13, pp. 211-224.

Popov, T., Gnjato, S., & Trbić, G. 2019a. Changes in precipitation over the East Herzegovina region. Bulletin of the Serbian Geographical Society. 99(1), pp. 29-44.

Popov, T., Gnjato, S., & Trbić, G. 2019b. Analysis of extreme precipitation over the Peripannonian region of Bosnia and Hercegovina. Időjárás. 122(4), pp. 433-452. doi:10.28974/idojaras.2018.4.5

Putniković, S., & Tošić, I. 2018. Relationship between atmospheric circulation weather types and seasonal precipitation in Serbia. Meteorology and Atmospheric Physics, 130(4), pp. 393-403. doi: 10.1007/s00703-017-0524-y

Radaković, G. M., Tošić, A. I., Bačević, R. N., Mađan, D., Marković, S. B. & Gavrilov, M. B. 2017. The analysis of aridity in Central Serbia from 1949-2015. Theoretical and Applied Climatology, 133(3-4), pp. 887-898. doi:10.1007/s00704-017-2220-8

Rahman, M.A., Yunsheng, L., &Sultana, N. 2017. Analysis and prediction of rainfall trends over Bangladesh using Mann–Kendall, Spearman's rho tests and ARIMA model. Meteorology and Atmospheric Physics. 129(4), pp. 409-424.

Rakićević, T. 1980. Climate zoning of SR of Serbia. Collection of Papers of Geographical Instite "Jovan Cvijić", 27, pp. 29-42.

RHSS, 2019. Official Website RHSS, http://www.hidmet.gov.rs/ciril/meteorologija/klimatologija_godisnjaci.php (retrieved 10 November 2019)

Savić, S., Milošević, D., Marković, V., & Kujundžić-Dačović, R. 2012. Homogenisation of Mean AirTemperature Time Series from Vojvodina (North Serbia). Geographica Pannonica. 16(2), pp. 38-43.

Spinoni, J., Naumann, G., & Vogt, V. J. 2017. Pan-European seasonal trends and recent changes of drought frequency and severity. Global and Planetary Change. 148, pp. 113-130.

Tošić, I., Hrnjak, I., Gavrilov, M. B., Unkašević, M., Marković, S. B., & Lukić, T. 2014a. Annual and seasonal variability of precipitation in Vojvodina. Theoretical and Applied Climatology, 117,pp. 331-341. doi:10.1007/s00704-013-1007-9

Tošić, I., & Unkašević, M. 2014b. Analysis of wet and dry periods in Serbia. International Journal of Climatology. 34(5), pp. 1357-1368.

Tošić, I., Zorn, M., Ortar, J., Unkašević, M., Gavrilov, M. B., & Marković, S. B. 2016. Annual and seasonal variability of precipitation and temperatures in Slovenia from 1961 to 2011. Atmospheric Research. 168, pp. 220-233.

Trbić, G., Popov, T. & Gnjato, S. 2017. Analysis of Air Temperature Trends in Bosnia and Herzegovina. Geographica Pannonica, 21(2), pp. 68-84.

Unkašević, M., & Tošić, I. 2013. Trends in temperature indices over Serbia: relationships to large-scale circulation patterns. International Journal of Climatology, 33(15), pp. 3152-3161.

Wibig, J., & Glowicki, B. 2002. Trends of minimum and maximum temperature in Poland. Climate Research, 20, pp. 123-133.

XLSTAT,http://www.xlstat.com/en/ (retrieved 10 December 2019)

UNIVERSITY THOUGHT
Publication in Natural Sciences, Vol.10, No.1, 2020, pp. 44-50.
DOI: https://doi.org/10.5937/univtho10-24982
Original Scientific Paper

THE EXTERNAL AGGREGATION NEWTON'S METHOD FOR SOLVING NONLINEAR EQUATIONS AND APPLICATIONS

MARIJA PAUNOVIĆ[1], DEJAN ĆEBIĆ[2], NEBOJŠA RALEVIĆ[3,⋆]

[1]Faculty of Hotel Management and Tourism in Vrnjacka Banja, University of Kragujevac, Vrnjacka Banja, Serbia
[2]Faculty of Mining and Geology, University of Belgrade, Belgrade, Serbia
[3]Faculty of Technical Sciences, University of Novi Sad, Novi Sad, Serbia

ABSTRACT

Different modified Newton's methods are widely used in modern computational engineering science, applied mechanics, economics, optimization problems and other disciplines. On the other hand aggregation of information takes a significant place in many knowledge-based systems, where aggregation of data or values is needed. In this paper we theoretically analysed a new modification of Newton's method based on aggregation function applied on finding multiple roots of nonlinear equations, and numerically verified theoretical results on the examples with simple and multiple roots. Numerical analysis of the proposed approach with obtained results and the related discussion are presented on examples in practice.

Keywords: Newton's method, Aggregation function, Order of convergence.

INTRODUCTION

Having in mind that Newton's methods have a wide range of applications, a new modification of Newton's method is presented. Proposed method for solving nonlinear equations is based on aggregation function. Some existing well-known modifications of Newton's method, based on arithmetic, geometric, harmonic and root-power mean are very closely related to the special members of this method. The convergence properties of the proposed method are discussed and it is shown that the order of convergence for multiple roots is one. It is proved that the iterative sequence defined by this method converges to roots, for any initial iteration sufficiently close to root.

The rest of the paper is as follows. In Section 2 we briefly describe the concepts of aggregation functions. Definition of the method and analysis of its convergence are presented in Section 3. Finally, sections 4 we show the computational results of some relevant numerical tests to compare the efficiencies of the proposed aggregation methods (including Newton's method).

AN AGGREGATION FUNCTIONS

In this section we present a brief recall of definitions, examples and properties of aggregation functions. Let I be interval real number.

Definition 1. An $n-$ary **aggregation function** is a function $\mathcal{A}_{[n]} : I^n \to I$ such that

i) $\mathcal{A}_{[n]}(x_1, ..., x_n) \leq \mathcal{A}_{[n]}(y_1, ..., y_n)$ whenever $x_i \leq y_i$ for all $i \in \{1, ..., n\}$ ($\mathcal{A}$ is monotonically increasing function in all its arguments).

ii) $\inf\limits_{x\in I^n} \mathcal{A}_{[n]}(x) = \inf I$ and $\sup\limits_{x\in I^n} \mathcal{A}_{[n]}(x) = \sup I$, $x = (x_1, ..., x_n)$ (boundary condition).

An **aggregation function** is a function $\mathcal{A} : \bigcup\limits_{n\in\mathbb{N}} I^n \to I$ such that for $n = 1$ holds $\mathcal{A}(x) = x$, for all $x \in I$, whose restriction is $\mathcal{A}|_{I^n} = \mathcal{A}_{[n]}$, for any $n \in \mathbb{N}$.

For aggregation function is required to comply with additional features such as

iii) $\mathcal{A}_{[n]}(x, x, ..., x) = x$ for all $x \in I$ ($\mathcal{A}_{[n]}$ is idempotent function).
iv) $\mathcal{A}_{[n]}(x_1, ..., x_n) = \mathcal{A}_{[n]}(x_{p_1}, ..., x_{p_n})$ for any permutation $(p_1, ..., p_n)$ of set $\{1, ..., n\}$ ($\mathcal{A}_{[n]}$ is symmetric function in all its arguments).
v) $\mathcal{A}_{[n]}$ is continuous function.
vi) $\mathcal{A}_{[n]} \in C^{\ell}((I^{\circ})^n)$ (The function $\mathcal{A}_{[n]}$ has continuous derivatives up to the order ℓ in all variables).

Remark. It is customary to take the $I = [0, 1]$. In this case boundary condition reduces to $\mathcal{A}(0, ..., 0) = 0$ and $\mathcal{A}(1, ..., 1) = 1$.

Here are some examples that we will use in our future work, in the case that is $n = 2$, when the aggregation function is defined Table 1.

Root-power means

$$M_p(a, b) = (\frac{a^p + b^p}{2})^{1/p} \quad (p \neq 0).$$

Marginal members of these classes are $M_0 = G = M_{\log a}$, which is the geometric mean, while $M_{\infty} = Max$ and $M_{-\infty} = Min$. So, $A = M_1$, $Q = M_2$ and $C = M_3$.

Thus, we are going to present a definition, some examples and properties of aggregation functions (see (Grabisch et al., 2009; Klement et al., 2000; Klir & Yuan, 1995)).

⋆ Corresponding author: nralevic@uns.ac.rs

Table 1.

$\mathcal{A}(a,b) =$	Mean	Parameter
$\frac{a+b}{2}$	Arithmetic (A)	
$\frac{2}{\frac{1}{a}+\frac{1}{b}}$	Harmonic (H)	
$\sqrt{ab}$	Geometric (G)	
$\sqrt{\frac{a^2+b^2}{2}}$	Quadratic (Q)	
$\sqrt[3]{\frac{a^3+b^3}{2}}$	Cubic (C)	
$\frac{a^p b^{1-p}+a^{1-p}b^p}{2}$	Heinz (Z_p)	$0 \leqslant p \leqslant \frac{1}{2}$
$(\frac{a^p+(ab)^{p/2}+b^p}{3})^{1/p}$	Generalized Heron (H_p)	$p \neq 0$
$\frac{a^s b^t+a^t b^s}{2}$	Symmetric Q_p	$s = \frac{1+\sqrt{p}}{2}, t = \frac{1-\sqrt{p}}{2}$
$\frac{a^2+b^2}{a+b}$	Contraharmonic (CH)	
$\frac{a^p+b^p}{a^{p-1}+b^{p-1}}$	Generalized Contraharmonic (GCH)	

Here we consider the aggregation functions as functions of two variables.

The methods obtained for a given aggregation function will be given the appropriate name. Thus, the quadratic and cubic mean give *quadratic mean Newton's method* (shortly QN method) and *cubic mean Newton's method* (shortly CN method). The contraharmonic mean, generalized contraharmonic mean, Heinz mean, Heron mean, symmetric mean, give *contraharmonic mean Newton's method* (shortly CHN method), *generalized contraharmonic mean Newton's method* (shortly GCHN method), *Heinz mean Newton's method* (shortly HZN method), *Heron mean Newton's method* (shortly HRN method) and *symmetric mean Newton's method* (shortly SMN method), respectively.

Definition 2. A quasi aggregation function of class ℓ is a function $\mathcal{A} : I^n \to I$, $n \in \mathbb{N}$ (where I is the interval of real numbers) such that $\mathcal{A}$ is idempotent, symmetric and $\mathcal{A} \in C^\ell(I^\circ)$, $\ell \in \mathbb{N}$.

Lemma 3. *If $\mathcal{A} : I^n \to I$, $n \in \mathbb{N}$ is a quasi aggregation function of class ℓ, then*

i) $\mathcal{A}_{x_i}(x, x, ..., x) = \mathcal{A}_{x_j}(x, x, ..., x)$, $x \in I$, $i, j = 1, ..., n$.
ii) $\mathcal{A}_{x_i}(x, x, ..., x) = \frac{1}{n}$, $x \in I$, $i, j = 1, ..., n$,

where $\mathcal{A}_{x_i}$ is $\frac{\partial \mathcal{A}}{\partial x_i}$.

For $n = 2$, $\mathcal{A}_x(x, x) = \mathcal{A}_y(x, x) = \frac{1}{2}$.

Lemma 4. *If $\mathcal{A} : \bigcup_{n\in\mathbb{N}} I^n \to I$ is a quasi aggregation function of class ℓ, (signed $\frac{\partial \mathcal{A}}{\partial x_i}$ with $\mathcal{A}_{x_i}$) then holds*

i) $\mathcal{A}_x(x, y) = \mathcal{A}_y(y, x)$;
ii) $\mathcal{A}_{xx}(x, y) = \mathcal{A}_{yy}(y, x)$;
iii) $\mathcal{A}_{xy}(x, y) = \mathcal{A}_{yx}(y, x)$;
iv) $\mathcal{A}_{xy}(x, y) = \mathcal{A}_{xy}(y, x)$ *(A_{xy} is symetric function);*
v) $\mathcal{A}_{xxy}(x, y) = A_{yyx}(y, x)$;
vi) $\mathcal{A}_{xxx}(x, y) = \mathcal{A}_{yyy}(y, x)$.

DEFINITION OF THE METHOD AND ANALYSIS OF ITS CONVERGENCE

Calculating the real root α of nonlinear equation

$$f(x) = 0, \quad f : I \subseteq \mathbb{R} \to \mathbb{R}. \tag{1}$$

is a common problem in the field of applied mathematics.

The root α is said to be *simple* if $f(\alpha) = 0$ and $f'(\alpha) \neq 0$. If $f(\alpha) = f'(\alpha) = ... = f^{(k-1)}(\alpha) = 0$ and $f^{(k)}(\alpha) \neq 0$ for $k \geq 1$ then α is of *multiplicity* k.

If the sequence $\{x_n\}$ tends to a limit α such that

$$\lim_{n\to\infty} \frac{x_{n+1} - \alpha}{(x_n - \alpha)^q} = C, \tag{2}$$

for some $C \neq 0$ and $q \geq 1$, then the *order of convergence* of the sequence $\{x_n\}$ is q and C is known as the *asymptotic error constant* (AEC) (see (Wait, 1979)). If $q = 1$, $q = 2$ or $q = 3$, the convergence is said to be *linear*, *quadratic* or *cubic*, respectively. Let $e_n = x_n - \alpha$ be the error in the n^{th} iteration of the method which produces the sequence $\{x_n\}$. Then, the relation (2) can be rewritten as

$$e_{n+1} = Ce_n^q + O(e_n^{q+1}) = O(e_n^q)$$

which is called the *error equation*. The value of q is called the *order of convergence* and C is known as the *asymptotic error constant of this method*.

There are several classical methods for solving the equation (1) and the most famous is Newton's method (shortly N method) defined by

$$x_{n+1} = x_n - \frac{f(x_n)}{f'(x_n)}, \quad n = 0, 1, \ldots, \tag{3}$$

where x_0 is the initial guess that is sufficiently close to α. Newton's method is quadratical convergence techniques for simple roots with the error equation

$$e_{n+1} = \frac{f''(\alpha)}{2f'(\alpha)} \cdot e_n^2 + O(e_n^3).$$

Below are some examples of two-step Newton's methods determined with

$$x_{n+1} = x_n - \frac{f(x_n)}{F(f'(x_n), f'(\tilde{x}_n))}, \tag{4}$$

where $\tilde{x}_n = x_n - \frac{f(x_n)}{f'(x_n)}$, $n = 0, 1, \ldots$.

The special cases of this method, defined by (4), for simple zeros can be founded in Weerakoon and Fernando (Weerakoon & Fernando, 2000) ($F = A$), Özban (Özban, 2004) ($F = H$), Lukić and Ralević (Lukić & Ralević, 2008) ($F = G$), Also Ralević and Lukić in (Ralević & Lukić, 2005),(Lukić et al., 2006) ($F = M_p$). Certain generalizations, modifications, improvements and further analysis of the mentioned mean-based methods one can find in (Babajee & Dauhoo, 2006; Frontini & Sormani, 2003; Herceg & Herceg, 2013b,a; Homeier, 2003; McDougall & Wotherspoon, 2014).

For reasons of feasibility of the method, the authors of (Lukić & Ralević, 2008; Lukić et al., 2006) and (Ralević & Lukić, 2005) take $\text{sign}(f'(x_0)) \cdot G(|f'(x_n)|, |f'(\tilde{x}_n)|)$ and $\text{sign}(f'(x_0)) \cdot M_p(|f'(x_n)|, |f'(\tilde{x}_n)|)$ instead of $G(f'(x_n), f'(\tilde{x}_n))$ and $M_p(f'(x_n), f'(\tilde{x}_n))$ in given methods, respectively.

The following is a generalized method based on on aggregation functions, *external aggregation Newton's method* will be introduced.

Let A be quasi aggregation function of class ℓ. The method which under consideration defined by

$$\begin{aligned} x_{n+1} &= x_n - \frac{f(x_n)}{\mathcal{A}(f'(x_n), f'(\tilde{x}_n))}, \\ \text{where } \tilde{x}_n &= x_n - \frac{f(x_n)}{f'(x_n)}, \quad n = 0, 1, \ldots \end{aligned} \tag{5}$$

we call *external aggregation Newton's method, shortly EANM*.

The next theorem (see Ralević & Ćebić (2019)) hold.

Theorem 5. *Let $f : I \subseteq \mathbb{R} \to \mathbb{R}$ where I is an open interval. Assume that f is sufficiently differentiable function in the interval I and f has a simple root $\alpha \in I$. If x_0 is sufficiently close to α, then the EANM converges cubically and satisfies the following error equation:*

$$e_{n+1} = e_n^3\Big(c_2^2(2f'(\alpha)\mathcal{A}_{xx}(f'(\alpha), f'(\alpha)) + 1) + \frac{1}{2}c_3\Big) + o(e_n^3), \tag{6}$$

where $e_n = x_n - \alpha$, $c_j = \frac{f^{(j)}(\alpha)}{j!\, f'(\alpha)}$ for $j = 1, 2, 3, \ldots$ are constants, and A is a generalized aggregation operator of class 3.

Example 6. If $\mathcal{A}(x, y) = M_p(x\, y) = (\frac{x^p + y^p}{2})^{\frac{1}{p}}$, we have that the error equation is:

$$e_{n+1} = \frac{1}{2}((p+1)c_2^2 + c_3)e_n^3 + o(e_n^3).$$

In the following Theorem we give the error equation of EANM method in a case when we approximate multiple roots.

Theorem 7. *Let $f : I \subseteq \mathbb{R} \to \mathbb{R}$, where I is an open interval. Assume that f is sufficiently differentiable function on the interval I and f has a multiple root of multiplicity $k > 1$ in $\alpha \in I$. If x_0 is sufficiently close to α, then the method (5) converges linearly to α and satisfies the following error equation:*

$$e_{n+1} = (1 - \frac{2}{k(1 + (\frac{k-1}{k})^{k-1})})e_n + \frac{2(K-1)d_{k+1}}{k(1 + (\frac{k-1}{k})^{k-1})}e_n^2 + o(e_n^2) \tag{7}$$

where $e_n = x_n - \alpha$, $d_{k+i} = \frac{f^{(k+i)}(\alpha)/(k+i)!}{f^{(k)}(\alpha)/k!}$ and $K = \frac{\frac{k+1}{k} + (\frac{k-1}{k})^{k-1} \cdot \frac{k^2+k-1}{k^2}}{1 + (\frac{k-1}{k})^{k-1}}$.

Proof. Since the function f has the multiple root α of multiplicity k, i.e. $f(\alpha) = f'(\alpha) = ... = f^{(k-1)}(\alpha) = 0$, $f^{(k)}(\alpha) \neq 0$, using Taylor expansion of $f(x_n)$ at α, we obtain

$$\begin{aligned} f(x_n) &= f(\alpha) + f'(\alpha)e_n + \frac{1}{2!}f''(\alpha)e_n^2 + ... \\ &\quad + \frac{1}{k!}f^{(k)}(\alpha)e_n^k + \frac{1}{(k+1)!}f^{(k+1)}(\alpha)e_n^{k+1} \\ &\quad + \frac{1}{(k+2)!}f^{(k+2)}(\alpha)e_n^{k+2} + o(e_n^{k+2}) \\ &= \frac{1}{k!}f^{(k)}(\alpha)e_n^k + \frac{1}{(k+1)!}f^{(k+1)}(\alpha)e_n^{k+1} \\ &\quad + \frac{1}{(k+2)!}f^{(k+2)}(\alpha)e_n^{k+2} + o(e_n^{k+2}) \\ &= \frac{f^{(k)}(\alpha)}{k!}[e_n^k + \frac{f^{(k+1)}(\alpha)}{(k+1)f^{(k)}(\alpha)}e_n^{k+1} \\ &\quad + \frac{f^{(k+2)}(\alpha)}{(k+2)(k+1)f^{(k)}(\alpha)}e_n^{k+2} + o(e_n^{k+2})], \\ &= \frac{f^{(k)}(\alpha)}{k!}[e_n^k + d_{k+1}e_n^{k+1} + d_{k+2}e_n^{k+2} + o(e_n^{k+2})]. \end{aligned} \tag{8}$$

Similarly,

$$\begin{aligned} & f'(x_n) \\ &= f'(\alpha) + f''(\alpha)e_n + \frac{f'''(\alpha)}{2!}e_n^2 + ... + \frac{f^{(k)}(\alpha)}{(k-1)!}e_n^{k-1} \\ &\quad + \frac{f^{(k+1)}(\alpha)}{k!}e_n^k + \frac{f^{(k+2)}(\alpha)}{(k+1)!}e_n^{k+1} + o(e_n^{k+1}) \\ &= \frac{f^{(k)}(\alpha)}{(k-1)!}e_n^{k-1} + \frac{f^{(k+1)}(\alpha)}{k!}e_n^k + \frac{f^{(k+2)}(\alpha)}{(k+1)!}e_n^{k+1} + o(e_n^{k+1}) \\ &= \frac{f^{(k)}(\alpha)}{k!}[ke_n^{k-1} + (k+1)d_{k+1}e_n^k + (k+2)d_{k+2}e_n^{k+1} + o(e_n^{k+1})] \\ &= \frac{f^{(k)}(\alpha)}{(k-1)!}e_n^{k-1}[1 + \frac{k+1}{k}d_{k+1}e_n + \frac{k+2}{k}d_{k+2}e_n^2 + o(e_n^2)] \end{aligned} \tag{9}$$

If we divide (8) by (9), we have

$$\begin{aligned} \frac{f(x_n)}{f'(x_n)} &= \tfrac{1}{k}e_n\Big(1 + d_{k+1}e_n + d_{k+2}e_n^2 + o(e_n^2)\Big) \\ &\quad \cdot\Big(1 + \tfrac{k+1}{k}d_{k+1}e_n + \tfrac{k+2}{k}d_{k+2}e_n^2 + o(e_n^2)\Big)^{-1} \\ &= \tfrac{e_n}{k}\Big(1 + d_{k+1}e_n + d_{k+2}e_n^2 + o(e_n^2)\Big) \cdot \Big[1 - \Big(\tfrac{k+1}{k}d_{k+1}e_n \\ &\quad + \tfrac{k+2}{k}d_{k+2}e_n^2 + o(e_n^2)\Big) + \\ &\quad \Big(\tfrac{k+1}{k}d_{k+1}e_n + \tfrac{k+2}{k}d_{k+2}e_n^2 + o(e_n^2)\Big)^2 + o(e_n^2)\Big] \\ &= \tfrac{e_n}{k}\Big(1 + d_{k+1}e_n + d_{k+2}e_n^2 + o(e_n^2)\Big) \cdot \Big[1 - \tfrac{k+1}{k}d_{k+1}e_n \\ &\quad + ((\tfrac{k+1}{k})^2 d_{k+1}^2 - \tfrac{k+2}{k}d_{k+2})e_n^2 + o(e_n^2)\Big] \\ &= \tfrac{e_n}{k}\Big[1 - \tfrac{1}{k}d_{k+1}e_n + (\tfrac{k+1}{k^2}d_{k+1}^2 - \tfrac{2}{k}d_{k+2})e_n^2 + o(e_n^2)\Big]. \end{aligned}$$

From $\tilde{x}_n = x_n - \frac{f(x_n)}{f'(x_n)}$, we get

$$\begin{aligned} &\tilde{x}_n - \alpha = e_n - \tfrac{f(x_n)}{f'(x_n)} \\ &= \tfrac{k-1}{k}e_n + \tfrac{1}{k^2}d_{k+1}e_n^2 + \tfrac{1}{k^3}(2kd_{k+2} - (k+1)d_{k+1}^2)e_n^3 + o(e_n^3) \\ &= \tfrac{k-1}{k}e_n\Big(1 + \tfrac{1}{k(k-1)}d_{k+1}e_n + \tfrac{1}{k^2(k-1)}(2kd_{k+2} - (k+1)d_{k+1}^2)e_n^2 + o(e_n^2)\Big), \end{aligned}$$

and

$$\begin{aligned} & f'(\tilde{x}_n) \\ &= f'(\alpha) + f''(\alpha)(\tilde{x}_n - \alpha) + \tfrac{1}{2!}f'''(\alpha)(\tilde{x}_n - \alpha)^2 + ... \\ &\quad + \tfrac{1}{(k-1)!}f^{(k)}(\alpha)(\tilde{x}_n - \alpha)^{k-1} + \tfrac{1}{k!}f^{(k+1)}(\alpha)(\tilde{x}_n - \alpha)^k \\ &\quad + \tfrac{1}{(k+1)!}f^{(k+2)}(\alpha)(\tilde{x}_n - \alpha)^{k+1} + o((\tilde{x}_n - \alpha)^{k+1}) \end{aligned}$$

$$
\begin{aligned}
&= \tfrac{1}{(k-1)!}f^{(k)}(\alpha)(\tilde{x}_n-\alpha)^{k-1}\Big[1+\tfrac{k+1}{k}d_{k+1}(\tilde{x}_n-\alpha)+\\
&\quad \tfrac{k+2}{k}d_{k+2}(\tilde{x}_n-\alpha)^2+o((\tilde{x}_n-\alpha)^2)\Big]\\
&= \tfrac{f^{(k)}(\alpha)}{(k-1)!}(\tfrac{k-1}{k})^{k-1}e_n^{k-1}\Big(1+\tfrac{1}{k(k-1)}d_{k+1}e_n+\\
&\quad \tfrac{1}{k^2(k-1)}(2kd_{k+2}-(k+1)d_{k+1}^2)e_n^2+o(e_n^2)\Big)^{k-1}\\
&\quad \cdot\Big[1+\tfrac{k+1}{k}d_{k+1}\cdot\tfrac{k-1}{k}e_n\Big(1+\tfrac{1}{k(k-1)}d_{k+1}e_n+\\
&\quad \tfrac{1}{k^2(k-1)}(2kd_{k+2}-(k+1)d_{k+1}^2)e_n^2+o(e_n^2)\Big)\\
&\quad +\tfrac{k+2}{k}d_{k+2}\cdot(\tfrac{k-1}{k}e_n)^2\Big(1+\tfrac{1}{k(k-1)}d_{k+1}e_n+\tfrac{1}{k^2(k-1)}(2kd_{k+2}\\
&\quad -(k+1)d_{k+1}^2)e_n^2+o(e_n^2)\Big)^2+o(e_n^2)\Big]\\
&= \tfrac{f^{(k)}(\alpha)}{(k-1)!}(\tfrac{k-1}{k})^{k-1}e_n^{k-1}\Big[1+(k-1)\Big(\tfrac{1}{k(k-1)}d_{k+1}e_n+\tfrac{1}{k^2(k-1)}\\
&\quad (2kd_{k+2}-(k+1)d_{k+1}^2)e_n^2+o(e_n^2)\Big)\\
&\quad +\tfrac{(k-1)(k-2)}{2}\Big(\tfrac{1}{k(k-1)}d_{k+1}e_n+o(e_n)\Big)^2+o(e_n^2)\Big]\\
&\quad \cdot\Big[1+\tfrac{k+1}{k}d_{k+1}\cdot\tfrac{k-1}{k}e_n(1+\tfrac{1}{k(k-1)}d_{k+1}e_n+o(e_n))\\
&\quad +\tfrac{k+2}{k}d_{k+2}(\tfrac{k-1}{k})^2e_n^2+o(e_n^2)\Big]\\
&= \tfrac{f^{(k)}(\alpha)}{(k-1)!}(\tfrac{k-1}{k})^{k-1}e_n^{k-1}\Big[1+\tfrac{1}{k}d_{k+1}e_n+\tfrac{1}{k^2}(2kd_{k+2}\\
&\quad -(k+1)d_{k+1}^2)e_n^2+\tfrac{(k-1)(k-2)}{2}\cdot\tfrac{1}{k^2(k-1)^2}d_{k+1}^2e_n^2+o(e_n^2)\Big]\\
&\quad \cdot\Big[1+\tfrac{k^2-1}{k^2}d_{k+1}e_n+\tfrac{k+1}{k^3}d_{k+1}^2e_n^2+\tfrac{(k+2)(k-1)^2}{k^3}d_{k+2}e_n^2+o(e_n^2)\Big]\\
&= \tfrac{f^{(k)}(\alpha)}{(k-1)!}(\tfrac{k-1}{k})^{k-1}e_n^{k-1}\Big[1+\tfrac{1}{k}d_{k+1}e_n+\tfrac{1}{k^2}(2kd_{k+2}\\
&\quad -(k+1)d_{k+1}^2+\tfrac{k-2}{2(k-1)}d_{k+1}^2)e_n^2+o(e_n^2)\Big]\\
&\quad \cdot\Big[1+\tfrac{k^2-1}{k^2}d_{k+1}e_n+\tfrac{1}{k^3}((k+2)(k-1)^2d_{k+2}\\
&\quad +(k+1)d_{k+1}^2)e_n^2+o(e_n^2)\Big]\\
&= \tfrac{f^{(k)}(\alpha)}{(k-1)!}(\tfrac{k-1}{k})^{k-1}e_n^{k-1}\Big[1+\tfrac{k^2+k-1}{k^2}d_{k+1}e_n+\\
&\quad (\tfrac{k^3+2k^2-3k+2}{k^3}d_{k+2}+\tfrac{k-2}{2k^2(k-1)}d_{k+1}^2)e_n^2+o(e_n^2)\Big]
\end{aligned}
$$

By lema , the properties $\mathcal{A}_x(\alpha,\alpha)=\mathcal{A}_y(\alpha,\alpha)=\frac{1}{2}$ holds, and by idempotency of $\mathcal{A}$ (i.e. $\mathcal{A}(\alpha,\alpha)=\alpha$), and taking $a=b=\frac{f^{(k)}(\alpha)}{(k-1)!}e_n^{k-1}$, and $x=f'(x_n)$, $y=f'(\tilde{x}_n)$, in Taylor's expansion

$$\mathcal{A}(x,y)=\mathcal{A}(a,b)+\frac{1}{1!}[\mathcal{A}_x(a,b)(x-a)+\mathcal{A}_y(a,b)(y-b)]$$
$$+o(\|(x-a,y-b)\|),$$

follows

$$\mathcal{A}(f'(x_n),f'(\tilde{x}_n)) = \tfrac{f^{(k)}(\alpha)}{(k-1)!}e_n^{k-1}+\tfrac{1}{2}\Big[\tfrac{f^{(k)}(\alpha)}{(k-1)!}e_n^{k-1}[\tfrac{k+1}{k}d_{k+1}e_n+\tfrac{k+2}{k}d_{k+2}e_n^2+o(e_n^2)]+\Big(\tfrac{f^{(k)}(\alpha)}{(k-1)!}(\tfrac{k-1}{k})^{k-1}e_n^{k-1}[1+\tfrac{k^2+k-1}{k^2}d_{k+1}e_n+o(e_n)]-\tfrac{f^{(k)}(\alpha)}{(k-1)!}e_n^{k-1}\Big)\Big]+o(e_n^k)=\tfrac{1}{2}\tfrac{f^{(k)}(\alpha)}{(k-1)!}e_n^{k-1}\Big[1+(\tfrac{k-1}{k})^{k-1}+(\tfrac{k+1}{k}+(\tfrac{k-1}{k})^{k-1}\cdot\tfrac{k^2+k-1}{k^2})d_{k+1}e_n+o(e_n)\Big].$$

Now, the formula (5) is transformed into

$$x_{n+1}-\alpha=x_n-\alpha-\tfrac{f(x_n)}{A(f'(x_n),f'(\tilde{x}_n))},\ \text{i.e.,}$$

$$
\begin{aligned}
e_{n+1} &= e_n-\tfrac{f(x_n)}{\mathcal{A}(f'(x_n),f'(\tilde{x}_n))}\\
&= e_n-\frac{\frac{f^{(k)}(\alpha)}{k!}e_n^k\Big[1+d_{k+1}e_n+d_{k+2}e_n^2+o(e_n^2)\Big]}{\frac{1}{2}\frac{f^{(k)}(\alpha)}{(k-1)!}e_n^{k-1}\Big[1+(\frac{k-1}{k})^{k-1}+\Big(\frac{k+1}{k}+(\frac{k-1}{k})^{k-1}\cdot\frac{k^2+k-1}{k^2}\Big)d_{k+1}e_n+o(e_n)\Big]}\\
&= e_n-\tfrac{2}{k(1+(\frac{k-1}{k})^{k-1})}e_n\Big[1+d_{k+1}e_n+d_{k+2}e_n^2+o(e_n^2)\Big]\\
&\quad \cdot\Big[1+Kd_{k+1}e_n+o(e_n)\Big]^{-1}\\
&= e_n-\tfrac{2}{k(1+(\frac{k-1}{k})^{k-1})}e_n\Big[1+d_{k+1}e_n+d_{k+2}e_n^2+o(e_n^2)\Big]\\
&\quad \cdot\Big[1-Kd_{k+1}e_n+o(e_n)\Big]\\
&= e_n-\tfrac{2}{k(1+(\frac{k-1}{k})^{k-1})}e_n\Big[1+\Big(d_{k+1}-Kd_{k+1}\Big)e_n+o(e_n)\Big]\\
&= (1-\tfrac{2}{k(1+(\frac{k-1}{k})^{k-1})})e_n+\tfrac{2}{k(1+(\frac{k-1}{k})^{k-1})}(K-1)d_{k+1}e_n^2+o(e_n^2)
\end{aligned}
$$

where is $K=\frac{\frac{k+1}{k}+(\frac{k-1}{k})^{k-1}\cdot\frac{k^2+k-1}{k^2}}{1+(\frac{k-1}{k})^{k-1}}$. □

Remark. In the proofs of the theorems we used the known properties of the function o:

i) $o(f)+o(f)=o(f)$, *ii)* $o(o(f))=o(f)$, *iii)* $f_1\cdot o(f_2)=o(f_1f_2)$,

iv) $o(cf)=o(f)$, $(c-const.)$ *v)* $o(f+o(f))=o(f)$.

Recall some notions from functional analysis (see Rudin (1991)).

If f is a mapping of the set of X to itself, then the point $x\in X$ is called a *fixed* (*stationary*) *point* of map f if $f(x)=x$.

We say that a map $f: X\to Y$ of the metric space (X,d_1) in the metric space (Y,d_2), is a *contraction* if there exists a real number $\lambda\in(0,1)$ such that for every $x_1,x_2\in X$

$$d_2(f(x_1),f(x_2))\le\lambda d_1(x_1,x_2).$$

The number λ is called the *coefficient of contraction*, and f a *contraction mapping*.

Banach fixed point theorem Rudin (1991):

Theorem 8. *If (X,d) is a complete metric space and $f: X\to X$ a contraction with coefficient λ, then there is one and only one fixed point $x\in X$ of the mapping f.*

Consider the function $\varphi(x)=x-\frac{f(x)}{g(x)}$, where $g(x)=\mathcal{A}(f'(x),f'(x-\frac{f(x)}{f'(x)}))$. Then EANM method can be written as

$$x_{n+1}=\varphi(x_n). \tag{10}$$

Theorem 9. *Let f be a real valued and $f\in C^3(I)$ on the closed interval I, α a simple root of f belonging to the interior of I, then the function φ a contraction in some neighbourhood of α where the function value is assumed to be small enough.*

Proof. It is easy to see that

$$\varphi'(x)=1-\frac{f'(x)}{g(x)}+\frac{f(x)g'(x)}{(g(x))^2}.$$

If we denote $\frac{\partial\mathcal{A}}{\partial a}(a,b)$ as $\mathcal{A}_a(a,b)$ and $\frac{\partial\mathcal{A}}{\partial b}(a,b)$ as $\mathcal{A}_b(a,b)$, then

$$g'(x)=\mathcal{A}_a(f'(x),f'(x-\frac{f(x)}{f'(x)}))\cdot\frac{\partial a}{\partial x}+\mathcal{A}_b(f'(x),f'(x-\frac{f(x)}{f'(x)}))\cdot\frac{\partial b}{\partial x}$$
$$=\mathcal{A}_a(f'(x),f'(x-\frac{f(x)}{f'(x)}))\cdot f''(x)$$
$$+\mathcal{A}_b(f'(x),f'(x-\frac{f(x)}{f'(x)}))\cdot f''(x-\frac{f(x)}{f'(x)})\cdot\frac{f(x)f''(x)}{(f'(x))^2}.$$

Because $f(\alpha)=0$ and idempotency of $\mathcal{A}$ follows $g(\alpha)=\mathcal{A}(f'(\alpha),f'(\alpha))=f'(\alpha)$ and by lema , $g'(\alpha)=\mathcal{A}_a(f'(\alpha),f'(\alpha))\cdot f''(\alpha)+\mathcal{A}_b(f'(\alpha),f'(\alpha))\cdot f''(\alpha))\cdot 0=\frac{f''(\alpha)}{2}$.

Using Taylor expansion of $F_1(x)=\frac{f'(x)}{g(x)}$ at α, we obtain

$$
\begin{aligned}
F_1(x) &= F_1(\alpha)+F_1'(\alpha)(x-\alpha)+O((x-\alpha)^2)\\
&= \tfrac{f'(\alpha)}{g(\alpha)}+\tfrac{g'(\alpha)f'(\alpha)-g(\alpha)f''(\alpha)}{(f'(\alpha))^2}(x-\alpha)+O((x-\alpha)^2)\\
&= 1-\tfrac{f''(\alpha)}{2f'(\alpha)}(x-\alpha)+O((x-\alpha)^2)
\end{aligned}
\tag{11}
$$

Similarly, using Taylor expansion of $F_2(x) = \frac{f(x)g'(x)}{(g(x))^2}$ at α, we obtain

$$F_2(x) = F_2(\alpha) + F_2'(\alpha)(x-\alpha) + O((x-\alpha)^2) = \frac{f(\alpha)g'(\alpha)}{(g(\alpha))^2} + \frac{(f'(\alpha)g'(\alpha) + f(\alpha)g''(\alpha)) \cdot g^2(\alpha) - f(\alpha)g'(\alpha) \cdot 2g(\alpha)(g'(\alpha))^2}{g^4(\alpha)} \cdot (x-\alpha) + O((x-\alpha)^2) = \frac{f''(\alpha)}{2f'(\alpha)}(x-\alpha) + O((x-\alpha)^2).$$

Now,

$$\begin{aligned} |\varphi'(x)| &= |1 - F_1(x) + F_2(x)| && (12)\\ &= |1 - 1 + \frac{f''(\alpha)}{2f'(\alpha)} + O((x-\alpha)^2) && (13)\\ &\quad + \frac{f''(\alpha)}{2f'(\alpha)} + O((x-\alpha)^2)|\\ &= |\frac{f''(\alpha)}{f'(\alpha)}(x-\alpha) + O((x-\alpha)^2)|\\ &\leq |\frac{f''(\alpha)}{f'(\alpha)}| \cdot |x-\alpha| + |O((x-\alpha)^2)| && (14) \end{aligned}$$

If we use the definition of the function O, we have that there exists a positive real number M and a positive real number δ such that for all x from the neighbourhood $(\alpha-\delta, \alpha+\delta)$ of point α

$$O((x-\alpha)^2) \leq M|x-\alpha|^2,$$

is satisfied.

If we introduce the label $L = \frac{f''(\alpha)}{f'(\alpha)}$, it follows

$$\begin{aligned} |\varphi'(x)| &\leq (L + M \cdot |x-\alpha|)|x-\alpha|\\ &\leq (L + M\delta)|x-\alpha| && (15) \end{aligned}$$

If we choose the neighbourhood $(\alpha-\varepsilon, \alpha+\varepsilon)$ of the point α such that

$$\varepsilon = \min\{\delta, \frac{1}{2(L+M\delta)}\},$$

we get that $|\varphi'(x)| < \frac{1}{2}$, i.e., φ is a contraction.

For arbitrary $x \in [\alpha-\varepsilon, \alpha-\varepsilon] = I$ we have

$$|\varphi(x) - \alpha| = |\varphi(x) - \varphi(\alpha)| = |\varphi'(\overline{x})| \cdot |x-\alpha| < |x-\alpha| < \varepsilon,$$

i.e., $\varphi(x) \in [\alpha-\varepsilon, \alpha-\varepsilon]$ and $\varphi : I \to I$. □

Conditions of the Banach fixed point theorem are fulfilled. Thus, the mapping φ has a unique fixed point in thats neighbourhood, and therefore the same follows for the function f, then EANM method ensures the sequence $\{x_n\}$ defined by (10) converges to α for any initial iteration x_0 sufficiently close to α.

NUMERICAL RESULTS AND CONCLUSIONS

In Tables 1-5 we show the computational results of some relevant numerical tests derived from the real-life applications, to compare the efficiencies of the proposed aggregation methods (including Newton's method) for simple and multiple roots. All the tables display the number of iterations N and the number of functional evaluations N_f, required to satisfy the stopping criterion $|x_{n+1} - x_n| + |f(x_{n+1})| < 10^{-7}$ where the maximum number of iterations is 500. Moreover, the computational order of convergence COC given in (Weerakoon & Fernando, 2000) has been calculated with following formula

$$\frac{\ln|(x_{n+1}-\alpha)/(x_n-\alpha)|}{\ln|(x_n-\alpha)/(x_{n-1}-\alpha)|}.$$

Test functions:

$f_1(x) = e^{-x} - 1 - x/5,$

$f_2(x) = 2e^{-\sqrt{x}}(\sqrt{x}+1) - 2e^{-\sqrt{x+1}}(\sqrt{x+1} - e^{-1}),$

$f_3(x) = x - 0.5\cos x + \pi/4,$

$f_4(x) = x^4 + 4x^3 - 24x^2 + 16x + 16,$

$f_5(x) = x^4 + 11.5x^3 + 47.49x^2 + 83.06325x + 51.23266875.$

All test examples are the real-life problems. The first function has been derived from the Planck's radiation law (see Jain (2013)), the second is the problem of minimum insurance premium determination, while the third describes the trajectory of the electron in the air gap between two parallel plates (see Maroju et al. (2017)). Here we are interested in finding simple roots 4.965114..., 0.541919808... and −0.3090932... respectively. In the fourth and the fifth example, we are searching for multiple roots −2.85 and 2 respectively. The fourth test function arised from the beam positioning problem (see Zachary (2012)), and fifth problem is also known as a continuous stirred tank reactor problem (see Douglas (1972)).

Table 2. Numerical results for $f_1(x)$ and $x_0 = 3$.

method	N	N_f	COC
N	4	8	1.9504
AN	4	12	2.9970
HN	4	12	2.9944
GN	4	12	2.9958
QN	4	12	2.9981
CN	3	9	3.1845
CHN	3	9	3.1791
HZN ($p = 1/4$)	4	12	2.9961
HRN	4	12	2.9966
SMN ($p = 9$)	4	12	2.9999
GCHN ($p = 3$)	3	9	2.7593

Table 3. Numerical results for $f_2(x)$ and $x_0 = 0.25$.

method	N	N_f	COC
N	5	10	1.9998
AN	4	12	2.9979
HN	3	9	2.9479
GN	4	12	2.9988
QN	-	-	-
CN	-	-	-
CHN	4	12	2.9959
HZN (p=1/4)	4	12	2.9986
HRN	-	-	-
SMN (p=9)	4	12	2.9882
GCHN (p=3)	4	12	2.9937

Table 4. Numerical results for $f_3(x)$ and $x_0 = -1.4$.

method	N	N_f	COC
N	5	10	1.9963
AN	4	12	3.0424
HN	4	12	3.0082
GN	4	12	3.0232
QN	4	12	3.0628
CN	4	12	3.0816
CHN	4	12	3.0856
HZN (p=1/4)	4	12	3.0277
HRN	4	12	3.0357
SMN (p=9)	5	15	3.0109
GCHN (p=3)	5	15	3.0013

Table 5. Numerical results for $f_4(x)$ and $x_0 = 1.7$.

method	N	N_f	COC
N	22	44	1.0000
AN	15	45	1.0000
HN	12	36	1.0000
GN	13	39	1.0000
QN	12	36	3.0006
CN	27	81	1.0000
CHN	17	51	1.0000
HZN (p=1/4)	14	42	1.0000
HRN	15	45	1.0000
SMN (p=9)	25	75	1.0000
GCHN (p=3)	19	57	1.0000

Table 6. Numerical results for $f_5(x)$ and $x_0 = -3$.

method	N	N_f	COC
N	21	42	1.0000
AN	14	42	1.0000
HN	12	36	1.0000
GN	13	39	1.0000
QN	15	45	1.0000
CN	16	48	1.0000
CHN	16	48	1.0000
HZN (p=1/4)	13	39	1.0000
HRN	14	42	1.0000
SMN (p=9)	24	72	1.0000
GCHN (p=3)	18	54	1.0000

All computational results have been carried out by the *Mathematica* programming package. The failure of the method is denoted by -.

All calculated COC numbers for each member of the aggregation family of methods are very close to 3 for simple roots, and very close to 1 for multiple roots, which means that those numerical results clearly confirm the theoretical analysis from previous sections. In general, it is impossible to conclude which choice of the aggregation function is the best, although it seems that for this set of test functions the harmonic mean aggregation method shows slightly better numerical results for multiple roots.

ACKNOWLEDGMENT

The author acknowledge the financial support of the Ministry of Education, Science and Technological Development of the Republic of Serbia, within the Projects No. ON 174009.

REFERENCES

Babajee, D. K. R. & Dauhoo, M. Z. 2006. An analysis of the properties of the variants of Newton's method with third order convergence, Applied Mathematics and Computation, 183(1), pp. 659-684. doi:10.1016/j.amc.2006.05.116.

Douglas, J. M. 1972. Process Dynamics and Control: Control System Synthesis, Prentice Hall, 2. doi:10.1002/aic.690190246.

Frontini, M. & Sormani, E. 2003. Some variant of Newton's method with third order convergence, Applied Mathematics and Computation, 140(2-3), pp. 419-426, doi:10.1016/S0096-3003(02)00238-2.

Grabisch, M., Marichal, J. L., Mesiar, R., & Pap, E. 2009. Aggregation Function, Cambridge University Press.

Herceg, D. & Herceg, D. 2013a. Means based modifications of Newton's method for solving nonlinear equations, Applied Mathematics and Computation, 219(11), pp. 6126-6133.

Herceg, D. & Herceg, D. 2013b. Third-order modifications of Newton's method based on Stolarsky and Gini means, Journal of Computational and Applied Mathematics, 245, pp. 53-61. doi:10.1016/j.cam.2012.12.008.

Homeier, H. H. H. 2003. A modified Newton method for rootfinding with cubic convergence, J. Comput. Appl. Math., 157(1), pp. 53-61. doi:10.1016/S0377-0427(03)00391-1.

Jain, D. 2013. Families of Newton-like methods with fourthorder convergence, International Journal of computer mathematics, 90(5), pp. 1072-1082. doi:10.1080/00207160.2012.746677.

Klement, E. P., Mesiar, R., & Pap, E. 2000. Triangular Norms, Kluwer Academic Publishers, Dordrecht. doi:10.1007/978-94-015-950-7.

Klir, G. J. & Yuan, B. 1995. Fuzzy sets and fuzzy logic, Theory and applications, Prentice Hall, New Jersey.

Lukić, T. & Ralević, N. M. 2008. Geometric Mean Newton's Method for Simple and Multiple Roots, Applied Mathematics Letters, 21, pp. 30-36. doi:10.1016/j.aml.2007.02.010.

Lukić, T., Ralević, N. M., & Lukity, A. 2006. Application of Aggregation Operators in Solution of Nonlinear Equations, 4th Serbian-Hungarian Joint Symposium on Intelligent Systems, September 29-30, 2006, Subotica, Serbia and Montenegro, pp. 329-339.

Maroju, P., Behl, R., & Motsa, S. S. 2017. Some novel and optimal families of King's method with eighth and sixteenth-order of convergence, Journal of Computational and Applied Mathematics, 318, pp. 136-148. doi:10.1016/j.cam.2016.11.018.

McDougall, T. J. & Wotherspoon, S. J. 2014. A simple modification of Newton's method to achieve convergence of order $1+2^{(1/2)}$, Applied Mathematics Letters, 29, pp. 20-25. doi:10.1016/j.aml.2013.10.008.

Özban, A. Y. 2004. Some new variants of Newton's method, Appl. Math. Lett., 17, pp. 677-682. doi:10.1016/S0893-9659(04)90104-8.

Ralević, N. M. & Ćebić, D. 2019. The Newton Method for Solving Nonlinear Equations Based on Aggregation operator, SYM-OP-IS 2019, XLVI International Symposium on Operational Research, Kladovo, September 15-18, 2019, pp. 367-372.

Ralević, N. M. & Lukić, T. 2005. Modification of Newton's Method Based on Root-Power Mean, Applied Linear Algebra 2005, October 13-15, Palic, Serbia and Montenegro.

Rudin, W. 1991. Functional analysis (McGraw-Hill) Wait, R. 1979. The Numerical Solution of Algebraic Equations, John Wiley Sons.

Wait, R. 1979. The Numerical Solution of Algebraic Equations. John Wiley & Sons.

Weerakoon, S. & Fernando, T. G. I. 2000. A variant of Newton's method with accelarated third-order convergence, Appl. Math. Lett., 13(8), pp. 87-93. doi:10.1016/S0893-9659(00)00100-2.

Zachary, J. L. 2012. Introduction to scientific programming: computational problem solving using Maple and C, Springer-Verlag New York, doi:10.1007/978-1-4612-2366-5.

UNIVERSITY THOUGHT
Publication in Natural Sciences, Vol.10, No.1, 2020, pp. 51-56.
DOI: https://doi.org/10.5937/univtho10-20589
Original Scientific Paper

ANALYSIS OF GEODESICS ON DIFFERENT SURFACES

MIROSLAV MAKSIMOVIĆ[1,⋆], TANJA JOVANOVIĆ[1], EUGEN LJAJKO[1], MILICA IVANOVIĆ[1]

[1]Faculty of Natural Sciences and Mathematics, University of Priština, Kosovska Mitrovica, Serbia

ABSTRACT

It is widely known that some surfaces contain special curves as a geodesics, while a lots of geodesics on surface have complicated shapes. Goal of this research is to find on what surfaces are u- and v- parameter curves geodesics. Developable surfaces that contain a given plane curve as a geodesic are studied in the article, whereas the plane curve is also an initial u-parameter curve on that surface. Parametric equations of the minimal surfaces that contain an epicycloid as a geodesic are also given. Visualization of geodesics was done in *Mathematica*.

Keywords: Geodesics, u- and v- parameter curve, Developable surface, Minimal surface.

INTRODUCTION

Geodesics are those curves on the surface that are not "geodesically curved". Considering their role on surfaces, they can be compared to straight lines in plane and they are called "the most straight lines" on surface. A geodesic can be obtained as the solution of the nonlinear system of second-order differential equations with the given points and its tangent direction for the initial conditions. This system can be solved in special cases for plane surface, revolution surface and ruled surface. But, in the general case, for other surfaces it is difficult to solve this system. In Khuangsatung (2012) geodesics are presented and classified by Clairauts relation on some surfaces of revolution. For example, at Hyperboloid just the initial parallel is a geodesic and any other meridian is geodesic. That means they are actually initial u- and v- parameter curve that are geodesics. In articles Abdel-All (2013) and Lewis (2002) it is shown that this system can be solved numerically for the given initial conditions, and for this purpose a *Mathematica* package code was written, that solves the system and shows obtained geodesics on the surfaces.

NOTATION AND PRELIMINARIES

Let $r : D \to \mathbb{R}^3, (u, v) \mapsto (x(u, v), y(u, v), z(u, v))$ denote a mapping of an open set $D \subset \mathbb{R}^2$.

Definition 1. (Abbena (2006)) Let us give a surface $\mathcal{S} : r = r(u, v)$. For the point $(u_0, v_0) \in D$, curves

$$u \to r(u, v_0) \text{ and } v \to r(u_0, v)$$

are called u- parameter curve and v- parameter curve on the surface $\mathcal{S}$.

For surface $\mathcal{S}$ denote with $E = r_u \cdot r_u$, $F = r_u \cdot r_v$, $G = r_v \cdot r_v$ coefficients of the first fundamental form

$$I = Edu^2 + 2Fdudv + Gdv^2.$$

Gaussian curvature K and mean curvature H of the surface $\mathcal{S}$ are given with formulas

$$K = \frac{LN - M^2}{EG - F^2}, \quad H = \frac{EN - 2FM + GL}{2(EG - F^2)}.$$

A surface with $H = 0$ is called minimal surface. A surface with $K = 0$ is called developable surface.

Definition 2. (Abbena (2006)) The Christoffel symbols Γ^i_{jk}, $i, j, k = 1, 2$, of a regular surface $\mathcal{S}$ are given by

$$\Gamma^1_{11} = \frac{GE_u - 2FF_u + FE_v}{2(EG-F^2)}, \qquad \Gamma^2_{11} = \frac{2EF_u - EE_v - FE_u}{2(EG-F^2)},$$

$$\Gamma^1_{12} = \frac{GE_v - FG_u}{2(EG-F^2)}, \qquad \Gamma^2_{12} = \frac{EG_u - FE_v}{2(EG-F^2)},$$

$$\Gamma^1_{22} = \frac{2GF_v - GG_u - FG_v}{2(EG-F^2)}, \qquad \Gamma^2_{22} = \frac{EG_v - 2FF_v + FG_u}{2(EG-F^2)},$$

where is $\Gamma^1_{12} = \Gamma^1_{21}$ and $\Gamma^2_{12} = \Gamma^2_{21}$.

For geodesic its said that it is the path of particles without acceleration and it is not affected by any outside factors, but it accelerates perpendicularly to the surface. According to that, we give the following definition.

Definition 3. (Pressley (2012)) Let $r(t) = r(u(t), v(t))$ be a smooth curve on a surface $\mathcal{S}$. The curve $r(t)$ is called a *geodesic* if $r''(t)$ is zero or perpendicular to the tangent plane of the surface at the point $r(t)$, for all values of the parameter t.

Definition 3 implies that $r''(t)$ and the normal to the surface are parallel.

Theorem 4. *(Pressley (2012)) A curve $r(t) = r(u(t), v(t))$ on a surface $\mathcal{S}$ is a geodesic if and only if, for any part of $r(t)$ contained in a surface patch of $\mathcal{S}$, the following two equations are satisfied*

$$\begin{cases} u'' + \Gamma^1_{11}u'^2 + 2\Gamma^1_{12}u'v' + \Gamma^1_{22}v'^2 = 0 \\ v'' + \Gamma^2_{11}u'^2 + 2\Gamma^2_{12}u'v' + \Gamma^2_{22}v'^2 = 0. \end{cases}$$

⋆ Corresponding author: miroslav.maksimovic@pr.ac.rs

where Γ^i_{jk} a Christoffel symbols.

Theorem 5. *(Do Carmo (1976)) Through any surface point in each direction passes one and only one geodesic.*

This theorem tells us that each geodesic is determined by initial point and the speed in that point. Any geodesics has a constant speed, and, taking that into consideration, any straight line, or its part is a geodesics on a surface. This result gives us a motivation for some researches in this work.

Theorem 6. *(Do Carmo (1976)) On the surface of revolution*

$$r(u, v) = (f(u)\cos v, f(u)\sin v, g(u)),$$

every meridian ($v = v_0$) is a geodesic and parallel $u = u_0$ is a geodesic if and only if u_0 is a stationary point of a function $f(u)$.

More about geodesics can be found in Do Carmo (1976), Abbena (2006), Pressley (2012) and Toponogov (2006).

u- AND *v*- PARAMETER CURVES AS GEODESICS

In this research we came to a conclusion that for some surfaces initial u- and v- parameter curve satisfies conditions of geodesics. We are going to use red color to mark a u- parameter curve, blue for a v- parameter curve and green for other geodesics.

Eight surface

Eight surface is a surface of revolution with parametrization

$$r(u, v) = (\sin(2u)\cos v, \sin(2u)\sin v, \sin u).$$

Based on theorem 6. it is clear that its meridians will be geodesic. Solutions of the equation $f'(u) = 0$ are $u_{1,2} = \pm\pi/4$, which means that the Eight surface has two parallels , $u_1 = \pi/4$ and $u_2 = -\pi/4$, that satisfy conditions for geodesics (fig. 1. a)). Other geodesics on the Eight surface "stay" only on one of its parts (fig. 1. b)), so the meridians are only geodesic of this surface that contains the coordinate origin.

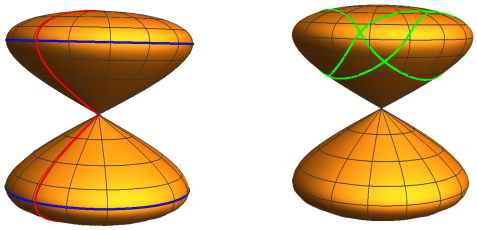

a) b)

Figure 1. Geodesics on Eight surface.

Two banana surface

Two banana surface is parametrized by

$$r(u, v) = ((2 + \cos u)\cos v, \sin u \cos v, \sin v).$$

On the Two banana surface initial u- and v- parameter curves are geodesics (fig. 2 a)). Other geodesics stay on one banana and have complicated shapes (Lewis (2002)) (fig. 2 b)).

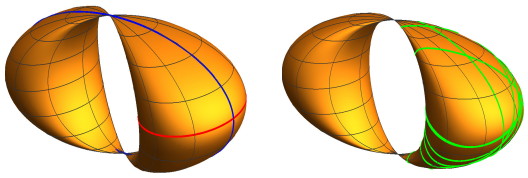

a) b)

Figure 2. Geodesics on Two banana surface.

Monkey saddle

Geodesics on monkey saddle, which has parametrization $r(u, v) = \left(u, v, u^3 - 3uv^2\right)$, are shown in fig. 3.

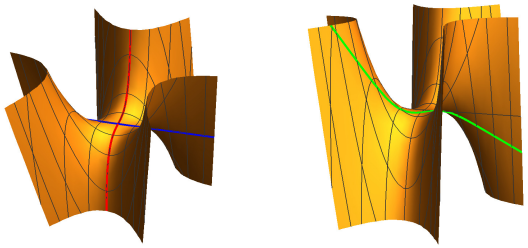

a) b)

Figure 3. Initial u- and v- parameter curve like a geodesic a) and other geodesic b).

Gaudi's surface

At Gaudi's surface with parametrization $r(u, v) = \left(u, v, au\sin\frac{v}{b}\right)$, for parameters a and b, initial v- parameter curve is a geodesic, while every u- parameter curves are geodesics (fig. 4).

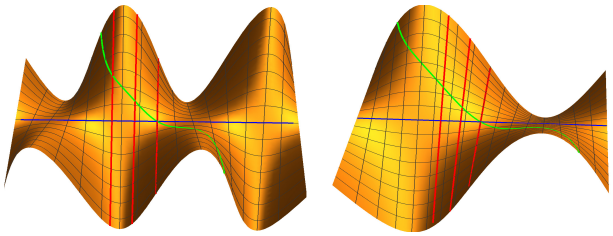

a) b)

Figure 4. Geodesics on Gaudi's surfaces with parameter (1,1) and (1,2).

Hyperbolic paraboloid

u- and v- parameter curves on Hyperbolic paraboloid with parametrization $r(u, v) = (u, v, uv)$ are straight lines, and they are also geodesics (fig. 5 a)), while at the surfaces with the parametrization $r(u, v) = \left(u, v, u^2 - v^2\right)$ (fig. 5 b)) only initial u- and v- parameter curves are geodesics.

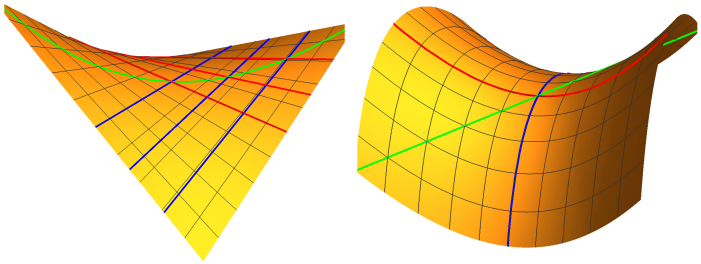

a) b)

Figure 5. Geodesics on hyperbolic paraboloid.

Developable surfaces

Firstly we are going to define a regular plane curve

$$curve(t) = (x(t), y(t), c), \quad c = const.$$

Then, the surface

$$surface(u, v) = (x(u), y(u), cg(u)f(v)), \quad g(u)f(v) \neq 0,$$

is a surface with $K = 0$, i.e. developable surface, that contains the given curve as a geodesic, where $g(u)$ and $f(v)$ are taken arbitrarily. Mean curvature of this surface will be

$$H = \frac{g^3(u)f'^3(v)(x''(u)y'(u) - x'(u)y''(u))}{2(g^2(u)f'^2(v)(x'^2(u) + y'^2(u)))^{3/2}}.$$

It is clear that given plane curve represents an initial u- parameter curve, while every v- parameter curve is a straight line, and is a geodesic on this surface.

For example, one of surfaces that contains sinusoid as a geodesic can be obtained for $g(u) = \cos u$ and $f(v) = \sin v$:

$$\mathcal{S}: \quad r(u, v) = (u, \sin u, \cos u \sin v).$$

This surface $\mathcal{S}$ (fig. 6) has curvatures

$$K = 0, \qquad H = \frac{\cos v \sin 2u}{2(3 + \cos 2u)\sqrt{\cos^2 u \cos^2 v(1 + \cos^2 u)}}.$$

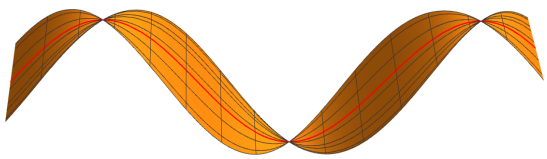

Figure 6. Sinusoid like a geodesic on surface with $K = 0$.

Minimal surfaces

It is well known that some minimal surfaces contain special curves as a geodesics (see Abbena (2006)). For example, the Enneper surface contains the *Tschirnhausen* cubic as a geodesic and that curve is also initial u-parameter curve and v-parameter curve of this surface. Also Catalan's surface contains a cycloid as a geodesics and it is its initial u- parameter curve.

The Scherk's surface and the Scherk's fifth surface contains initial u- and v- parameter curves as a geodesics (fig. 7).

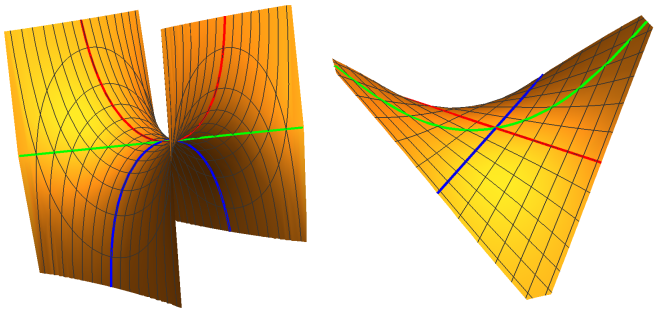

a) b)

Figure 7. Geodesics on Scherk's surfaces

Considering that the Catenoid is a surface of revolution, its meridians (v- parameter curves) are geodesics, and only the initial parallel satisfies conditions for geodesics (fig. 8 a)). Since the catenoid is locally isometrical to the helicoid, all its properties are same as those of the helicoid. (fig. 8 b)).

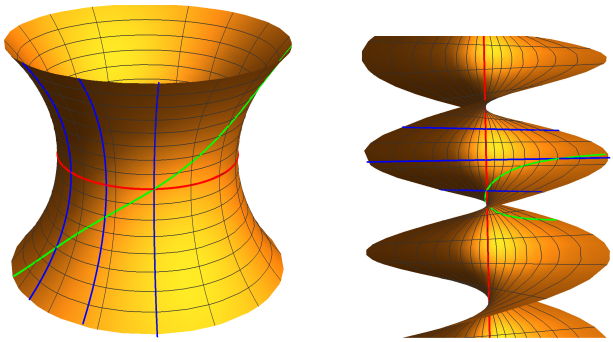

a) b)

Figure 8. Catenoid and Helicoid

CONSTRUCTION OF THE MINIMAL SURFACES THAT CONTAIN EPICYCLOID AS A GEODESIC

Construction of the minimal surfaces that contain some curve as a geodesic represents Björling's problem. Construction of these surfaces in *Mathematica* based on a given curve is represented in Abbena (2006).

One of the simplest Björling's surfaces that contains a known curve as a geodesic is the Catalan's minimal surface (fig. 9). At this surface one of geodesics is cycloid.

Also, at Enneper surface initial u- and v- parameter curves are geodesics and represent the Tschirnhausen cubic (fig. 10).

Epicycloid represents a curve that is given as a trail of a determined point of the circle $k_1 = (O_1, b)$ that spins around the circle $k_0 = (O, a)$. For different relations of their radii they get

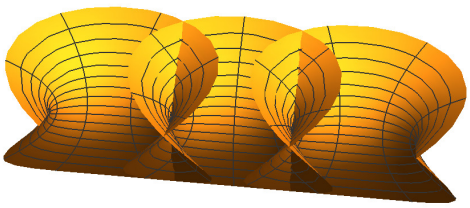

Figure 9. Catalan surface.

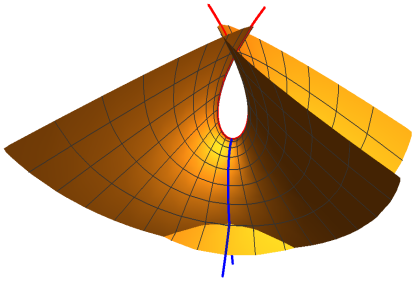

Figure 10. Enneper surface.

different epicycloids. Out of the group of epicycloids, cardioids, nephroids and ranuncloids are best known.

Parametric equations of epicycloid with parameters a and b are:

$$\begin{cases} x = (a+b)\cos t - b\cos\left(\frac{a+b}{b}t\right) \\ y = (a+b)\sin t - b\sin\left(\frac{a+b}{b}t\right). \end{cases}$$

Parametric equations of the minimal surface that contains arbitrarily epicycloid as a geodesic are:

$$\begin{cases} x = (a+b)\cos u\cosh v - b\cos\left(\frac{a+b}{b}u\right)\cosh\left(\frac{a+b}{b}v\right) \\ y = (a+b)\sin u\cosh v - b\sin\left(\frac{a+b}{b}u\right)\cosh\left(\frac{a+b}{b}v\right) \\ z = \frac{4b(a+b)}{a}\sin\left(\frac{a}{2b}u\right)\sinh\left(\frac{a}{2b}v\right). \end{cases}$$

We will discuss minimal surfaces obtained on the epicycloid depending on the parameters (values of the parameters are given in the table 1.) Their graphic representation is given on fig. 11, 12, 13, 14 and 15.

Table 1. Values of the parameters.

$[a,b]$	t	u, v
$[1,1]$	$0 \le t \le 2\pi$	$0 \le u \le 2\pi$, $-0.5 \le v \le 0.5$
$[2,1]$	$0 \le t \le 2\pi$	$0 \le u \le 2\pi$, $-0.5 \le v \le 0.5$
$[5,1]$	$0 \le t \le 2\pi$	$0 \le u \le 2\pi$, $-0.3 \le v \le 0.3$
$[7,2]$	$0 \le t \le 4\pi$	$0 \le u \le 4\pi$, $-0.3 \le v \le 0.3$
$[3,2]$	$0 \le t \le 4\pi$	$0 \le u \le 4\pi$, $-0.5 \le v \le 0.5$

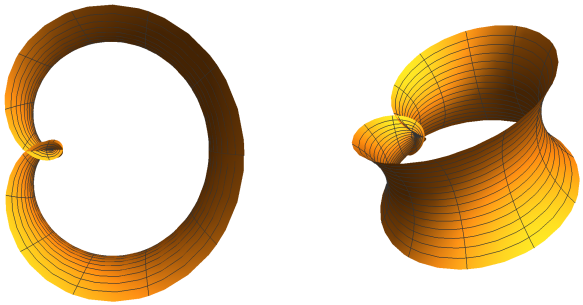

Figure 11. Minimal surface with parameters [1,1].

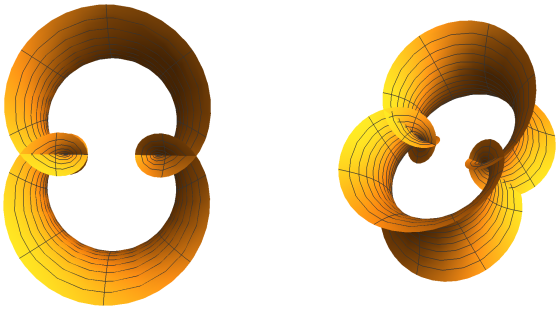

Figure 12. Minimal surface with parameters [2,1].

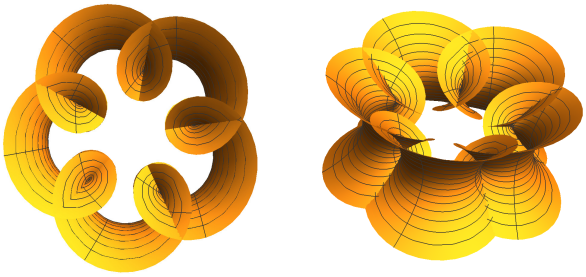

Figure 13. Minimal surface with parameters [5,1].

We see that these surfaces represent "closed Catalan's surfaces". The Gaussian curvature of the minimal surface given for parameters [2, 1] is a shown on fig. 16.

For $a < b$ there is a very special group epicycloids that are called pericycloids. Minimal surfaces whose pericycloids are geodesic are shown on fig. 17, 18, 19 and values of the parameters are given in the table 2.

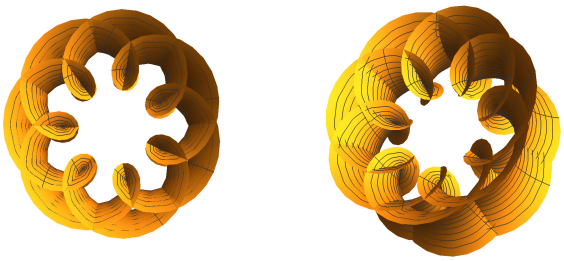

Figure 14. Minimal surface with parameters [7,2].

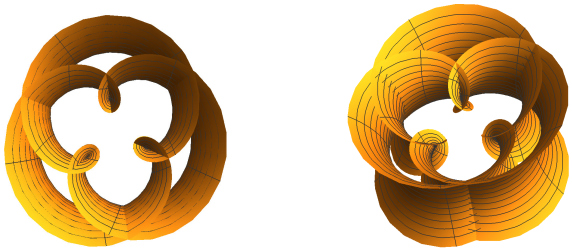

Figure 15. Minimal surface with parameters [3,2].

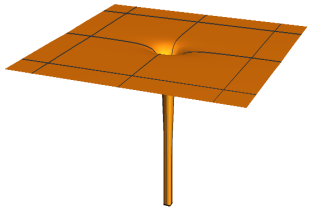

Figure 16. Gaussian curvature of minimal surface with parameters [2,1].

Table 2. Values of the parameters

$[a,b]$	t	u,v
$[1,2]$	$0 \le t \le 4\pi$	$0 \le u \le 4\pi$, $-0.5 \le v \le 0.5$
$[1,3]$	$0 \le t \le 4\pi$	$0 \le u \le 4\pi$, $-0.5 \le v \le 0.5$
$[2,3]$	$0 \le t \le 6\pi$	$0 \le u \le 6\pi$, $-0.5 \le v \le 0.5$

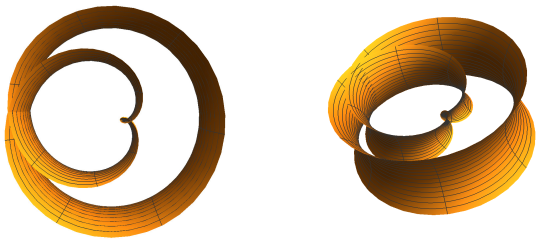

Figure 17. Minimal surface with parameters [1,2].

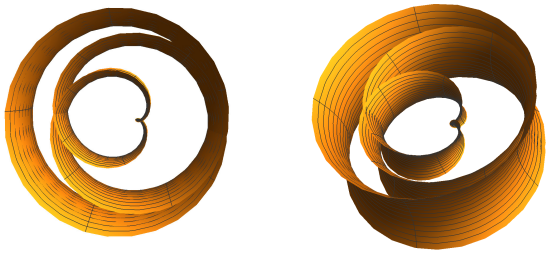

Figure 18. Minimal surface with parameters [1,3].

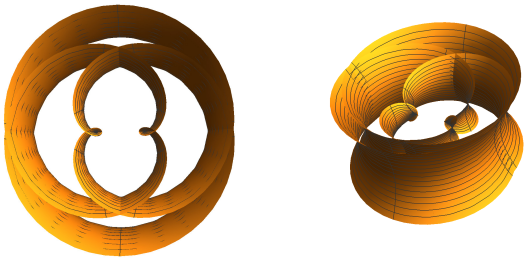

Figure 19. Minimal surface with parameters [2,3].

APPENDIX

Geodesic vs shortest path

Due to the analogy with the straight lines in plane, geodesics are often connected with the shortest path between two points on the surface. However, its not always possible to identify this terms. As one of the examples, we are going to give the distance between two points A and B on sphere, that belong to a great circle of the sphere and that are not diametrally opposite to each other (fig. 20).

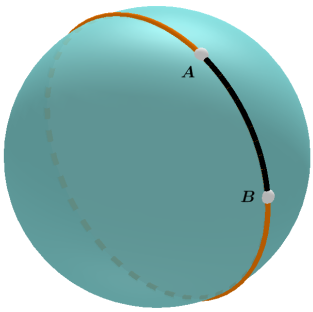

Figure 20. Distance of points on the sphere.

Observer points divide a great circle into two arcs, one of which is shorter than the other. Its clear that both arcs are the parts of the same geodesic, but if points are connected with the longer arc, then it is not the shortest path between them.

ACKNOWLEDGEMENT

The first author was supported by the research project 174025 of the Serbian Ministry of Science.

REFERENCES

Abbena, E., S. S. . G.-A. 2006, Modern differential geometry of curves and surfaces with Mathematica.Boca Raton: Chapman and Hall CRC. 3rd ed.

Abdel-All, N. H., . A.-G. E. I. 2013, Numerical treatment of geodesic differential equations on a surface in $\mathbb{R}^3$. International Mathematical Forum, 8, pp. 15-29. doi:10.12988/imf.2013.13003

Do Carmo, M. 1976, Differential Geometry of Curves and Surfaces. Prentice-Hall

Khuangsatung, W. C. P. 2012, Some geodesics in open surfaces classified by Clairauts relation, World Academy of Science. Engineering and Technology, 6(9), pp. 1360-1364.

Lewis, J. 2002, Geodesics Using Mathematica. Rose-Hulman Undergraduate Mathematics Journal, 3(1).

Pressley, A. 2012, Elementary Differential Geometry. London: Springer Science and Business Media LLC. doi:10.1007/978-1-84882-891-9

Toponogov, V. 2006, Differential geometry of curves and surfaces. Birkhauser: Boston

UNIVERSITY THOUGHT
Publication in Natural Sciences, Vol. 10, No. 1, 2020, pp. 57-62.
DOI: https://doi.org/10.5937/univtho10-23091
Original Scientific Paper

FIRST ORDER OUTAGE STATISTICS OF ASYMMETRICAL RF-OW DUAL-HOP RELAY COMMUNICATIONS

STEFAN PANIĆ[1*], SERGEI MOHANCHENKO[2], ČASLAV STEFANOVIĆ[1], MIHAJLO STEFANOVIĆ[3]

[1]Faculty of Natural Sciences and Mathematics, University of Priština, Kosovska Mitrovica, Serbia
[2]School of Computer Sciences and Robotics, National Research Tomsk Polytechnic University, Tomsk, Russia
[3]Faculty of Electronic Engineering, University of Niš, Niš, Serbia

ABSTRACT

This paper addresses the first-order outage statistics of asymmetrical radio frequency (RF)-optical wireless (OW) relay systems over non turbulent-induced-fading (nTIF) and turbulent-induced-fading (TIF) channels. We rely on dual-hop amplify-and-forward relay (AFR) scheme and provide detailed mathematical development for derivation of novel exact analytical as well as novel closed form approximative expressions for: *i*). cumulative distribution function, *ii*.) outage probability, and *iii*.) average bit-error-rate. The system under consideration is modeled as the product of independent Nakagmi-m and double squared Nakagami-m (also known as Gamma-Gamma) random processes. The obtained results of the proposed system are graphically presented for RF-OW TIF and nTIF channel sets of parameters. Moreover, the detailed comparisons of exact and approximated numerical results whose derivation resorts on exponential Laplace approximation method (LAM) are provided and thoroughly examined for the considered RF-OW statistical measures.

Keywords: Gamma-Gamma, Laplace approximation, Nakagami-m, Outage statistics, RF-FSO relay systems.

INTRODUCTION

Optical wireless (OW) communicationsas well as asymmetrical radio frequency (RF)-OW communications are relevant research topic within academia and industry for future 5G and even beyond 5G (B5G) network deployments (Hamza et al., 2018; Khalighi & Uysal, 2014; Illi et al., 2017; Douik et al., 2016). The OW communications are primarily intended to speed up the transmission rate and ensure higher capacity and wider bandwidth compared to RF links. Moreover, OW communications, especially free space optical (FSO) communications which operates at near infrared part of the spectrum are *i*.) cost effective, *ii*.) spectrum license free, *iii*.) channel interference free. On the other hand, one of the main FSO system performance impairments is the impact of atmospheric turbulence due to the small- and large-scales atmospheric cells. Weather conditions as well as misalignment of the system's transmitter-receiver apparatus can cause further degradation of the system performance stability.

The relay system techniques represent efficient way to speed up data-rate, extend coverage and save energy but also to efficiently merge different wireless technologies (Zedini et al., 2014; Anees & Bhatnagar, 2015; Petkovic et al., 2017; Zedini et al., 2015; Stefanovic et al., 2019a). Moreover, amplify-and-forward relay (AFR) scheme plays an important role in all-RF, RF-FSO and all-FSO relay systems (Stefanovic, 2017; Karimi & Masoumeh, 2011; Petkovic & Trpovski, 2018) and in some cases the signal envelope, signal-to-interference ratio (SIR) and signal-to-noise ratio (SNR) can be modeled as the product of two or more random processes (RPs) (Zlatanov et al., 2008; Stefanovic et al., 2018; Milosevic et al., 2018; Stefanovic et al., 2019b; Talha & Pätzold, 2007; Issaid & Alouini, 2019).

Namely, Nakagami-m (Nm) RP can address RF links over non turbulence induced fading (nTIF) channels (Nakagami, 1960) while double squared Nakagami-m (d-sNm), also known as gamma-gamma RP can address FSO links over moderate to strong turbulence induced fading (TIF) channels (Andrews & Phillips, 2005; Vetelino et al., 2007; Al-Ahmadi, 2014). The papers (Zedini et al., 2014; Anees & Bhatnagar, 2015; Petkovic et al., 2017) address mixed RF-FSO relay systems over Nm nTIF channels and d-sNm TIF channels and provide closed form analytical results for the first order statistical measures expressed through Meijer's G function. In paper (Zedini et al., 2015), Nm nTIF and d-sNm TIF are used to address cooperative mixed RF-FSO relay link and obtained analytical results are given in terms of H-fox and Meijer's G functions. Moreover, in (Stefanovic et al., 2019a) the closed form analytical expressions for second order statistics of the products of Nm, d-sNm and Nm RPs are derived by Laplace approximation method (LAM) and efficiently applied to address TIF and nTIF channels of mixed triple-hop RF-FSO-RF vehicle-to-vehicle (V2V) AFR communications.

It is important to note that LAM already plays an important role in performance analysis of wireless communicationsystems (Stefanovic et al., 2019a; Stefanovic, 2017; Zlatanov et al., 2008; Stefanovic et al., 2018; Milosevic et al., 2018; Stefanovic et al., 2019b; Hajri et al., 2018). Moreover, LAM can provide precise

* Corresponding author: stefan.panic@pr.ac.rs

approximations by solving complex many-folded integrals and significantly decrease computational time of complex analytical expressions. The proofs that LAM is able to provide precise results even under sub-asymptotic conditions is provided in (Butler & Wood, 2002). Another remark of the LAM is its generality and simplicity of application, which in many cases can provide fast computing closed form accurate approximations derived from latent Gaussian models (Wang, 2010).

In this paper we provide comprehensive mathematical development for computing novel exact expressions as well as novel closed form approximative expressions for *i.*) cumulative distribution function, *ii*.) outage probability, *iii*.) and average bit error rate of the product of Nm and d-sNm RPs. Moreover, we rely on exponential LAM for derivation of closed form analytical expressions for the first order statistical measures. The obtained results are further used to address asymmetrical RF-FSO dual-hop AFR system in the case when nTIF (fading over RF channel) and TIF (turbulence induced fading over FSO channel) are the main cause of the system model performance degradation.

To the best of author's knowledge there is no paper in open technical literature that applies exponential LAM for derivation of the first order outage statistics of RF-FSO AFR system over Nm nTIF and d-sNm TIF channels.

SYSTEM MODEL OF RF-FSO DUAL-HOP AFR COMMUNICATIONS

We model the mixed RF-FSO dual-hop AFR system as the product of the independent Nm random process (RP), y_{Nm_1} and gamma-gamma (GG) RP, y_{GG}. Further, we express GG as double squared Nakagami-m (d-sNm) RP, $y_{GG} = y_{Nm_2}^2 y_{Nm_3}^2$. Thus, we model the output signal envelope x_{out} as the product of the independent RPs, $x_{out} = \underbrace{y_{Nm_1}}_{RF}\underbrace{y_{GG}}_{FSO} = \underbrace{y_{Nm_1}}_{RF}\underbrace{y_{Nm_2}^2 y_{Nm_3}^2}_{FSO}$. where,

$$p_{Y_{Nm_i}}\left(y_{Nm_i}\right) = \frac{2\left(m_i/\Omega_i\right)^{m_i}}{\Gamma\left(m_i\right)} y_{Nm_i}^{2m_i-1} e^{-\frac{m_i y_{Nm_i}^2}{\Omega_i}}, i = 1,3. \quad (1)$$

whose average powers and fading severity parameters of RF Nm and FSO d-sNm RPs are, respectively, $\Omega_1 = \Omega_{RF}$, $m_1 = m_{RF}$.

$$\Omega_2 = \Omega_3 = 1, \quad (2)$$

$$m_2 = \alpha = \left[\exp\left(\frac{0.49\delta^2}{\left(1+0.18d^2+0.56\delta^{12/5}\right)^{7/6}}\right)-1\right]^{-1}, \quad (3)$$

$$m_3 = \beta = \left[\exp\left(\frac{0.51\delta^2\left(1+0.69\delta^{12/5}\right)^{-5/6}}{\left(1+0.9d^2+0.62d^2\delta^{12/5}\right)^{5/6}}\right)-1\right]^{-1}. \quad (4)$$

where α and β are small-scale and large-scale cells related to atmospheric conditions, respectively, $\delta^2 = 0.5C_n^2 k^{7/6} L^{11/6}$ is the Rytov variance and $d = \sqrt{kD^2/4L}$ is the optical wave number. Further, C_n^2 is Refractive index, $k=2\pi/\lambda$ is wave-number (λ-wavelength), D is receiver aperture diameter and L is propagation distance.

FIRST ORDER STATISTICS OF RF-FSO DUAL-HOP AFR COMMUNICATIONS

Probability Density Function (PDF)

The PDF of x_{out} can be expressed through joint and conditional probabilities as:

$$p_{X_{out}}\left(x_{out}\right) = \int_0^\infty dy_{Nm_2} \int_0^\infty \left|\frac{dy_{Nm_1}}{dx_{out}}\right| p_{Y_{Nm_1}}\left(\frac{x_{out}}{y_{Nm_2}^2 y_{Nm_3}^2}\right) \times p_{Y_{Nm_2}}\left(y_{Nm_2}\right) p_{Y_{Nm_3}}\left(y_{Nm_3}\right) dy_{Nm_3}. \quad (5)$$

Cumulative Distribution Function (CDF)

The CDF of x_{out} can be calculated by using (Simon & Alouini, 2000; Gradshteyn & Ryzhik, 2000, Equation 3.381.1 and Equation 8.352.1), respectively for the case where m_{RF} is positive integer,

$$F_{X_{out}}\left(x_{out}\right) = \int_0^{x_{out}} p_{X_{out}}\left(t\right)dt = \frac{4\alpha^\alpha \beta^\beta}{\Gamma\left(m_{RF}\right)\Gamma\left(\alpha\right)\Gamma\left(\beta\right)}\left(m_{RF}-1\right)! \times \left(\frac{\Gamma\left(\alpha\right)\Gamma\left(\beta\right)}{4\alpha^\alpha\beta^\beta} - \sum_{k=0}^{m_{RF}-1} \frac{\left(\frac{m_{RF}x_{out}^2}{\Omega_{RF}}\right)^k \left(\frac{\Omega_{RF}}{m_{RF}}\right)^{m_{RF}}}{k!} J_1\right) \quad (6)$$

where,

$$J_1 = \int_0^\infty dy_{Nm_2} \times \int_0^\infty e^{-\alpha y_{Nm_2}^2 - \beta y_{Nm_3}^2 - \frac{m_{RF}x_{out}^2}{\Omega_{RF} y_{Nm_2}^2 y_{Nm_3}^2} + (2\alpha-4k-1)\ln\left(y_{Nm_2}\right) + (2\beta-4k-1)\ln\left(y_{Nm_3}\right)} dy_{Nm_3}.$$

The integral J_1 in (6) can be solved by applying exponential LAM for two folded integrals (Zlatanov et al., 2008, Equation I.3).

$$\int_0^\infty dy_{Nm_2} \int_0^\infty df_1\left(y_{Nm_2}, y_{Nm_3}\right) e^{-Tf_2\left(y_{Nm_2}, y_{Nm_3}\right)} dy_{Nm_3} \approx \frac{2\pi}{T} \frac{f_1\left(y_{Nm_2}, y_{Nm_3}\right)}{\sqrt{\det H}} e^{-Tf_2\left(y_{Nm_2}, y_{Nm_3}\right)}. \quad (7)$$

It has been shown in (Butler & Wood, 2002) that accurate results can be obtained for real value parameter, T=1. Further, the LAM, also known as exponential LAM for constant multivariate function f_1 and variable multivariate function f_2 is considered in

(Harding & Hausman, 2007). Accordingly, the arguments in Eq. 7 are, respectively, T=1, $f_1\left(y_{Nm_{20}}, y_{Nm_{30}}\right)=1$,

$$f_1\left(y_{Nm_{20}}, y_{Nm_{30}}\right)=-\alpha y_{Nm_{20}}^2-\beta y_{Nm_{30}}^2-\frac{m_{RF}x_{out}^2}{\Omega_{RF}y_{Nm_{20}}^4 y_{Nm_{30}}^4} +\left(2\alpha-4k-1\right)\ln\left(y_{Nm_{20}}\right)+\left(2\beta-4k-1\right)\ln\left(y_{Nm_{30}}\right) \tag{8}$$

Further, the Hessian matrix H in Eq. 7 is,

$$H=\begin{vmatrix} \frac{\partial^2 f_2\left(y_{Nm_{20}}, y_{Nm_{30}}\right)}{\partial y_{Nm_{20}}^2} & \frac{\partial^2 f_2\left(y_{Nm_{20}}, y_{Nm_{30}}\right)}{\partial y_{Nm_{20}}\partial y_{Nm_{30}}} \\ \frac{\partial^2 f_2\left(y_{Nm_{20}}, y_{Nm_{30}}\right)}{\partial y_{Nm_{30}}\partial y_{Nm_{20}}} & \frac{\partial^2 f_2\left(y_{Nm_{20}}, y_{Nm_{30}}\right)}{\partial y_{Nm_{30}}^2} \end{vmatrix}, \tag{9}$$

while, $y_{Nm_{20}}$ and $y_{Nm_{30}}$ are real and positive values obtained from the following equations,

$$\frac{\partial f_2\left(y_{Nm_{20}}, y_{Nm_{30}}\right)}{\partial y_{Nm_{20}}}=0, \tag{10}$$

$$\frac{\partial f_2\left(y_{Nm_{20}}, y_{Nm_{30}}\right)}{\partial y_{Nm_{30}}}=0. \tag{11}$$

Outage Probability (Pout)

The Pout of RF-FSO AFR proposed system is defined as the probability that the output signal goes below the outage threshold $x_{th,RF-FSO}$ (Simon & Alouini, 2000):

$$P_{out}\left(x_{th,RF-FSO}\right)=\int_0^{x_{th,RF-FSO}} p_{x_{out}}(t)\,dt=F_{x_{out}}\left(x_{th,RF-FSO}\right). \tag{12}$$

Average Bit Error Rate (BER)

The average BER, $BER_{RF\text{-}FSO}$ by definition for different binary modulations can be evaluated with (Anees & Bhatnagar, 2015, Equation 23):

$$BER_{RF-FSO}=\frac{q^p}{2\Gamma(p)}\int_0^{\infty}\exp\left(-qx_{out}\right)x_{out}^{p-1}F_{X_{out}}\left(x_{out}\right)dx_{out}. \tag{13}$$

By substituting (5) in (Anees & Bhatnagar, 2015, Equation 23), we obtain:

$$BER_{RF-FSO}=\frac{q^p}{2\Gamma(p)}\frac{4\alpha^{\alpha}\beta^{\beta}}{\Gamma\left(m_{RF}\right)\Gamma(\alpha)\Gamma(\beta)}\left(m_{RF}-1\right)! \times\left(\frac{\Gamma(\alpha)\Gamma(\beta)\Gamma(p)}{4\alpha^{\alpha}\beta^{\beta}q^p}-\sum_{k=0}^{m_{RF}-1}\frac{\left(m_{RF}\right)^k}{k!}J_2\right). \tag{14}$$

where,

$$J_2=\int_0^{\infty}dy_{Nm_2}\int_0^{\infty}dy_{Nm_3}\int_0^{\infty}e^{-\alpha y_{Nm_2}^2-\beta y_{Nm_3}^2-\frac{m_{RF}x_{out}^2}{\Omega_{RF}y_{Nm_2}^4 y_{Nm_3}^4}} \times e^{qx_{out}(2\alpha-4k-1)\ln\left(y_{Nm_2}\right)+\left(2\beta-4k-1\right)\ln\left(y_{Nm_3}\right)+\left(p+2k-1\right)\ln\left(x_{out}\right)}dx_{out}.$$

where p and q denote parameters for different binary modulation such as:

- coherent binary frequency shift keying (CBFSK) for p=0.5 and q=0.5,
- coherent binary phase shift keying (CBPSK) for p=0.5 and q=1,
- non-coherent binary frequency shift keying (NBFSK) for p=1, q=0.5,
- differential binary phase shift keying (DBPSK) for p=1, q=1.

The closed form approximation for $BER_{RF\text{-}FSO}$ can be obtained by evaluating J_2 in Eq. (13) by using exponential LAM for three folded integrals (Zlatanov et al., 2008, Equation I.3):

$$\int_0^{\infty}dy_{Nm_2}\int_0^{\infty}dy_{Nm_3}\int_0^{\infty}df_1\left(y_{Nm_2}, y_{Nm_3}, x_{out}\right)e^{-Tf_2\left(y_{Nm_2}, y_{Nm_3}, x_{out}\right)}dx_{out} \approx\frac{2\pi}{T}\frac{f_1\left(y_{Nm_{20}}, y_{Nm_{30}}, x_{out}\right)}{\sqrt{\det H}}e^{-Tf_2\left(y_{Nm_{20}}, y_{Nm_{30}}, x_{out}\right)}. \tag{15}$$

where the parameters in Eq. 15 are, respectively, T=1, $f_1\left(y_{Nm_2}, y_{Nm_3}, x_{out}\right)=1$,

$$f_2\left(y_{Nm_{20}}, y_{Nm_{30}}, x_{out}\right)=-\alpha y_{Nm_{20}}^2-\beta y_{Nm_{30}}^2-\frac{m_{RF}x_{out}^2}{\Omega_{RF}y_{Nm_{20}}^4 y_{Nm_{30}}^4} -qx_{out0}+\left(2\alpha-4k-1\right)\ln\left(y_{Nm_{20}}\right)+\left(2\beta-4k-1\right)\ln\left(y_{Nm_{30}}\right) +\left(p+2k-1\right)\ln\left(x_{out0}\right)$$

Further, $y_{Nm_{20}}, y_{Nm_{30}}, x_{out0}$ and H in Eq. 14 can be evaluated from the following equations, respectively,

$$\frac{\partial^2 f_2\left(y_{Nm_{20}}, y_{Nm_{30}}, x_{out0}\right)}{\partial y_{Nm_{20}}}=0, \qquad \frac{\partial^2 f_2\left(y_{Nm_{20}}, y_{Nm_{30}}, x_{out0}\right)}{\partial y_{Nm_{30}}}=0,$$

$$\frac{\partial^2 f_2\left(y_{Nm_{20}}, y_{Nm_{30}}, x_{out0}\right)}{\partial x_{out0}}=0.$$

$$H=\begin{vmatrix} \frac{\partial^2 f_2\left(y_{Nm_{20}}, y_{Nm_{30}}, x_{out0}\right)}{\partial y_{Nm_{20}}^2} & \frac{\partial^2 f_2\left(y_{Nm_{20}}, y_{Nm_{30}}, x_{out0}\right)}{\partial y_{Nm_{20}}\partial y_{Nm_{30}}} & \frac{\partial^2 f_2\left(y_{Nm_{20}}, y_{Nm_{30}}, x_{out0}\right)}{\partial y_{Nm_{20}}\partial x_{out0}} \\ \frac{\partial^2 f_2\left(y_{Nm_{20}}, y_{Nm_{30}}, x_{out0}\right)}{\partial y_{Nm_{30}}\partial y_{Nm_{20}}} & \frac{\partial^2 f_2\left(y_{Nm_{20}}, y_{Nm_{30}}, x_{out0}\right)}{\partial y_{Nm_{30}}^2} & \frac{\partial^2 f_2\left(y_{Nm_{20}}, y_{Nm_{30}}, x_{out0}\right)}{\partial y_{Nm_{30}}\partial x_{out0}} \\ \frac{\partial^2 f_2\left(y_{Nm_{20}}, y_{Nm_{30}}, x_{out0}\right)}{\partial x_{out0}\partial y_{Nm_{20}}} & \frac{\partial^2 f_2\left(y_{Nm_{20}}, y_{Nm_{30}}, x_{out0}\right)}{\partial x_{out0}\partial y_{Nm_{30}}} & \frac{\partial^2 f_2\left(y_{Nm_{20}}, y_{Nm_{30}}, x_{out0}\right)}{\partial x_{out}^2} \end{vmatrix},$$

NUMERICAL RESULTS

In numerical results we provide performance analysis as well as comparison of exact and approximated results of the first order outage statistics under weak, moderate and strong nTIF and TIF conditions of the RF-FSO dual-hop AFR system.

First order Statistics

The FSO section of dual-hop RF- FSO AFR relay link is modeled with d-sNmRP, where numerical results are evaluated for different optical fading severity parameters (α, β) and for different values of irradiance variance $\sigma_{d-sN_m^2} = \frac{1}{\alpha} + \frac{1}{\beta} + \frac{1}{\alpha\beta}$. The RF section of dual-hop RF-FSO AFR is modeled with *Nm* RP and evaluated for RF fading severity parameter m_{RF}.

- Outage Probability

The $P_{out}\left(x_{th,RF-FSO}\right)$ for normalized Ω_{RF}=1 under weak (α=4, β=4, m_{RF}=4), moderate to weak (α=3, β=3, m_{RF}=3), moderate to strong (α=2, β=2, m_{RF}=2) and strong (α=1, β=1, m_{RF}=1) nTIF and TIF channel conditions is shown in Figure 1. It can be seen that $P_{out}\left(x_{th,RF-FSO}\right)$ approximated by exponential LAM for the considered nTIF and TIF severity values fits well with exact analytical expression (Eq. 6) especially for higher $P_{out}\left(x_{th,RF-FSO}\right)$ dB values. It is evident that the system performance improvement can be achieved by increasing TIF and nTIF severity parameters since $P_{out}\left(x_{th,RF-FSO}\right)$ decreases.

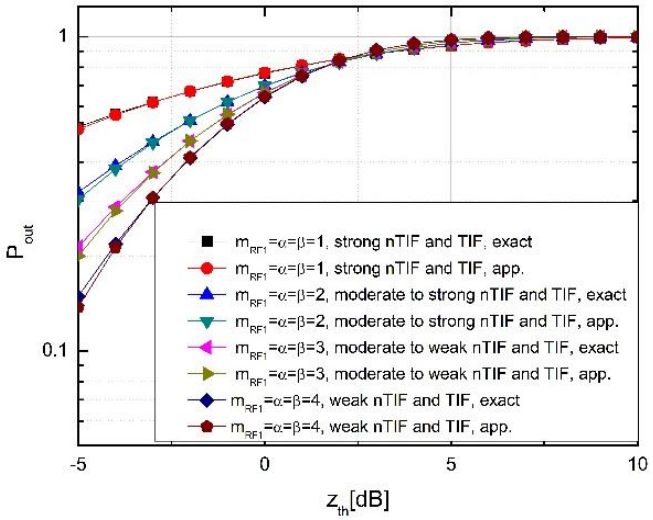

Figure 1. Comparison of exact and approximated results for P_{out} under weak, moderate and strong TIF and nTIF channel conditions.

- Average Bit Error Rate

The average bit error rate versus Ω_{RF} for different binary modulation schemes under weak (α=3, β=3, m_{RF}=3) , moderate (α=2, β=2, m_{RF}=2) and strong (α=1, β=1, m_{RF}=1) nTIF and TIF channel conditions is presented in Figure 2. As expected, under moderate and weak TIF and nTIF channel conditions, BER noticeably decreases what can enable RF-FSO AFR system performance improvement.

Moreover, it can be seen that nTIF and TIF severity parameters (α, β, m_{RF}) have stronger impact on $BER_{RF\text{-}FSO}$ than considered binary modulations. In most of the observed range and under considered nTIF and TIF channel conditions the best performance results relating to $BER_{RF\text{-}FSO}$ can be achieved for CBPSK. The comparison of exact analytical expression and approximated closed form expression for $BER_{RF\text{-}FSO}$ of DBPSK modulated signal are provided in Figure 3. It can be noticed that exponential LAM fails to match approximation with exact analytical results for higher Ω_{RF} dB values.

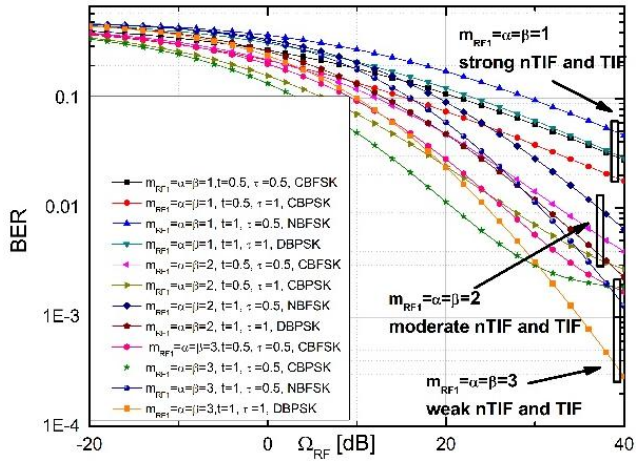

Figure 2. BER versus Ω_{RF} under weak, moderate and strong TIF and nTIF channel conditions and for different binary modulation schemes.

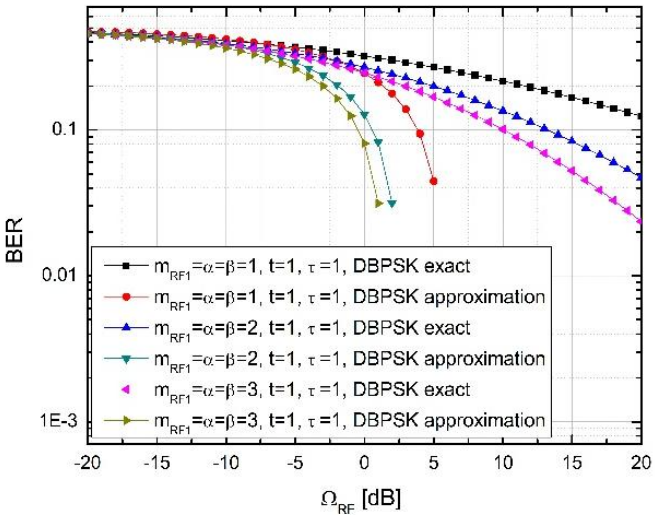

Figure 3. Comparison of exact and approximated results for BER versus Ω_{RF} under weak, moderate and strong TIF and nTIF channel conditions.

CONCLUSION

This paper addresses the first -order outage statistics of the RF-FSO AFR dual-hop relay link. In particular, we provide closed form analytical expressions for *i*.) cumulative distribution function, *ii*.) outage probability and *iii*.) average bit error rate of the product of *Nm* and d-sNmRPs. Moreover, we provide comparison of novel exact analytical and LAM approximated closed form expressions under weak, strong and moderate nTIF and TIF channel conditions. Numerical examples show that exponential LAM approximations fit well with exact expressions for cumulative distribution function especially for higher output threshold dB values. On the other hand, exponential LAM fails to perform well in the case of $BER_{RF\text{-}FSO}$, especially in higher RF average power dB regime. In general, nTIF and TIF severity parameters have more dominant impact on first order statistics then other observed parameters such as: type of binary modulation in case of $BER_{RF\text{-}FSO}$. Our future works are going to include cooperative RF-FSO AFR relay systems.

ACKNOWLEGMENTS

The authors would like to acknowledge the COST Action 15104.This work has been partially funded from the VIU project of Tomsk Polytechnic University, Russia, No. 216/2019.

REFERENCES

Al-Ahmadi, S. 2014. The Gamma-Gamma Signal Fading Model: A Survey [Wireless Corner]. IEEE Antennas and Propagation Magazine, 56(5), pp. 245-260. doi:10.1109/map.2014.6971962

Andrews, L. C., & Phillips, R. L. 2005. Laser Beam Propagation through Random Media. Washington: SPIE-Intl Soc Optical Eng. doi:10.1117/3.626196

Anees, S., & Bhatnagar, M. R. 2015. Performance of an Amplify-and-Forward Dual-Hop Asymmetric RF–FSO Communication System. Journal of Optical Communications and Networking, 7(2), p. 124. doi:10.1364/jocn.7.000124

Butler, R. W., & Wood, A. T. A. 2002. Laplace approximations for hypergeometric functions with matrix argument. The Annals of Statistics, 30(4), pp. 1155-1177. doi:10.1214/aos/1031689021

Douik, A., Dahrouj, H., Al-Naffouri, T. Y., & Alouini, M. 2016. Hybrid Radio/Free-Space Optical Design for Next Generation Backhaul Systems. IEEE Transactions on Communications, 64(6), pp. 2563-2577. doi:10.1109/tcomm.2016.2557789

Gradshteyn, I. S., & Ryzhik, I. M. 2010. Table of Integrals, Series, and Products. New York: Academic. 6th ed.

Hajri, N., Youssef, N., Kawabata, T., Patzold, M., & Dahech, W. 2018. Statistical Properties of Double Hoyt Fading With Applications to the Performance Analysis of Wireless Communication Systems. IEEE Access, 6, pp. 19597-19609. doi:10.1109/access.2018.2820746

Hamza, A. S., Deogun, J. S., & Alexander, D. R. 2019. Classification Framework for Free Space Optical Communication Links and Systems. IEEE Communications Surveys and Tutorials, 21(2), pp. 1346-1382. doi:10.1109/comst.2018.2876805

Harding, M. C., & Hausman, J. 2007. Using a Laplace approximation to estimate the random coefficients logit model by nonlinear least squares. International Economic Review, 48(4), pp. 1311-1328. doi:10.1111/j.1468-2354.2007.00463.x

Illi, E., Bouanani, F. E., & Ayoub, F. 2017. A performance study of a hybrid 5G RF/FSO transmission system. In 2017 International Conference on Wireless Networks and Mobile Communications (WINCOM). Institute of Electrical and Electronics Engineers (IEEE)., pp. 1-7. doi:10.1109/wincom.2017.8238167

Issaid, C. B., & Alouini, M. 2019. Level Crossing Rate and Average Outage Duration of Free Space Optical Links. IEEE Transactions on Communications, 67(9), pp. 6234-6242. doi:10.1109/tcomm.2019.2918324

Karimi, M., & Masoumeh, N. 2011. Free space optical communications via optical amplify-and-forward relaying. Jour. of Light. Technology, 29(2), pp. 242-248.

Khalighi, M. A., & Uysal, M. 2014. Survey on Free Space Optical Communication: A Communication Theory Perspective. IEEE Communications Surveys and Tutorials, 16(4), pp. 2231-2258. doi:10.1109/comst.2014.2329501

Milosevic, N., Stefanovic, M., Nikolic, Z., Spalevic, P., & Stefanovic, C. 2018. Performance Analysis of Interference-Limited Mobile-to-Mobile κ-μ Fading Channel. Wireless Personal Communications, 101(3), pp. 1685-1701.

Nakagami, M. 1960. The m-distribution-A general formula of intensity distribution of rapid fading. In W. G. Hoffman Ed., Statistical Methods in Radio Wave Propagation. Oxford: Pergamon.

Petkovic, M., Djordjevic, G. T., & Djordjevic, I. B. 2017. Analysis of mixed RF/FSO system with imperfect CSI estimation. In 2017 19th International Conference on Transparent Optical Networks (ICTON). Institute of Electrical and Electronics Engineers (IEEE)., pp. 1-7. doi:10.1109/icton.2017.8024759

Petkovic, M. I., & Trpovski, Z. 2018. Exact Outage Probability Analysis of the Mixed RF/FSO System With Variable-Gain Relays. IEEE Photonics Journal, 10(6), pp. 1-14. doi:10.1109/jphot.2018.2882611

Simon, M. K., & Alouini, M. 2000. Digital Communication Over Fading Channels. New York, USA: Wiley. doi:10.1002/0471200697

Stefanovic, C. 2017. LCR of amplify and forward wireless relay systems in general alpha-Mu fading environment. In Proceedings 25th Telecommunication Forum. pp. 1-6.

Stefanovic, C., Pratesi, M., & Santucci, F. 2018. Performance evaluation of cooperative communications over fading channels in vehicular networks. In Proceedings 2nd URSI Atalntic Science Radio Meeting (AT-RASC). pp. 1-4.

Stefanovic, D., Stefanovic, C., Djosic, D., Milic, D., Rancic, D., & Stefanovic, M. 2019. LCR of the Ratio of the Product of Two Squared Nakagami-m Random Processes and Its Application to Wireless Communication Systems. In 2019 18th International Symposium INFOTEH-JAHORINA (INFOTEH).Institute of Electrical and Electronics Engineers (IEEE)., pp. 1-4. doi:10.1109/infoteh.2019.8717765

Stefanovic, C., Pratesi, M., & Santucci, F. 2019. Second Order Statistics of Mixed RF-FSO Relay Systems and its Application to Vehicular Networks. In Proceedings 2019 IEEE International Conference on Communications (ICC). pp. 1-6.

Talha, B., & Pätzold, M. 2007. On the statistical properties of double Rice channels. In Proceedings 10th International Symposium on Wireless Personal Multimedia Communications, WPMC. pp. 517-522.

Vetelino, F. S., Young, C., Andrews, L., & Recolons, J. 2007. Aperture averaging effects on the probability density of irradiance fluctuations in moderate-to-strong turbulence. Applied Optics, 46(11), p. 2099. doi:10.1364/ao.46.002099

Wang, J. 2010. Dirichlet Processes in Nonlinear Mixed Effects Models. Communications in Statistics - Simulation and Computation, 39(3), pp. 539-556. doi:10.1080/03610910903511745

Zedini, E., Ansari, I. S., & Alouini, M. 2015. Performance Analysis of Mixed Nakagami- m and Gamma–Gamma Dual-Hop FSO Transmission Systems. IEEE Photonics Journal, 7(1), pp. 1-20. doi:10.1109/jphot.2014.2381657

Zedini, E., Ansari, I. S., & Alouini, M. 2015. Unified performance analysis of mixed line of sight RF-FSO fixed gain dual-hop transmission systems. In 2015 IEEE Wireless Communications and Networking Conference (WCNC). Institute of Electrical and Electronics Engineers (IEEE)., pp. 46-51. doi:10.1109/wcnc.2015.7127443

Zlatanov, N., Hadzi-Velkov, Z., & Karagiannidis, G. 2008. Level crossing rate and average fade duration of the double Nakagami-m random process and application in MIMO keyhole fading channels. IEEE Communications Letters, 12(11), pp. 822-824. doi:10.1109/lcomm.2008.081058

UNIVERSITY THOUGHT
Publication in Natural Sciences, Vol.10, No.1, 2020, pp. 63-68.
DOI: https://doi.org/10.5937/univtho10-25351
Original Scientific Paper

COOPERATIVE MOBILE DATA COLLECTION IN SMART CITIES

IZZET FATIH SENTURK[1,⋆]

[1]Faculty of Engineering and Natural Sciences, Bursa Technical University, Bursa, Turkey

ABSTRACT

Smart cities are driven by huge amount of data collected from sensors deployed across the city. Sensors typically form a multi-hop network with a base station (BS) in order to send their data to the command and control center. However, sparse deployment of sensors can leave subsets of the network partitioned from the rest of the network. In such a case, isolated partitions cannot forward their data to the BS. Consequently, network coverage and data fidelity decline. A possible solution to link partitions and provide connectivity is employing mobile data collectors (MDCs). A smart vehicle supporting wireless communication can act as an MDC and carry data between sensors and the BS. Using a single MDC extends the average tour length. To minimize the maximum tour length, multiple MDCs can be employed. To identify sensors to be visited by each MDC, this paper clusters partitions as many as the number of MDCs and assigns an MDC for each cluster. Then two different cooperative data collection schemes are considered based on the availability of inter-MDC data exchange. If MDCs collaborate in data delivery, they meet at certain meeting points for data exchange. Such a cooperation avoids the requirement of visiting the BS for some MDCs and reduces tour lengths. On the other hand, MDCs closer to the BS can experience data loss due to buffer overflow given the higher volume of the accumulated data. Presented approaches are evaluated in terms of maximum tour length, data latency, and data loss. The smart city application is simulated with deployment of sensors on certain amenity types. Geographic data is obtained from a volunteered geographic information system and MDC mobility is restricted with the road network. Obtained results indicate that MDC cooperation decreases maximum tour length at the expense of increased rate of data loss and data latency.

Keywords: Wireless sensor networks, Caching, Buffer overflow, Latency, Energy consumption.

INTRODUCTION

The smart city phenomenon is a reaction against the continuous worldwide urbanization which leads to increased demand on limited resources in urban areas. Resource efficiency is a must for cities and gathering required data in a timely manner is essential to make better decisions regarding the management of urban infrastructure and services. The decision making part is handled by the the data analytics platform of the smart city framework by integrating big data and artificial intelligence. This framework is fueled with the data loop between sensors deployed across the city, urban infrastructure and services, and the data analytics platform. Wireless communication technology is the link in this loop which provides the most efficient solution for connectivity.

Despite availability of various wireless communication technologies, sensors are often restricted with limited transmission ranges to reduce energy consumption of the radio module. Therefore, sensors typically form a multi-hop Wireless Sensor Network (WSN) connected to the rest of the world with a base station (BS). However, smart city applications require sensor deployment across a large area and network connectivity can be partitioned due to the sparsity of the network. To link the partitions, various solutions can be pursued. Given the sensors are stationary, either additional nodes can be added between partitions to link them or a mobile data collector (MDC) can be used to carry data between partitions and the BS.

According to a recent study, linking partitions with additional nodes requires deploying nodes more than 94% of the network size (Senturk & Kebe, 2019) when low-rate wireless communication technologies are employed. To avoid the complexity of additional node deployment, this paper considers mobile data collection to sustain connectivity in smart city applications. An MDC can be a smart vehicle with wireless communication support. MDCs can be dedicated vehicles employed for mainly data collection. In such a case, mobility of the vehicle can be controlled and optimized based on considered metrics such as travel length or delay. It is also possible to use public transport vehicles following pre-determined paths. This approach eliminates the additional cost of vehicles in the expense of increased tour lengths and data latency due to the lack of mobility control. Worse, some regions will be likely out of network coverage. To ensure network connectivity, this paper assumes controlled mobility with dedicated vehicles. Nevertheless, the emergence of connected vehicles and the distributed ledger technology are promising to avoid the requirement of dedicated vehicles while ensuring data privacy. A sample demonstration of mobile data collection can be found in Figure 1.

Using a single MDC to link the whole network extends the resulting tour length. On the other hand, employing multiple MDCs can reduce the maximum tour length if the workload can be distributed uniformly between MDCs. To ensure a fair distribution of sensors to be visited between MDCs, this paper employs

⋆ Corresponding author:izzet.senturk@btu.edu.tr

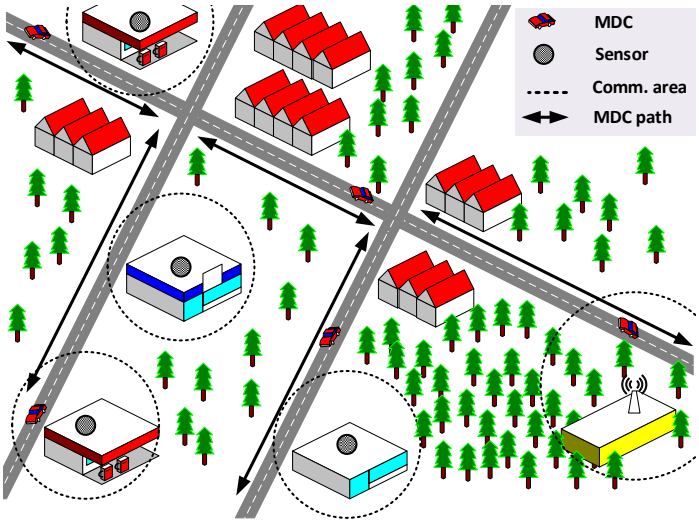

Figure 1. Mobile data collection with smart vehicles.

Un-weighted Pair-Group Method using Arithmetic Averages (UPGMA) clustering algorithm. The idea is grouping partitions according to the number of available MDCs. Subsequently, each MDC is assigned to a cluster. Each cluster can contain multiple partitions comprising several sensors. Visiting one of the sensors enables data collection from the whole partition considering the availability of multi-hop routing. Thus, it is sufficient to visit only a subset of sensors to collect data from the network. Visiting a sensor implies approaching close enough to establish wireless communication. Based on the distance between sensors, MDC can collect data from multiple sensors of different partitions at certain locations. It can be argued that total tour length of MDCs can be reduced by minimizing the number of locations to be visited. However, minimizing the locations to be visited to provide full network coverage is a complicated problem. This paper follows the Steiner Zone with Partitions (SZP) approach to identify locations to be visited in each cluster. SZP defines circular disks to represent communication areas assuming omnidirectional antennas and evaluates the degree of disk overlaps. SZP designates visiting points within the overlapping regions and favors overlaps with the highest degrees first.

When multiple MDCs are available, MDCs can cooperate in data delivery through inter-MDC data exchange. To exchange data, two or more MDCs meet at a certain meeting point. Based on the direction of the data exchange, this cooperation can be modeled as a tree where the *BS* is the root and data moves from leaf nodes to the root through parent nodes. Each parent node waits at the meeting point until collecting data from its children. The size of the data accumulated at parent nodes increases and MDCs closer to the *BS* can experience data loss due to buffer overflow. On the other hand, the tree structure obtained through inter-MDC data exchange avoids visiting the *BS* for most of the nodes and reduces tour lengths. To avoid extended tour lengths, this paper assumes availability of multiple MDCs and considers two different use-cases based on the availability of MDC cooperation in data exchange. Cooperative mobile data collection (C-MDC) assumes availability of inter-MDC data exchange. Individual mobile data collection (I-MDC) avoids this assumption and requires all MDCs to visit the *BS* to deliver their data. Limited cache size is assumed for MDCs. This paper evaluates both approaches in terms of maximum tour length, data latency and data loss through simulations considering metropolitan cities in Turkey.

RELATED WORK

Determining the order of visits among the given set of cities which yields the shortest tour is regarded as the traveling salesman problem (TSP). In TSP, the tour is circular and the salesman returns to the initial city. This paper considers a variation of the TSP problem known as TSP with neighborhoods (TSPN). TSPN seeks the shortest tour visiting a set of polygons. Unlike TSP which considers discrete points, the search space is continuous in TSPN. Considered problem is regarded as TSPN since we assume availability of wireless communication for sensors. Assuming omnidirectional antenna, regions to be visited can be represented with disks. For each sensor, a disk is defined centered at the location of the respective sensor. The radius of the disk is equal to the transmission range (R). Disks overlap if the distance between sensors is less than $2 \times R$. After defining disks, the problem of visiting sensors and returning to the *BS* with the shortest tour length becomes TSPN.

In the literature, various solutions are available to solve TSPN (Alatartsev et al., 2013a,b; Shuttleworth et al., 2008; Gulczynski et al., 2006). CIH (Alatartsev et al., 2013a) and C3-Opt (Alatartsev et al., 2013b) consider the TSPN problem as the combination of TSP and TPP (Touring a sequence of Polygons Problem). The idea is applying one of the tour improvement algorithms (e.g. 3-Opt (Frederick, 1958), Rubber-band algorithm (Pan et al., 2010)) as the TPP solver and then applying one of the available TSP solutions to the obtained set of points. (Shuttleworth et al., 2008) considers the problem of automated meter reading using radio frequency identification (RFID) technology. The goal is collecting readings from meters by approaching close enough while minimizing the tour length. The problem is formulated as the close enough TSP (CETSP). The problem defined in (Shuttleworth et al., 2008) is very similar to the considered problem since they also assume a road network with street segments. However, they employ a propriety software to solve the problem. Several heuristics are presented in (Gulczynski et al., 2006) for CETSP. This paper employs SZP to identify positions to be visited in the two-dimensional Euclidean space. SZP extends Steiner Zone approach presented in (Gulczynski et al., 2006). However, unlike Steiner Zone approach, SZP can handle partitions with multiple sensors.

Presented work is different from earlier studies due to the additional complexity of considered assumptions. First of all, this paper employs multiple MDCs to collect data. Therefore, the goal is not only minimizing the total tour length but also balancing the

load uniformly between MDCs. In the literature, assuming multiple salesmen is regarded as the multiple traveling salesmen problem (mTSP) (Bektas, 2006). In mTSP, a single depot node exists. Tours of all salesmen start and end at the depot. Presented problem is similar to mTSP since multiple MDCs are available with a single *BS*. This paper employs Un-weighted Pair-Group Method using Arithmetic Averages (UPGMA) clustering algorithm to divide the workload between MDCs. The idea is grouping partitions according to the number of available MDCs. In this work, two different data collection approaches are proposed based on the availability of cooperation between MDCs. *I-MDC* requires each MDC to visit *BS* in order to deliver its data. *C-MDC*, on the other hand, exploits inter-MDC cooperation in data delivery.

Another challenge is restricting mobility with the road network. Most of the earlier studies assume availability of a direct path between nodes. This paper models the road network as a weighted graph with directed edges for corresponding road segments. The road data is obtained from OSM (OpenStreetMap contributors, 2020). OSM is a volunteered geographic information (VGI) system. OSM data is collected using OSMnx (Boeing, 2017). Elevation data is obtained from Google Maps Elevation API (Platform, 2020).

DATA COLLECTION AND THE SIMULATION SETUP

This paper simulates data sampling from sensors deployed across a city and employs presented mobile data collection schemes to collect sampled data assuming a smart city application at the top. To simulate considered scenarios in a realistic manner, sensor locations and corresponding data generation rates are determined using OSM, a geographic information system. OSM follows a participatory approach to collect geospatial data. OSM models the real world using three basic data elements: node, way, and relation. Node denotes a point in the space. Way is an ordered list of nodes. Relation signifies how different elements interact. To designate sensor locations, Points of Interest (POIs) are obtained through OSM and sensors are deployed on certain POIs. This paper considers three POIs, namely school, hospital, and police station for sensor deployment. Data generation rates are as follows: 1, 2, and 3 sampling per second for hospitals, police stations, and schools respectively.

A POI can be represented as a node or as a polygon (i.e. way) to denote the boundary of the building. If the POI is represented as a polygon, multiple sensors are deployed to monitor the building. The actual sensor location is determined according to the drivable road network where MDCs can travel to ensure data collection from the sensor. Therefore, sensors are located at the closest road segment. A common transmission range is used for both sensors and MDCs. The transmission range is varied between 20 and 50 in the experiments. OSM also provides drivable road segments and mobility of MDCs is restricted with the road network. To calculate latency in a realistic manner, velocity of the MDCs are set dynamically according to the speed limit of the crossed road segment. OSM provides speed limits. If the maximum speed limit is not available on OSM for the considered road segment, a default limit of 50 km/h is used.

We assume availability of multi-hop routing between sensors. Thus, sensors can form a connected component (i.e. partition). Multi-hop communication enables data collection from the whole network upon visiting one of the sensors in the partition. Identifying the minimum set of sensors to be visited which ensures full network coverage is a complicated problem and this paper employs Steiner Zone with Partitions (SZP) approach as discussed earlier. SZP provides visiting points for data collection. Visiting points are not necessarily sensor locations but coordinates in the two-dimensional Euclidean space given the availability of wireless communication. On the other hand, visiting points are always part of the drivable road network. Based on the employed transmission range, the average number of visiting points vary as shown in Table 1.

Table 1. The number of points visited by MDCs with respect to the employed transmission range. The average number for 30 cities is reported. The average sensor count is 103,73.

Transmission range	The number of visiting points
20	38,77
30	34,00
40	28,37
50	24,20

In the experiments, the number of MDCs is set to 3. Sensors are clustered using UPGMA (Wikipedia, 2020c) and each MDC is assigned to a cluster. The first sensor in the list of sensors is regarded as the *BS*. As mentioned earlier, two different approaches are considered for mobile data collection. I-MDC does not assume MDC cooperation and requires MDCs to visit the *BS* to deliver their data. In C-MDC, MDCs meet at certain meeting points to forward their data to the next MDC. MDC meeting points are determined according to cluster size of the respective MDCs. For two MDCs MDC_a and MDC_b assigned to clusters $cluster_a$ and $cluster_b$ respectively, two visiting points vp_a and vp_b are selected from respective clusters such that the distance between visiting points are the minimum. If the size of $cluster_a$ is smaller, MDC_a visits MDC_b at vp_b, and vice-versa.

After designating clusters along with the set of visiting points, data collection paths are computed for each MDC. Visiting a set of points and returning to the starting point with a path minimizing the objective function is regarded as the Traveling Salesman Problem (Wikipedia, 2020b). In this paper, we aim to minimize the path length of MDCs. Given the availability of multiple MDCs, the goal can be defined as minimizing the maximum path length. Inter-MDC data exchange can minimize the maximum path length by avoiding the requirement of visiting the *BS* for certain MDCs. On the other hand, cooperation in data delivery can increase latency and data loss due to the additional waiting

times and the extended size of the accumulated data. Data latency is computed based on the path length, velocity of the MDCs and the waiting time for other MDCs. Waiting time and the size of the accumulated data are computed by modeling the inter-MDC cooperation as a tree where the *BS* is the root. Each sensor sampling is assumed be sent in packets of 4 bytes. A buffer size of 1 MB is assumed for MDCs. TSP is solved using OR-Tools library (OR-Tools, 2020).

This paper considers 30 metropolitan cities of Turkey (Wikipedia, 2020a). Obtained spatial data is limited within the bounding box of 1 km from city centers. For statistical significance, the average results are reported.

EXPERIMENTAL EVALUATION

Performance metrics

- *Maximum path length*: As the name suggests, this metric reports the length of the longest path among MDCs. Shorter path length reduces the cost of mobility. If the MDC is battery operated this metric suggests the network lifetime.
- *Latency*: This metric denotes the time required to complete the path. Two main sources of delay are considered; the duration of mobility and the waiting time for other MDCs.
- *Total overflow*: This metric indicates the ratio of data loss due to buffer overflow.

Results

Experiment results in terms of maximum path length are shown in Figure 2. According to the obtained results, C-MDC outperforms I-MDC thanks to inter-MDC data exchange. The results indicate that MDC cooperation in data delivery alleviates the cost of mobility by reducing the length of the longest path up to 12 per cent. The decline in the maximum path length can be attributed to the lack of requirement of visiting the *BS* in order to deliver data. Mobile data collection scheme imposes extended paths for MDCs assigned to partitions with sensors deployed far from the *BS*. Cooperation in data delivery, on the other hand, enables forwarding collected data to the next MDC instead of visiting the *BS*. This paper considers an application area of 1 km and it can be argued that the performance gap between two approaches can increase with an extended application area.

It can also be noticed from Figure 2 that the maximum path length declines when the employed transmission range is extended. The decline in the maximum path length can be attributed to the decreased number of visiting points when the transmission range is increased as indicated in Table 1.

Figure 3 portrays experiment results in terms of data latency. Two main sources of latency are considered in the experiments, namely mobility delay and waiting delay. Mobility delay denotes the duration which the data is moved on MDCs until reaching the *BS*. Mobility delay is based on the MDC velocity and the length of the travel path. Considering the performance of C-MDC in terms

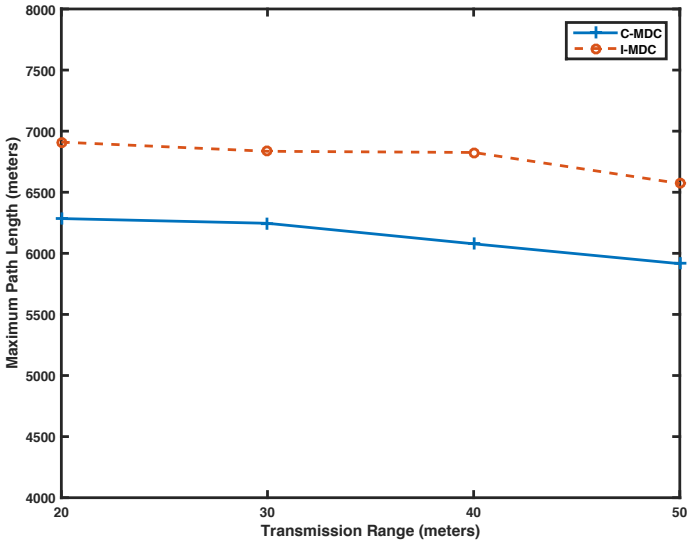

Figure 2. Experiment results in terms of maximum path length with respect to the employed transmission range.

of maximum path length, one can expected reduced mobility delay as well for C-MDC. However, obtained results indicate increased data latency up to 68 per cent for C-MDC compared to I-MDC. These results suggest the overwhelming impact of waiting delay in data latency.

Recall that the inter-MDC cooperation leads to a tree structure in data collection. The *BS* acts as the root and the direction of data transfer is from child nodes to their parents. Parent nodes wait at the meeting points to collect data until all of the child nodes arrive. Consequently, waiting delay can be considerably high to dominate the latency results. Note that the waiting time is zero for I-MDC since MDCs do not have to wait each other and rather forward the data to the *BS* directly.

According to obtained results, transmission range has limited impact on latency. For C-MDC, the latency declines slightly when the transmission range is extended. On the other hand, the latency is almost constant for I-MDC.

The results of the experiments to assess the ratio of total data loss due to buffer overflow are given in Figure 4. For both of the approaches, the rate of the total data loss is less than 3 per cent. However, C-MDC leads to increased data loss up to 75 per cent compared to I-MDC. Note that the size of the sampled data increases if the data collection is delayed. The main source of delay for I-MDC is mobility delay. As denoted in Figure 2, I-MDC leads to increased maximum path length which implies extended mobility delay. On the other hand, as illustrated in Figure 3, waiting delay dominates the overall latency for C-MDC. Consequently, I-MDC outperforms C-MDC by reducing data loss.

Another factor which impairs the performance of C-MDC is the cooperation in data delivery and the resulting tree structure. In I-MDC, MDCs carry data exclusively from their respective clusters. On the other hand, C-MDC leads to a tree structure and imposes parent MDCs to carry the data of their children. Given the

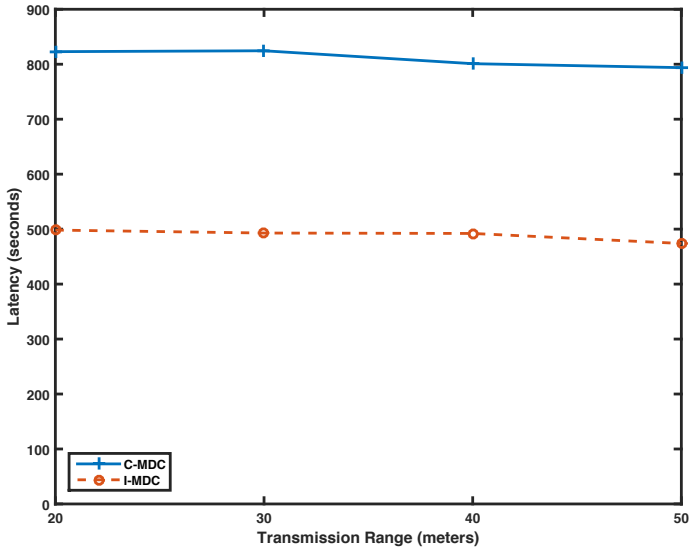

Figure 3. Experiment results in terms of latency with respect to employed transmission range.

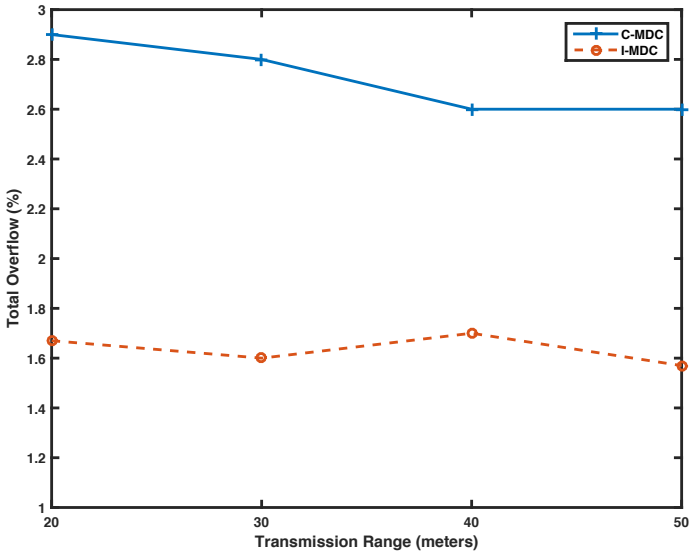

Figure 4. Experiment results in terms of data loss with respect to employed transmission range.

large volume of the accumulated data for MDCs closer to the *BS*, data loss is more likely for C-MDC compared to I-MDC.

The results indicate that increased transmission range can alleviate data loss for C-MDC. The rate of the data loss fluctuates for I-MDC for varying transmission ranges.

CONCLUSION

This paper presents two approaches for mobile data collection considering a smart city application. The idea is employing smart vehicles to collect sensor data in a sparse wireless sensor network deployed at city scale. One of the approaches, C-MDC, exploits cooperation of the vehicles in data delivery to the *BS*. C-MDC leads to a tree structure modeling the data collection. In this tree, the *BS* acts as the root and the data is forwarded from children to parents. This scheme avoids the requirement of interacting with the *BS* directly as in the other approach, I-MDC. To analyze the trade-offs, both approaches are evaluated in terms of maximum path length, data latency, and the rate of data loss. The results show that C-MDC decreases maximum tour length at the expense of increased rate of data loss and data latency. To simulate the smart city application in a realistic manner, sensor locations and data generation rates as well as the mobility path of the vehicles are determined according to geospatial data obtained from a volunteered geographic information system.

ACKNOWLEDGEMENT

This work was supported by the Scientific and Technical Research Council of Turkey (TUBITAK) under Grant No. EEEAG-117E050.

REFERENCES

Alatartsev, S., Augustine, M., & Ortmeier, F. 2013a

Alatartsev, S., Mersheeva, V., Augustine, M., & Ortmeier, F. 2013b

Bektas, T. 2006, The multiple traveling salesman problem: an overview of formulations and solution procedures, Omega, 34(3), pp. 209-219. doi.org/10.1016/j.omega.2004.10.004

Boeing, G. 2017, OSMnx: New methods for acquiring, constructing, analyzing, and visualizing complex street networks, Computers, Environment and Urban Systems, 65, pp. 126-139. doi.org/10.1016/j.compenvurbsys.2017.05.004

Frederick, B. 1958, An algorithm for solving travelling-salesman and related network optimization problems, Operations Research, 6(6), pp. 897-897.

Gulczynski, D. J., Heath, J. W., & Price, C. C. 2006, The Close Enough Traveling Salesman Problem: A Discussion of Several Heuristics. Boston, MA: Springer US, pp. 271-283. doi.org/10.1007/978-0-387-39934-8$_1$6

OpenStreetMap contributors. 2020, Planet dump retrieved from https://planet.osm.org, https://www.openstreetmap.org. Accessed January 20, 2020.

OR-Tools, G. 2020, The OR-Tools Suite, https://developers.google.com/optimization. Accessed January 20, 2020.

Pan, X., Li, F., & Klette, R. 2010, Approximate shortest path algorithms for sequences of pairwise disjoint simple polygons (Citeseer).

Platform, G. M. 2020, Elevation API, `https://developers.google.com/maps/documentation/elevation/start`. Accessed January 20, 2020

Senturk, I. F. & Kebe, G. Y. 2019, in A New Approach to Simulating Node Deployment for Smart City Applications Using Geospatial Data, International Symposium on Networks, Computers and Communications (ISNCC'19), June 18-20, 2019, Istanbul, Turkey, pp. 1-5.

Shuttleworth, R., Golden, B. L., Smith, S., & Wasil, E. 2008, Advances in Meter Reading: Heuristic Solution of the Close Enough

Traveling Salesman Problem over a Street Network. Boston, MA: Springer US, pp. 487-501. doi.org/10.1007/978-0-387-77778-8$_2$2

Wikipedia. 2020a, Metropolitan Municipalities in Turkey, https://en.wikipedia.org/wiki/Metropolitan_municipalities_in_Turkey. Accessed January 20, 2020.

Wikipedia. 2020b, Travelling Salesman Problem, https://en.wikipedia.org/wiki/Travelling_salesman_problem. Accessed January 20, 2020.

Wikipedia. 2020c, UPGMA (Unweighted Pair Group Method with Arithmetic Mean), https://en.wikipedia.org/wiki/UPGMA. Accessed January 20, 2020.

UNIVERSITY THOUGHT
Publication in Natural Sciences, Vol.10, No.1, 2020, pp. 69-71.
DOI: https://doi.org/10.5937/univtho10-26075
Original Scientific Paper

SOME REMARKS ON AN ALTERNATIVE APPROACH FOR BOLTZMANN DISTRIBUTION OF HYDROGEN ATOMS

NICOLA FABIANO[1,2,⋆], STOJAN RADENOVIĆ[3]

[1]Nonlinear Analysis Research Group, Ton Duc Thang University, Ho Chi Minh City, Vietnam
[2]Faculty of Mathematics and Statistics, Ton Duc Thang University, Ho Chi Minh City, Vietnam
[3]Faculty of Mechanical Engineering, University of Belgrade, Kraljice Marije 16, 11120 Beograd 35, Serbia

ABSTRACT

We propose an alternative approach to Boltzmann distribution concerning the hydrogen atom and compare our results to previous formalism for some observables.

Keywords: Hydrogen atom, Partition function, Tsallis model.

THE PROBLEM

The probability P_n for the Boltzmann distribution is given by

$$P_n = \frac{\exp -(\beta E_n)}{\sum_n \exp -(\beta E_n)} \, . \tag{1}$$

It gives the probabilty that a system in equilibrium with a heat reservoir is found in the energy level n. Here $\beta = 1/(k_B T)$, the inverse of the temperature, while E_n are the various energy states the system could have. Of particular interest is the partition function

$$Z = \sum_n \exp -(\beta E_n) \, , \tag{2}$$

from which it is possible to extract all the relevant thermodinamical quantities.

The hydrogen atom obeys to an attractive potential given by

$$V(r) = -\frac{e^2}{r} \, , \tag{3}$$

and when solved the two–body quantum mechanical problem gives us the binding energy levels

$$E_n = -\frac{R}{n^2}, \tag{4}$$

where R has the value of 1 Rydberg, 13.6 eV, the ionization energy of hydrogen atom, equivalent to a temperature of about 1.58×10^5 Kelvin.

Because of the symmetry of the Coulombic potential (3), apart from the angular momentum $\mathbf{L}$ there exists another conserved vector, the Laplace–Runge–Lenz vector given by

$$\mathbf{A} = \mathbf{p} \times \mathbf{L} - e^2 m_e \frac{\mathbf{r}}{r} \, . \tag{5}$$

That is due to a supplementary $SO(4)$ symmetry of the system Fock (1935); Bargmann (1936) besides the usual rotational invariance $SO(3)$ that gives the n^2 degeneracy to energy levels in (4).

Computing the partition function for the hydrogen atom and considering the degeneracy one obtains

$$Z = \sum_{n=1}^{+\infty} n^2 \exp\left(\frac{\beta R}{n^2}\right) \geq \sum_{n=1}^{+\infty} n^2 \, , \tag{6}$$

which contrary to some other known cases, like the quantum harmonic oscillator, is clearly a divergent quantity. This makes impossible to extract any meaningful thermodinamical quantity out of (6) for an otherwise well-defined problem with sound results for energy levels, fine structure, relativistic effects and so on.

A possible solution to this problem was proposed by Tsallis et al.(see Lucena et al. (1995) and references therein). Essentially it consists on deforming the exponential measure by means of a continuous parameter q

$$\exp_q(x) = \begin{cases} [1 + (1-q)x]^{\frac{1}{1-q}} & \text{for } 1 + (1-q)x > 0 \text{ and } q \neq 1 \\ \exp(x) & \text{for } q = 1 \\ 0 & \text{else} \end{cases} \tag{7}$$

The idea of the so–called q-deformation was first introduced by Box & Cox (1964) for statistical distributions. In this approach equation (6) becomes

$$Z = \sum_{n=1}^{+\infty} n^2 \left[1 + (1-q)\frac{\beta R}{n^2}\right]^{\frac{1}{1-q}} \, . \tag{8}$$

Setting $m = 1/(1-q)$ so that for $m = +\infty$ one recovers the usual Boltzmann distribution, and $t = \beta R$, one could write the Tsallis partition function as

$$Z_{Ts} := \sum_{n=1}^{+\infty} n^2 \left(1 + \frac{t}{mn^2}\right)^m \, . \tag{9}$$

⋆ Corresponding author: nicola.fabiano@tdtu.edu.vn

A DIFFERENT APPROACH

As we have seen in eq. (6) this partition function diverges. Rewriting the expression in a different way one obtains

$$Z = \sum_{n=1}^{+\infty} n^2 \exp\left(\frac{\beta R}{n^2}\right) = \sum_{n=1}^{+\infty} n^2 \sum_{k=0}^{+\infty} \frac{(\beta R)^k}{n^{2k}} \frac{1}{k!} = \sum_{k=0}^{+\infty} \frac{(\beta R)^k}{k!} \sum_{n=1}^{+\infty} \frac{1}{n^{2k-2}}$$
$$= \sum_{k=0}^{+\infty} \frac{(\beta R)^k}{k!} \zeta(2k-2) = \sum_{k=0}^{+\infty} \frac{t^k}{k!} \zeta(2k-2) =: Z_\zeta \,. \quad (10)$$

With this definition, owing to the fact that $\zeta(-2) = 0, \zeta(0) = -1/2, \zeta(2) = \pi^2/6$ and $\zeta(2k-2) < 2$ for $k > 1$, the partition function Z_ζ converges and is well defined.

Rearranging eq. (9) in the same way as done with eq. (10) one obtains

$$Z_{Ts} = \sum_{n=1}^{+\infty} n^2 \left(1 + \frac{\beta R}{mn^2}\right)^m = \sum_{n=1}^{+\infty} n^2 \sum_{k=0}^{m} \left(\frac{\beta R}{mn^2}\right)^k \binom{m}{k} =$$
$$\sum_{k=0}^{m} \left(\frac{\beta R}{m}\right)^k \binom{m}{k} \sum_{n=1}^{+\infty} \frac{1}{n^{2k-2}} = \sum_{k=0}^{m} \left(\frac{t}{m}\right)^k \binom{m}{k} \zeta(2k-2) \,. \quad (11)$$

The ζ function regularization allows to make sense of both partition functions Z_{Ts} and Z_ζ (the former, at least for finite m). However there is no way to obtain a closed form for either partition function. Therefore we shall compare the two results only for some special cases.

LOW TEMPERATURE EXPANSION

Starting from the partition function Z it is possible to extract the internal energy

$$\langle E \rangle = -\frac{\partial}{\partial \beta} \ln Z \quad (12)$$

along with the variation of energy

$$\langle E^2 - \langle E \rangle^2 \rangle = \left(-\frac{\partial}{\partial \beta}\right)^2 \ln Z \quad (13)$$

and its fluctuation

$$\frac{\langle E^2 - \langle E \rangle^2 \rangle}{\langle E \rangle^2} \,. \quad (14)$$

Comparing Z_{Ts} and Z_ζ at low temperature translates to keep only the highest β terms in the series, respectively

$$Z_{Ts} = \frac{(\beta R)^m}{m^m} \zeta(2m-2) + \frac{(\beta R)^{m-1}}{m^{m-2}} \zeta(2m-4) +$$
$$\frac{(\beta R)^{m-2}}{m^{m-3}} \left(\frac{m-1}{2}\right) \zeta(2m-6) + \dots \,, \quad (15)$$

and

$$Z_\zeta = \frac{(\beta R)^m}{m!} \zeta(2m-2) + \frac{(\beta R)^{m-1}}{(m-1)!} \zeta(2m-4) + \frac{(\beta R)^{m-2}}{(m-2)!} \zeta(2m-6) + \dots \,, \quad (16)$$

eventually letting $m \to +\infty$.

We will start with results given by Z_{Ts}:

$$\langle E \rangle = -m k_B T + \frac{m^2 \zeta(2m-4)}{\zeta(2m-2)} \frac{k_B^2 T^2}{R} +$$
$$\frac{\left[(m^4 - m^3)\zeta(2m-6)\zeta(2m-2) - m^4 \zeta(2m-4)^2\right]}{\zeta(2m-2)^2} \frac{k_B^3 T^3}{R^2} + \dots =$$
$$-m k_B T + m^2 \frac{k_B^2 T^2}{R} - m^3 \frac{k_B^3 T^3}{R^2} + \dots \,, \quad (17)$$

and the result for the internal energy is always consistently negative even before taking the limit $m \to +\infty$.

$$\langle E^2 - \langle E \rangle^2 \rangle = -m k_B^2 T^2 + \frac{2m^2 \zeta(2m-4)}{\zeta(2m-2)} \frac{k_B^3 T^3}{R} + \dots =$$
$$-m k_B^2 T^2 + 2m^2 \frac{k_B^3 T^3}{R} + \dots \,, \quad (18)$$

the energy variation is also negative irrespective of the value for m, and behaves like T^2 as expected.

$$\frac{\langle E^2 - \langle E \rangle^2 \rangle}{\langle E \rangle^2} = -\frac{1}{m} + \left[\frac{m^2 \zeta(2m-6)}{\zeta(2m-2)} + \frac{m\zeta(2m-4)^2}{\zeta(2m-2)^2} - \right.$$
$$\left. \frac{m\zeta(2m-6)}{\zeta(2m-2)} - \frac{m^2 \zeta(2m-4)^2}{\zeta(2m-2)^2}\right] \frac{k_B^2 T^2}{R^2} + \left[\frac{2m^4 \zeta(2m-4)^3}{\zeta(2m-2)^3} + \right.$$
$$\frac{7m^3 \zeta(2m-4)\zeta(2m-6)}{\zeta(2m-2)^2} + \frac{2m^2 \zeta(2m-4)^3}{\zeta(2m-2)^3} -$$
$$\frac{4m^2 \zeta(2m-4)\zeta(2m-6)}{\zeta(2m-2)^2} - \frac{4m^3 \zeta(2m-4)^3}{\zeta(2m-2)^3} -$$
$$\left. \frac{3m^4 \zeta(2m-4)\zeta(2m-6)}{\zeta(2m-2)^2}\right] \frac{k_B^3 T^3}{R^3} + \dots = -\frac{1}{m} -$$
$$m^2(m^2 - 3m + 2) \frac{k_B^3 T^3}{R^3} + \dots = -\frac{1}{m} - m^4 \frac{k_B^3 T^3}{R^3} + \dots \,, \quad (19)$$

the first term shows that the energy fluctuation goes to zero with increasing m independently from the temperature. Adding further terms in T in the expression above appears to cancel out, that is the energy fluctuation seems to be independent from the temperature at least for several terms in the expansion.

The ζ function regularized partition function Z_ζ furnishes us with the following results:

$$\langle E \rangle = -m k_B T + \frac{m! \zeta(2m-4)}{(m-1)! \zeta(2m-2)} \frac{k_B^2 T^2}{R} +$$
$$\frac{\left[2((m-1)!)^2 m! \zeta(2m-6)\zeta(2m-2) - (m-2)!(m!)^2 \zeta(2m-4)^2\right]}{(m-2)!((m-1)!)^2 \zeta(2m-2)^2} \times$$
$$\frac{k_B^3 T^3}{R^2} + \dots = -m k_B T + m \frac{k_B^2 T^2}{R} + m(m-2) \frac{k_B^3 T^3}{R^2} + \dots \,, \quad (20)$$

in this case also the internal energy turns out to be negative even before considering large m values, consistently with the previous case.

$$\langle E^2 - \langle E \rangle^2 \rangle = -m k_B^2 T^2 + \frac{2m! \zeta(2m-4)}{(m-1)! \zeta(2m-2)} \frac{k_B^3 T^3}{R} + \dots =$$
$$-m k_B^2 T^2 + 2m \frac{k_B^3 T^3}{R} + \dots \,, \quad (21)$$

and like in the previous case the energy variation turns out to be negative in the low temperature limit considered.

$$\frac{\langle E^2-\langle E\rangle^2\rangle}{\langle E\rangle^2} = -\frac{1}{m}+$$
$$\left[\frac{2\zeta(2m-6)}{\zeta(2m-2)}+\frac{\zeta(2m-4)^2}{m\zeta(2m-2)^2}-\frac{\zeta(2m-4)^2}{\zeta(2m-2)^2}-\frac{2\zeta(2m-6)}{m\zeta(2m-2)}\right]\frac{k_B^2T^2}{R^2}+$$
$$\left[\frac{14\zeta(2m-4)\zeta(2m-6)}{\zeta(2m-2)^2}+\frac{2m\zeta(2m-4)^3}{\zeta(2m-2)^3}+\frac{2\zeta(2m-4)^3}{m\zeta(2m-2)^3}-\right.$$
$$\left.\frac{8\zeta(2m-4)\zeta(2m-6)}{m\zeta(2m-2)^2}-\frac{6m\zeta(2m-4)\zeta(2m-6)}{\zeta(2m-2)^2}-\frac{4\zeta(2m-4)^3}{\zeta(2m-2)^3}\right]\times$$
$$\frac{k_B^3T^3}{R^3}+\cdots = -\frac{1}{m}+\left(\frac{m-1}{m}\right)\frac{k_B^2T^2}{R^2}+\left(\frac{10m-4m^2-6}{m}\right)\frac{k_B^3T^3}{R^3}+$$
$$\cdots = -\frac{1}{m}+\frac{k_B^2T^2}{R^2}-4m\frac{k_B^3T^3}{R^3}+\cdots\ , \tag{22}$$

the energy fluctuation approaches zero from below in the relevant limit, irrispective of the temperature. The only difference with the previous case is an additional term proportional to T^2 and independent from m, again not influent in the low temperature limit.

HIGH TEMPERATURE EXPANSION

We shall now discuss some results obtained in the high temperature limit. It is understood that whith this expression we mean a high value of T (that is, $\beta \to 0$) such that $k_BT < R$ in order that the discrete spectrum of eq. (4) is still valid, being below the ionization level.

In this regime the two partition functions are given by

$$Z_{Ts} = -\frac{m}{2}\beta R+\frac{\pi^2}{12}\frac{m-1}{2m}(\beta R)^2 \tag{23}$$

and

$$Z_\zeta = -\frac{1}{2}\beta R+\frac{\pi^2}{12}(\beta R)^2\ . \tag{24}$$

The results from Z_{Ts} are the following:

$$\langle E\rangle = -\frac{1}{\beta}+\frac{\pi^2}{12}\frac{(m-1)}{m^2}R+\frac{\pi^4}{144}\frac{(m-1)^2}{m^4}R^2\beta+\dots\ , \tag{25}$$

the internal energy approaches a negative value limited by the cutoff R as previously discussed. In the Boltzmann limit $m \to +\infty$ all other terms disappear irrispective of the temperature.

$$\langle E^2-\langle E\rangle^2\rangle = -\frac{1}{\beta^2}-\frac{\pi^4}{144}\frac{(m-1)^2}{m^4}R^2-\frac{\pi^6}{864}\frac{(m-1)^3}{m^6}R^3\beta+\dots\ , \tag{26}$$

the energy variation behaves just like the internal energy discussed above, assuming a negative value.

$$\frac{\langle E^2-\langle E\rangle^2\rangle}{\langle E\rangle^2} = -1-\frac{\pi^2}{6}\frac{(m-1)}{m^2}R\beta+\dots\ , \tag{27}$$

the energy fluctuation approaches the constant value -1 when either one of the limits $\beta \to 0$ or $m \to +\infty$ is considered.

The results given by the regularized Z_ζ are:

$$\langle E\rangle = -\frac{1}{\beta}+\frac{\pi^2}{6}R+\frac{\pi^4}{36}R^2\beta+\dots\ , \tag{28}$$

as in the previous case, the internal energy is negative. The presence of a constant term independent from the temperature cannot change its sign as we have that $k_BT < R$ by hypothesis.

$$\langle E^2-\langle E\rangle^2\rangle = -\frac{1}{\beta^2}-\frac{\pi^4}{36}R^2-\frac{\pi^6}{108}R^3\beta+\dots\ , \tag{29}$$

even the energy variation has the same behaviour of internal energy as a function of temperature. The presence of a negative constant term does not change the result. Notice that an analogous term is present in Z_{Ts} for finite m.

$$\frac{\langle E^2-\langle E\rangle^2\rangle}{\langle E\rangle^2} = -1-\frac{\pi^2}{3}R\beta+\dots\ , \tag{30}$$

the energy fluctuation assumes a constant negative value -1 for small β, in agreement with the previous model.

CONCLUSIONS

We have considered the problem of the thermodinamics for hydrogen atom in the canonical ensemble. We have compared the results given by an alternative distribution to the Boltzmann one with our approach of a ζ function regularization of the partition function. Comparing some thermodinamical quantities in the limits of low and high temperature we have shown that the results given by our approach are sound, do not contradict results of quantum mechanical bound states and are consistent with the continuosly deformed exponential measure.

REFERENCES

Bargmann, V. 1936, Zur theorie des Wasserstoffatoms, Zeitschrift für Physik, 99(7-8), pp. 576–582.

Box, G. E. & Cox, D. R. 1964, An analysis of transformations, Journal of the Royal Statistical Society: Series B (Methodological), 26(2), pp. 211–243.

Fock, V. 1935, Zur theorie des Wasserstoffatoms, Zeitschrift für Physik, 98(3-4), pp. 145–154.

Lucena, L. S., da Silva, L. R., & Tsallis, C. 1995, Departure from Boltzmann-Gibbs statistics makes the hydrogen-atom specific heat a computable quantity, Physical Review E, 51(6), 6247.

UNIVERSITY THOUGHT
Publication in Natural Sciences, Vol.10, No.1, 2020, pp. 72-77.
DOI: https://doi.org/10.5937/univtho10-26397
Original Scientific Paper

STARK BROADENING OF Tb III SPECTRAL LINES ORIGINATING FROM 6s-6p TRANSITIONS

MILAN S. DIMITRIJEVIĆ[1,2,⋆]

[1]Astronomical Observatory, Volgina 7, 11060 Belgrade, Serbia
[2]Sorbonne Université, Observatoire de Paris, Université PSL, CNRS, LERMA, F-92190, Meudon, France

ABSTRACT

Stark full widths at half maximum (FWHM) for 26 6s-6p transitions in Tb III spectrum have been calculated for electron density of 10^{17} cm^{-3} within a temperature range of 5 000 K to 80 000 K, by using the simplified modified semiempirical (SMSE) method. The results obtained are used for the consideration of Strak width regularities within the investigated transition array.

Keywords: Stark broadening, Spectral lines, Line profiles, Tb III.

INTRODUCTION

Spectral line profiles, broadened by impacts with charged particles (Stark broadening) are useful for many topics as e.g. in astrophysics, laboratory plasma diagnostics, and for different plasma technologies.

For analysis of stellar atmospheres line broadening data for spectral lines of many atoms and ions are needed since the chemical composition of a stellar atmospheres is various and with development of space astronomy, spectrographs on board produce spectral line profiles with increasingly high resolution and accuracy. Consequently, even the data on spectral lines of trace elements become important.

Terbium belongs to lanthanides, a group of fifteen elements from lanthanum to lutetium. Their atomic numbers are from 57 to 71. They are also known as the rare earth elements (REE). Because of the rare-earth peak in the cosmic abundance distribution of chemical elements, data on Stark broadening of their spectral lines is of considerable significance in astrophysics, particularly for stellar atmospheres modelling and investigations and radiative transfer calculation.

The existence of terbium and its ions in stellar atmospheres is confirmed by observation of its spectral lines in stellar spectra. As an example, Siqueira Mello et al. (2014) derived, using three weak Tb II lines, the abundance of terbium for the moderately r-process-enhanced star CS 30315-029. Elkin et al. (2015) found Tb III lines in the spectrum of ro Ap star HD 213637 and Sachkov et al. (2008) in ro Ap star 10 Aql. The spectrum of HD 101065, known as Przybylski's star, an extreme roAp star, contains Tb I, Tb II and Tb III spectral lines (Cowley et al., 2000).

Stark full widths at half maximum (FWHM) for five multiplets of Tb II and 8 multiplets of Tb IV have been published in Dimitrijević (2020). Since for Tb III there is neither experimental nor theoretical data for Stark broadening, we calculated here, in order to provide such data, Stark full widths at half maximum (FWHM) for 26 s-p transitions of Tb III by using the simplified modified semiempirical method (Dimitrijević & Konjević, 1987), since there is no enough reliable atomic data for more sophysticated calculations.

The obtained results will be implemented in the STARK-B (Sahal-Bréchot et al., 2015, 2020) database for Stark broadening parameters.

SIMPLIFIED MSE FORMULA

For calculation of Stark line widths for Tb III the simplified modified semiempirical formula (Dimitrijević & Konjević, 1987) applicable to isolated, singly, and multiply charged ion lines is used. It is applicable for temperatures when the condition $x_{jj'} = E/|E_{j'} - E_j| \leq 2$ is satisfied. Here, j=i,f, where i denotes initial and f final atomic energy level forming the considered transition, $E_{j'}$ (j'=i' or f') is the nearest atomic energy level with possibility to have an allowed dipole transition from or to the energy level i or f. In such a case, full width at half maximum is (Dimitrijević & Konjević, 1987):

$$W(\text{Å}) = 2.2151 \times 10^{-8} \frac{\lambda^2(\text{cm}) N(\text{cm}^{-3})}{T^{1/2}(\text{K})} (0.9 - \frac{1.1}{Z}) \times$$

$$\times \sum_{\text{j=i,f}} (\frac{3n_j^*}{2Z})^2 (n_j^{*2} - \ell_j^2 - \ell_j - 1). \quad (1)$$

where N is the electron density, T temperature, $E = 3kT/2$ the energy of perturbing electron, $Z-1$ the ionic charge, n^{*2} the effective principal quantum number, ℓ_j (j=i,f) orbital angular momentum quantum number and λ the wavelength.

RESULTS AND DISCUSSION

Here are calculated Full Stark wifths at half intensity maximum by using the simplified modified semiempirical (SMSE)

⋆ Corresponding author: mdimitrijevic@aob.rs

Table 1. This table gives electron-impact broadening (Stark broadening) Full Widths at Half Intensity Maximum (W) for Tb III spectral lines, for a perturber density of 10^{17} cm^{-3} and temperatures from 5 000 to 80 000 K. The configuration is $4f^8(^7F)n\ell$. Also, the $3kT/2\Delta E$, quantity is given, where ΔE is the energy difference between closest perturbing level and the closer of initial and final levels. In order that the used method is valid, this quantity should be less or equal two. One value larger of two is given for better interpolation.

Transition	T(K)	W[Å]	3kT/2ΔE
Tb III $6s^8F_{13/2}$-$6p_{1/2}(6,1/2)^o$	5000.	0.254	0.215
λ = 2900.4 Å	10000.	0.180	0.431
	20000.	0.127	0.861
	40000.	0.899E-01	1.72
	80000.	0.636E-01	3.45
Tb III $6s^8F_{13/2}$-$6p_{3/2}(6,3/2)^o$	5000.	0.204	0.177
λ = 2517.1 Å	10000.	0.144	0.354
	20000.	0.102	0.708
	40000.	0.721E-01	1.42
	80000.	0.510E-01	2.83
Tb III $6s^8F_{11/2}$-$6p_{1/2}(6,1/2)^o$	5000.	0.281	0.215
λ = 3032.8 Å	10000.	0.198	0.431
	20000.	0.140	0.861
	40000.	0.992E-01	1.72
	80000.	0.702E-01	3.45
Tb III $6s^8F_{11/2}$-$6p_{3/2}(6,3/2)^o$	5000.	0.222	0.177
λ = 2616.1 Å	10000.	0.157	0.354
	20000.	0.111	0.708
	40000.	0.786E-01	1.42
	80000.	0.556E-01	2.83
Tb III $6s^8F_{9/2}$-$6p_{1/2}(6,1/2)^o$	5000.	0.310	0.215
λ = 3174.1 Å	10000.	0.219	0.431
	20000.	0.155	0.861
	40000.	0.110	1.72
	80000.	0.776E-01	3.45
Tb III $6s^8F_{9/2}$-$6p_{3/2}(6,3/2)^o$	5000.	0.243	0.177
λ = 2720.6 Å	10000.	0.171	0.354
	20000.	0.121	0.708
	40000.	0.857E-01	1.42
	80000.	0.606E-01	2.83
Tb III $6s^8F_{7/2}$-$6p_{1/2}(6,1/2)^o$	5000.	0.333	0.215
λ = 3277.4 Å	10000.	0.235	0.431
	20000.	0.167	0.861
	40000.	0.118	1.72
	80000.	0.833E-01	3.45
Tb III $6s^8F_{7/2}$-$6p_{3/2}(6,3/2)^o$	5000.	0.258	0.177
λ = 2796.2 Å	10000.	0.182	0.354
	20000.	0.129	0.708
	40000.	0.911E-01	1.42
	80000.	0.644E-01	2.83
Tb III $6s^8F_{5/2}$-$6p_{1/2}(6,1/2)^o$	5000.	0.352	0.215
λ = 3359.2 Å	10000.	0.249	0.431
	20000.	0.176	0.861
	40000.	0.124	1.72
	80000.	0.879E-01	3.45

Table 1. Continued.

Transition	T(K)	W[Å]	3kT/2ΔE
Tb III $6s^8F_{5/2}$-$6p_{3/2}(6,3/2)^o$	5000.	0.270	0.177
λ = 2855.5 Å	10000.	0.191	0.354
	20000.	0.135	0.708
	40000.	0.955E-01	1.42
	80000.	0.675E-01	2.83
Tb III $6s^8F_{3/2}$-$6p_{1/2}(6,1/2)^o$	5000.	0.365	0.215
λ = 3418.1 Å	10000.	0.258	0.431
	20000.	0.183	0.861
	40000.	0.129	1.72
	80000.	0.913E-01	3.45
Tb III $6s^8F_{3/2}$-$6p_{3/2}(6,3/2)^o$	5000.	0.279	0.179
λ = 2898.0 Å	10000.	0.197	0.358
	20000.	0.140	0.716
	40000.	0.987E-01	1.43
	80000.	0.698E-01	2.86
Tb III $6s^8F_{1/2}$-$6p_{1/2}(6,1/2)^o$	5000.	0.374	0.215
λ = 3454.2 Å	10000.	0.264	0.431
	20000.	0.187	0.861
	40000.	0.132	1.72
	80000.	0.934E-01	3.45
Tb III $6s^8F_{1/2}$-$6p_{3/2}(6,3/2)^o$	5000.	0.285	0.181
λ = 2923.8 Å	10000.	0.201	0.362
	20000.	0.142	0.723
	40000.	0.101	1.45
	80000.	0.711E-01	2.89
Tb III $6s^6F_{11/2}$-$6p_{1/2}(6,1/2)^o$	5000.	0.303	0.215
λ = 3141.0 Å	10000.	0.214	0.431
	20000.	0.152	0.861
	40000.	0.107	1.72
	80000.	0.758E-01	3.45
Tb III $6s^6F_{11/2}$-$6p_{3/2}(6,3/2)^o$	5000.	0.238	0.177
λ = 2696.3 Å	10000.	0.168	0.354
	20000.	0.119	0.708
	40000.	0.840E-01	1.42
	80000.	0.594E-01	2.83
Tb III $6s^6F_{9/2}$-$6p_{1/2}(6,1/2)^o$	5000.	0.354	0.215
λ = 3369.4 Å	10000.	0.250	0.431
	20000.	0.177	0.861
	40000.	0.125	1.72
	80000.	0.885E-01	3.45
Tb III $6s^6F_{9/2}$-$6p_{3/2}(6,3/2)^o$	5000.	0.272	0.177
λ = 2862.9 Å	10000.	0.192	0.354
	20000.	0.136	0.708
	40000.	0.960E-01	1.42
	80000.	0.679E-01	2.83
Tb III $6s^6F_{7/2}$-$6p_{1/2}(6,1/2)^o$	5000.	0.378	0.215
λ = 3472.6 Å	10000.	0.267	0.431
	20000.	0.189	0.861
	40000.	0.134	1.72
	80000.	0.945E-01	3.45

Table 1. Continued.

Transition	T(K)	W[Å]	3kT/2ΔE
Tb III $6s^6F_{7/2}$-$6p_{3/2}(6,3/2)^o$	5000.	0.287	0.182
λ = 2937.1 Å	10000.	0.203	0.364
	20000.	0.144	0.727
	40000.	0.102	1.45
	80000.	0.719E-01	2.91
Tb III $6s^6F_{5/2}$-$6p_{1/2}(6,1/2)^o$	5000.	0.407	0.215
λ = 3591.1 Å	10000.	0.288	0.431
	20000.	0.204	0.861
	40000.	0.144	1.72
	80000.	0.102	3.45
Tb III $6s^6F_{5/2}$-$6p_{3/2}(6,3/2)^o$	5000.	0.306	0.188
λ = 3021.3 Å	10000.	0.216	0.376
	20000.	0.153	0.752
	40000.	0.108	1.50
	80000.	0.765E-01	3.01
Tb III $6s^6F_{3/2}$-$6p_{1/2}(6,1/2)^o$	5000.	0.425	0.215
λ = 3664.1 Å	10000.	0.301	0.431
	20000.	0.213	0.861
	40000.	0.150	1.72
	80000.	0.106	3.45
Tb III $6s^6F_{3/2}$-$6p_{3/2}(6,3/2)^o$	5000.	0.318	0.192
λ = 3072.9 Å	10000.	0.225	0.384
	20000.	0.159	0.767
	40000.	0.112	1.53
	80000.	0.794E-01	3.07
Tb III $6s^6F_{1/2}$-$6p_{1/2}(6,1/2)^o$	5000.	0.439	0.215
λ = 3715.7 Å	10000.	0.310	0.431
	20000.	0.219	0.861
	40000.	0.155	1.72
	80000.	0.110	3.45
Tb III $6s^6F_{1/2}$-$6p_{3/2}(6,3/2)^o$	5000.	0.326	0.195
λ = 3109.1 Å	10000.	0.231	0.389
	20000.	0.163	0.778
	40000.	0.115	1.56
	80000.	0.815E-01	3.11

method for 26 s-p transitions of Tb III. Calculations has been performed for an electron density of 10^{17} cm^{-3} and for temperature interval from 5 000 K to 80 000 K, for broadening of spectral lines by collisions with electrons. The needed energy levels and the ionization energy have been taken from Martin et al. (1978) and Kramida et al. (2020). The data on Tb III energy levels are not sufficient for a more sophysticated calculations, so that SMSE method, needing less atomic data, is the most advanced that could be successfully applied.

The additional complication with Tb III energy level system is that 6s levels are described with LS coupling and 6p levels with J_1j coupling. Moreover, in 6p terms only a part of energy levels is known. Consequently we calculated averaged term energies for $6p_{1/2}(6,1/2)^o$ and $6p_{3/2}(6,3/2)^o$ using existing energy levels and expression:

$$E = \frac{\sum_{\mathrm{J}}(2\mathrm{J}+1)E_{\mathrm{J}}}{\sum_{\mathrm{J}}(2\mathrm{J}+1)}, \qquad (2)$$

where E is the averaged energy and E_{J} and J energy and total angular momentum of a particular energy level. An average energy obtained for the term $6p_{1/2}(6,1/2)^o$ is 52154.1 cm^{-1} and for $6p_{3/2}(6,3/2)^o$ 57405.3 cm^{-1}. Also, we assumed that the perturber with $\Delta n = 0$ of the lower level is the upper level of the considered transition. Since the contribution of the lower level is smaller in comparison with the upper one, and the averaged energy is ob-

Table 2. This table gives electron-impact broadening (Stark broadening) Full Widths at Half Intensity Maximum (W) for Tb III $(^7F)6s^{(2S+1)}F_{j_1/2}$-$(^7F)6p_{j_2/2}(6,j_2/2)^o$ transition array, for a perturber density of 10^{17} cm^{-3} and temperature of 10 000 K, in [Å] and in [10^{12}s^{-1}] units.

Transition	W[Å]	W[10^{12} s^{-1}]
Tb III $6s^8F_{13/2}$-$6p_{1/2}(6,1/2)^o$ λ = 2900.4 Å	0.180	0.403
Tb III $6s^8F_{13/2}$-$6p_{3/2}(6,3/2)^o$ λ = 2517.1 Å	0.144	0.428
Tb III $6s^8F_{11/2}$-$6p_{1/2}(6,1/2)^o$ λ = 3032.8 Å	0.198	0.405
Tb III $6s^8F_{11/2}$-$6p_{3/2}(6,3/2)^o$ λ = 2616.1 Å	0.157	0.432
Tb III $6s^8F_{9/2}$-$6p_{1/2}(6,1/2)^o$ λ = 3174.1 Å	0.219	0.409
Tb III $6s^8F_{9/2}$-$6p_{3/2}(6,3/2)^o$ λ = 2720.6 Å	0.171	0.435
Tb III $6s^8F_{7/2}$-$6p_{1/2}(6,1/2)^o$ λ = 3277.4 Å	0.235	0.412
Tb III $6s^8F_{7/2}$-$6p_{3/2}(6,3/2)^o$ λ = 2796.2 Å	0.182	0.438
Tb III $6s^8F_{5/2}$-$6p_{1/2}(6,1/2)^o$ λ = 3359.2 Å	0.249	0.416
Tb III $6s^8F_{5/2}$-$6p_{3/2}(6,3/2)^o$ λ = 2855.5 Å	0.191	0.441
Tb III $6s^8F_{3/2}$-$6p_{1/2}$ $(6,1/2)^o$ λ = 3418.1 Å	0.258	0.416
Tb III $6s^8F_{3/2}$-$6p_{3/2}(6,3/2)^o$ λ = 2898.0 Å	0.197	0.442
Tb III $6s^8F_{1/2}$-$6p_{1/2}(6,1/2)^o$ λ = 3454.2 Å	0.264	0.417
Tb III $6s^8F_{1/2}$-$6p_{3/2}(6,3/2)^o$ λ = 2923.8 Å	0.201	0.443
Tb III $6s^6F_{11/2}$-$6p_{1/2}(6,1/2)^o$ λ = 3141.0 Å	0.214	0.409
Tb III $6s^6F_{11/2}$-$6p_{3/2}(6,3/2)^o$ λ = 2696.3 Å	0.168	0.435
Tb III $6s^6F_{9/2}$-$6p_{1/2}(6,1/2)^o$ λ = 3369.4 Å	0.250	0.415
Tb III $6s^6F_{9/2}$-$6p_{3/2}(6,3/2)^o$ λ = 2862.9 Å	0.192	0.441
Tb III $6s^6F_{7/2}$-$6p_{1/2}(6,1/2)^o$ λ = 3472.6 Å	0.267	0.417
Tb III $6s^6F_{7/2}$-$6p_{3/2}(6,3/2)^o$ λ = 2937.1 Å	0.203	0.443
Tb III $6s^6F_{5/2}$-$6p_{1/2}(6,1/2)^o$ λ = 3591.1 Å	0.288	0.421
Tb III $6s^6F_{5/2}$-$6p_{3/2}(6,3/2)^o$ λ = 3021.3 Å	0.216	0.446
Tb III $6s^6F_{3/2}$-$6p_{1/2}(6,1/2)^o$ λ = 3664.1 Å	0.301	0.422
Tb III $6s^6F_{3/2}$-$6p_{3/2}(6,3/2)^o$ λ = 3072.9 Å	0.225	0.449
Tb III $6s^6F_{1/2}$-$6p_{1/2}(6,1/2)^o$ λ = 3715.7 Å	0.310	0.423
Tb III $6s^6F_{1/2}$-$6p_{3/2}(6,3/2)^o$ λ = 3109.1 Å	0.231	0.450

tained without missing energy levels, we assume that the introduced error is acceptable.

The obtained results of our theoretical determination of Stark widths for spectral lines of doubly charged terbium ion are shown in Table 1. The extrapolation towards lower electron densities than 10^{17} cm^{-3} is linear while for higher it is linear if the influence of Debye screening is negligible or reasonably small. The wavelengths shown in Tables 1 and 2 are the calculated ones from the lower energy level and the averaged upper one, so that they are not equal with the observed ones. In the Table 1 the quantity $3kT/2\Delta E$ is given in the last column. This is the ratio of the average energy of free electrons, $E = 3kT/2$, and the larger of energy differences between the initial or final and the closest perturbing level.

$$\Delta E = \mathrm{Max}[E/\Delta E_{i,i'}, E/\Delta E_{f,f'}] \tag{3}$$

This ratio is one of the validity conditions for the used, simplified modified semiempirical method. Namely, the threshold for the corresponding inelastic transition is $3kT/2\Delta E = 1$. For values lower than one, elastic collisions dominate and the SMSE method is convenient and valid. In the case of values larger than one the inelastic collisions start to be more and more important but up to the value around two it is acceptable to neglect their influence. In Table 1, for the Stark width at T = 80 000 K, this value is higher than two. The width for this temperature is just a point for better interpolation.

The Stark widths obtained here, all belong to the 6s-6p transition array what enables to compare them in order to check their similarities. When such similarities exist, this gives possibility to use them for estimates of missing values, using the known ones. Wiese & Konjević (1982) demonstrated that Stark line widths, if expressed in angular frequency units, are usually very similar in a multiplet, in a supermultiplet they agree within about 30 per cent and, within up to 40 per cent within a transition array. In order to check their similarities within Tb III 6s-6p transition array we transformed the Stark widths expressed in Å-units to angular frequency units, using the expression:

$$W(\mathring{A}) = \frac{\lambda^2}{2\pi c} W(s^{-1}), \tag{4}$$

where c is the speed of light.

In Table 2 are shown Stark widths expressed in Å and in s^{-1} for a temperature of 10 000 K. We can see that values expressed in s^{-1} are much closer because they are liberated from the influence of wavelength. If expressed in Å, the highest value in the considered transition array is more than two times (115%) higher from the smallest one, while in angular frequeny units (s^{-1}) this difference is only 12%. If we look separately sextets and octets, the difference is in both groups 10%. For a fixed lower level, the difference betwen transitions with upper level $6p_{1/2}(6,1/2)^o$ and $6p_{3/2}(6,3/2)^o$ is 6-7% and for transitions with $6p_{1/2}$ only 5% as well as for the case of $6p_{1/2}$, even smaller if we separate octets and sextets, so that we look at multiplets. Than the difference is only 3.5%. In all considered cases the agreement is well within the maximal limits predicted by Wiese & Konjević (1982).

The results obtained in this investigation - Stark widths of Tb III spectral lines will be included in the STARK-B database (Sahal-Bréchot et al., 2015, 2020). This database is also one of the 33 databases entering in the european Virtual Atomic and Molecular Data Center - VAMDC (Dubernet et al., 2010; Rixon et al., 2011; Dubernet et al., 2016), which can be found on the web site http://portal.vamdc.eu.

CONCLUSION

With the help of the SMSE method we have calculated Stark widths for 26 Tb III transitions within the 6s-6p transition array as a function of temperature, for an electron density of 10^{17} cm^{-3} . The consideration of their similarities within the 6s-6p transition array of Tb III show that their differences are within 12 per cent for the transition array as a whole and up to 3.5% for multiplets. This can be used for the estimate of missing values in Tb III multiplets and transition arrays on the basis of the known ones. These data will be implemented in STARK-B database containing the calculated widths and shifts of isolated lines of atoms and ions due to electron and ion collisions. There is no other experimental or theoretical data for Stark broadening of Tb III lines so that it is not possible to make a comparison with other results. The new Stark broadening data for Tb III obtained in this work may be of interest for stellar physics and plasma diagnostics, especially for investigation of spectral lines and abundances of rare earth elements in atmospheres of white dwarfs and chemically peculiar stars .

REFERENCES

Cowley, C. R., Ryabchikova, T., Kupka, F., Bord, D. J., Mathys, G., Bidelman, W. P. 2000. Abundances in Przybylski's star. Monthly Notices of the Royal Astronomical Society, 317, pp. 299-309. doi.org/10.1046/j.1365-8711.2000.03578.x

Dimitrijević, M.S. 2019. Stark broadening data for spectral lines of rare-earth elements: Example of Tb II and Tb IV. Contrib. Astron. Obs. Skalnaté Pleso, 50, pp. 122-127. doi: 10.31577/caosp.2020.50.1.122

Dimitrijević, M. S., Konjević, N. 1987. Simple estimates for Stark broadening of ion lines in stellar plasma. Astronomy and Astrophysics, 172, pp. 345-349.

Dubernet, M. L., Antony, B. K., Ba, Y. A., Babikov, Yu. L., Bartschat, K., Boudon, V., ... Zwölf, C. M. 2016. The virtual atomic and molecular data centre (VAMDC) consortium. Journal of Physics B: Atomic, Molecular and Optical Physics, 49(7), 074003. doi: 10.1088/0953-4075/49/7/074003

Dubernet, M.L., Boudon, V., Culhane, J.L., Dimitrijević, M.S., Fazliev, A.Z., Joblin, C., ... Zeippen, C.J. 2010. Virtual atomic and molecular data centre. Journal of Quantitative Spectroscopy & Radiative Transfer, 111(15), pp. 2151-2159.

Elkin, V. G., Kurtz, D. W., Mathys, G. 2015. Time resolved spectroscopy of the cool Ap star HD 213637. Monthly Notices of the Royal Astronomical Society, 446, pp. 4126-4131. doi.org/10.1093/mnras/stu2406

Kramida, A., Ralchenko, Yu., Reader, J., -NIST ASD Team 2020, NIST Atomic Spectra Database. Gaithersburg, MD: National Institute of Standards and Technology. (ver. 5.5.1), Retrived from https://physics.nist.gov/asd, 2020, 1st of April.

Martin, W. C., Zalubas, R., Hagan, L. 1978. Atomic Energy Levels: The Rare-Earth Elements. Nat. Stand. Ref. Data Ser., NSRDS-NBS 60, pp. 1-422.

Rixon, G., Dubernet, M. L., Piskunov, N., Walton, N., Mason, N., Le Sidaner, P., ... Zeippen, C. J. 2011. VAMDC—The Virtual Atomic and Molecular Data Centre—A New Way to Disseminate Atomic and Molecular Data—VAMDC Level 1 Release. AIP Conference Proceedings, 1344, pp. 107-115.

Sachkov, M., Kochukov, O., Ryabchikova, T., Leone, F., Bagnulo, S., Weiss, W. W. 2008. Spectroscopic study of pulsations in the atmosphere of roAp star 10 Aql. Contrib. Astron. Obs. Skalnaté Pleso, 38, pp. 323-328.

Sahal-Bréchot, S., Dimitrijević, M. S., Moreau, N. 2020. STARK-B database. Observatory of Paris / LERMA and Astronomical Observatory of Belgrade. Retrieved from http://starkb.obspm.fr, 2020 May 1st.

Sahal-Bréchot, S., Dimitrijević, M. S., Moreau, N., Ben Nessib, N. 2015. The STARK-B database VAMDC node: a repository for spectral line broadening and shifts due to collisions with charged particles. Physica Scripta, 50, 054008.

Siqueira Mello, C., Hill, V., Barbuy, B., Spite, M., Spite, F., Beers, T. C., Ca_au, E., Bonifacio, P., Cayrel, R., François, P., Schatz, H., Wanajo, S. 2014. High-resolution abundance analysis of very metal-poor r-I stars. AA, 565, A93.

Wiese, W.L., Konjević, N. 1982. Regularities and similarities in plasma broadened spectral line widths (Stark widths). Journal of Quantitative Spectroscopy and Radiative Transfer, 28, pp. 185-198.

CIP - Каталогизација у публикацији
Народна библиотека Србије, Београд

5

The UNIVERSITY thought. Publication in natural sciences / editor in chief Nebojša Živić. - Vol. 3, no. 1 (1996)- . - Kosovska Mitrovica : University of Priština, 1996- (Kosovska Mitrovica : Art studio KM). - 29 cm

Polugodišnje. - Prekid u izlaženju od 1999-2015. god. - Je наставак: Универзитетска мисао. Природне науке =
ISSN 0354-3951
ISSN 1450-7226 = The University thought. Publication in natural sciences
COBISS.SR-ID 138095623

Available Online

This journal is available online. Please visit http://www.utnsjournal.pr.ac.rs or http://www.utnsjournal.com to search and download published articles.